A geophysical survey of a suspected Iron Age Fort on Newton Farm in Markinch, Fife

Stefan Froud
060005963

Submitted as an integral part of the Bsc Geoscience Honours Degree course in the School of Geography & Geosciences, University of St Andrews, March 2010. I certify that I have read the University's statement on Academic Misconduct, that the following work is my own work and that significant academic debts and borrowings have been properly acknowledged and referenced.

In association with:

Rathmell Archaeology Ltd

Fife Council Archaeological Unit

ABSTRACT

Cropmarks reveal the presence of a suggested Iron Age Fort complex positioned on Newton Hill in Markinch, Fife. The primary aim of this investigation was to use a range of geophysical techniques to understand the size and nature of the subsurface archaeology and any other subsurface features on Newton Farm. As the majority of the cropmarks are located within Field 1 (NGR: 3295 7029), this site was targeted with a more detailed geophysical survey. Two DC resistivity transects, electromagnetism, magnetometry and magnetic susceptibility were applied on the main site (Field 1). Electromagnetism was also applied to Field 2 (NGR: 3293 7028) and Field 3 (NGR: 3295 7031). By using geophysical modelling, interpretation of any underground subsurface features was possible. DC resistivity enabled interpretation of the contents of two ring ditches and several buried metallic bodies. Electromagnetism was less successful for mapping subsurface archaeology but showed a relationship between topography and soil water content with lower topographies showing increased soil water content. It was possible to interpret some archaeology with magnetometry and magnetic susceptibility and both also located a recent structure, a WWII spot light position.

Excavation enabled comparison of the ground truth with the geophysical results. The ring ditches causing the cropmarks were proven using XRF, XRD and grain size analysis to be very similar in composition and grain size to the surrounding drift sediment. As a consequence these ditches did not provide a significant variation in geophysical response and therefore could not be interpreted with use of the original geophysical model. Ground truth allowed a new adjusted geophysical model to be created for improved interpretation of the current and any future geophysical results. Additional application of electromagnetism over the trenches concluded that the topsoil covering on Newton Farm ‘masks’ the electromagnetic response.

This investigation proved that as long as a range of geophysical techniques are used and an accurate geophysical model can be created, the two can compliment each other to provide a successful and reliable survey of the subsurface features assuming ground conditions are suitable.

(**Cover photograph**. Newton Farm (Field 1) looking west, June 2009).

ACKNOWLEDGEMENTS

This project would not have been possible without the dedication of several people. I would therefore like to thank the following people for their assistance throughout different stages of the project.

- Dr. Richard Bates for assisting three days in the operation of the geophysical surveys and allowing me to use the geophysical equipment throughout June. I would also like to thank him for his support for the duration of the project.

- Dr. John Walden, Angus Calder and Donald Herd for their support with analytical laboratory methods.

- Melanie Chocholek for giving up valuable time to helping with the operation of the HiPer Pro Topcon DGPS.

- Dr. Ruth Robinson for her advice on the presentation of GIS data.

- Dr Margaret Watters and Dr Peter Morris for their contribution with data and opinions.

- Douglas Spiers and Stephen Liscoe, the Fife Council archaeologists, for allowing me to survey the site beforehand. I would also like to thank them both for the continued contact and information on the site.

- John Lethangie, the Newton Farm farmer, for allowing operation of the geophysical surveys on the farm.

- The Markinch Heritage Group and Rathmell Archaeology Ltd for making the excavation possible.

CONTENTS

"I declare that this dissertation is 9648 words in length, excluding appendices, references, tables and figures"
Signature……………………………………

"I declare that the School of Geography & Geosciences informed me of the Safety Guidelines which it has drawn up, that I signed a Safety Guidance Form, thereby agreeing to abide by these Guidelines."
Signature……………………………………

LIST OF FIGURES

CHAPTER 1: INTRODUCTION

CHAPTER 2: BACKGROUND INFORMATION

CHAPTER 3: FIELD SURVEY

CHAPTER 4: SURVEY RESULTS AND INTERPRETATION

CHAPTER 5: GROUND TRUTH - EXCAVATION

CHAPTER 6: DISCUSSION

CHAPTER 7: FUTURE WORK

LIST OF TABLES

CHAPTER 3: FIELD SURVEY

CHAPTER 5: GROUND TRUTH - EXCAVATION

CHAPTER 1: INTRODUCTION

1.1 General Introduction

First discovered during aerial archaeological reconnaissance work by the Royal Commission on the Ancient and Historical Monuments of Scotland (RCAHMS) in 1989, aerial photography over Newton Farm, Markinch, suggests previous existence of prehistoric settlements. The ringed nature of cropmarks visible from aerial photography suggests that this was the likely location of a hill fort presumed to be active during the Iron Age.

1.2 Aims and Objectives

Geophysics is increasingly being used to map archaeological landscapes both on broad- and fine-scale and can help provide a perspective to settlement context and enable landscape reconstruction. The main aims and objectives of this investigation were as follows:

- To perform a range of geophysical techniques over Newton Farm and interpret the results with the use of a geophysical model. This will enable prediction of the size and nature of the archaeology as well as showing general ground conditions.
- To collect soil samples on the site and test these in the laboratory for magnetic susceptibility, enabling the location of areas which have had significant previous human activity.

- Excavate and locate the main features of the settlement, recording any findings and link the ground truth with the geophysical results.
- To gain a better understanding of the relationship between geophysical survey data, subsurface archaeology and site soil/ground properties to enhance interpretation of geophysical surveys.

1.3 Site Description

Newton Farm is located less than 1 km north of Markinch, Fife, and lies approximately 100 m above Ordnance Datum (OD) (Figures 1.1 and 1.2). The main site (Field 1), where aerial photography reveals the main cropmark features, is bound by metal barbed wire fences and a stone wall on the eastern side. It measures an estimated 150 m x 150 m and is located at NGR: 3295 7029. There are two other fields with access available in close proximity. The field to the west (Field 2) of Field 1 measures approximately 200 m x 200 m at NGR: 3293 7028 and the field to the north (Field 3) of Field 1 measures approximately 350 m x 250 m at NGR: 3295 7031 (Figure 1.3).

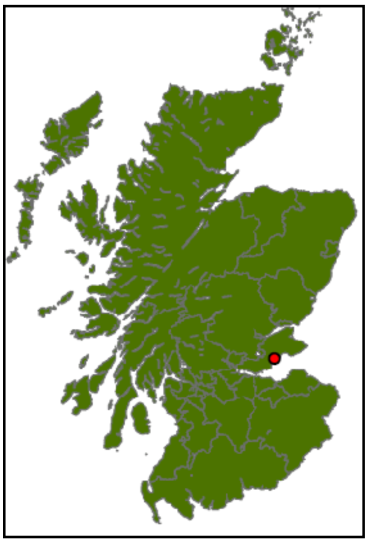

Figure 1.1. Markinch shown within Scotland in red.

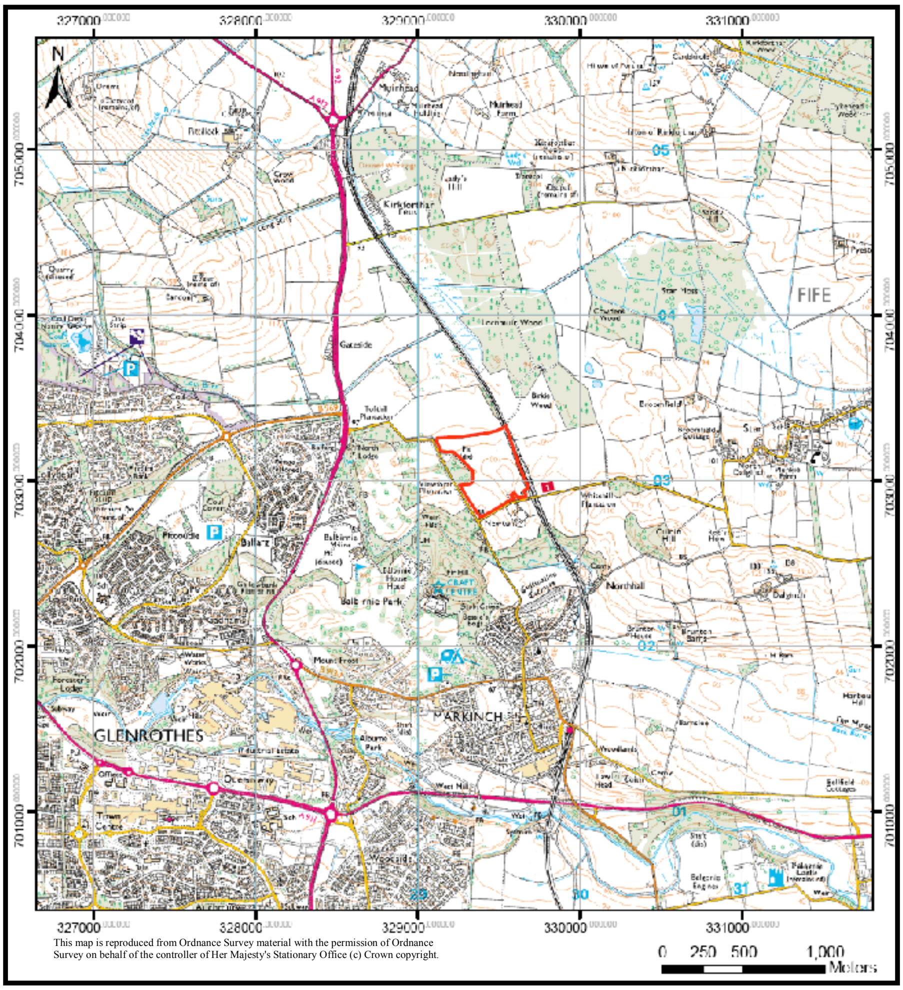

Figure 1.2. Map of the Markinch region with field area outlined in red.

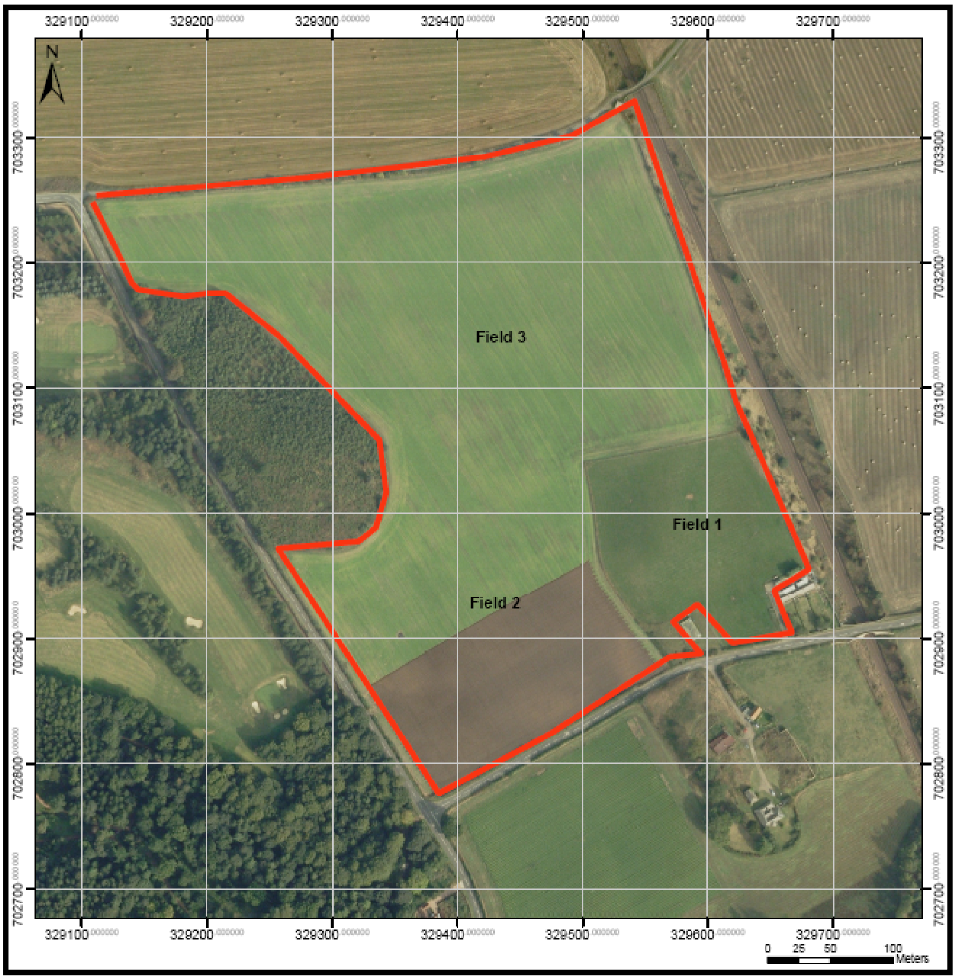

Figure 1.3. Aerial image of Newton with field area outlined in red (Imagery taken in 2005 and supplied by Fife Council).

Field 1 is covered with grass (Figure 1.4) but aerial imagery confirmed it was previously used for crop farming and it is thought to have been farmed in this way for many centuries (John Lethangie, *Personal Communication,* 2009). Fields 2 and 3 are both ploughed and consist of sprouting crops (e.g. carrots) (Figures 1.5 and 1.6). The land is gently undulating with the exception of Field 1 which is positioned on a distinct steep sided hillock (Figures 1.4 and 1.7). It is evident that the site drains very well and the soil appeared very dry throughout. This good drainage property is typical of the surrounding drift geology, composed of glacial gravel, sand and silt to at least 25 m deep (Section 2.3), which is renowned for its high permeability.

Figure 1.4. Field 1 showing steep side slope.

Figure 1.5. Field 2 showing ploughed land.

Figure 1.6. Field 3 showing ploughed land with sprouting crops.

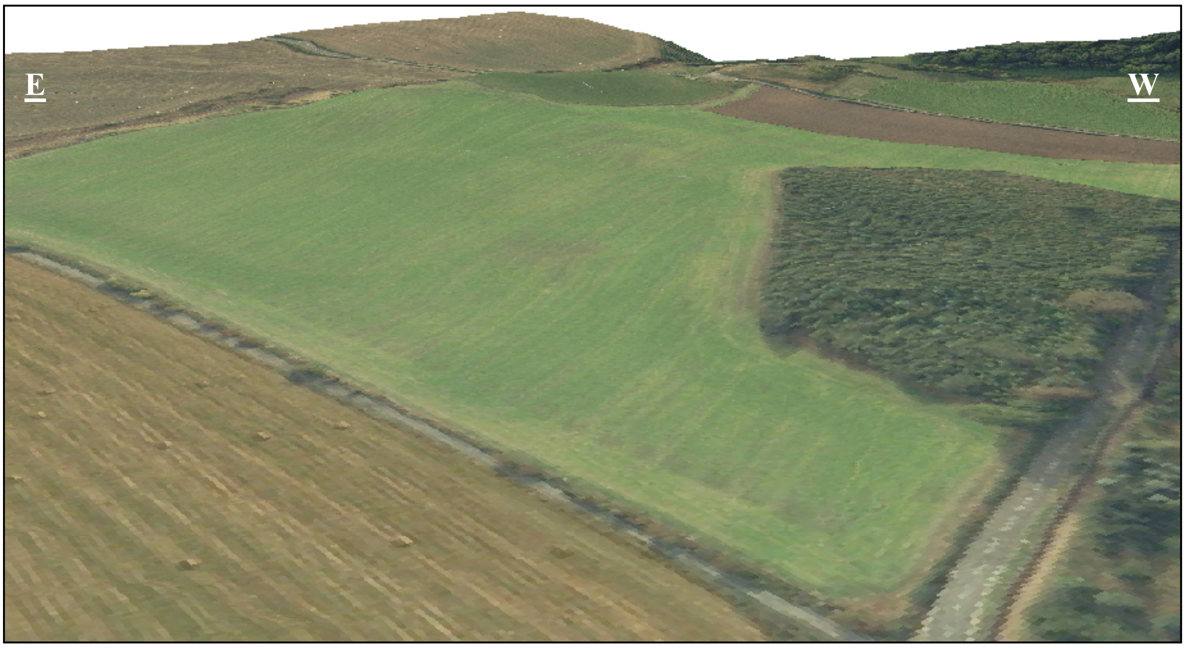

Figure 1.7. Aerial view of Newton Farm showing the undulation over the site (Aerial Imagery taken 2005 and supplied by Fife Council).

1.3.1 *Possible Noise (Interference) Sources*

In geophysical surveys it is important to note sources of interference in order to achieve accurate results. These were accurately recorded using the HiPer Pro Topcon integrated RTK GPS (Figure 1.8 and Appendix B.3). Field 1 is bound by a metal barbed wire fence (Figure 1.9) and a stone wall on the eastern side. On the other side of the wall lies a railway which could cause some interference. On the southern side of Field 1 at NGR: 329600 702900, there is a large water tank surrounded by a metal fence. Field 2 and Field 3 are also bound by barbed wire fences. Field 1 has an overhead power cable (Figure 1.10) trending in a north-south direction from NGR: 329627 703064 to 329649 702899. There are also two metal drain covers on Field 1 at NGR: 329659 702993 and 329595 703037.

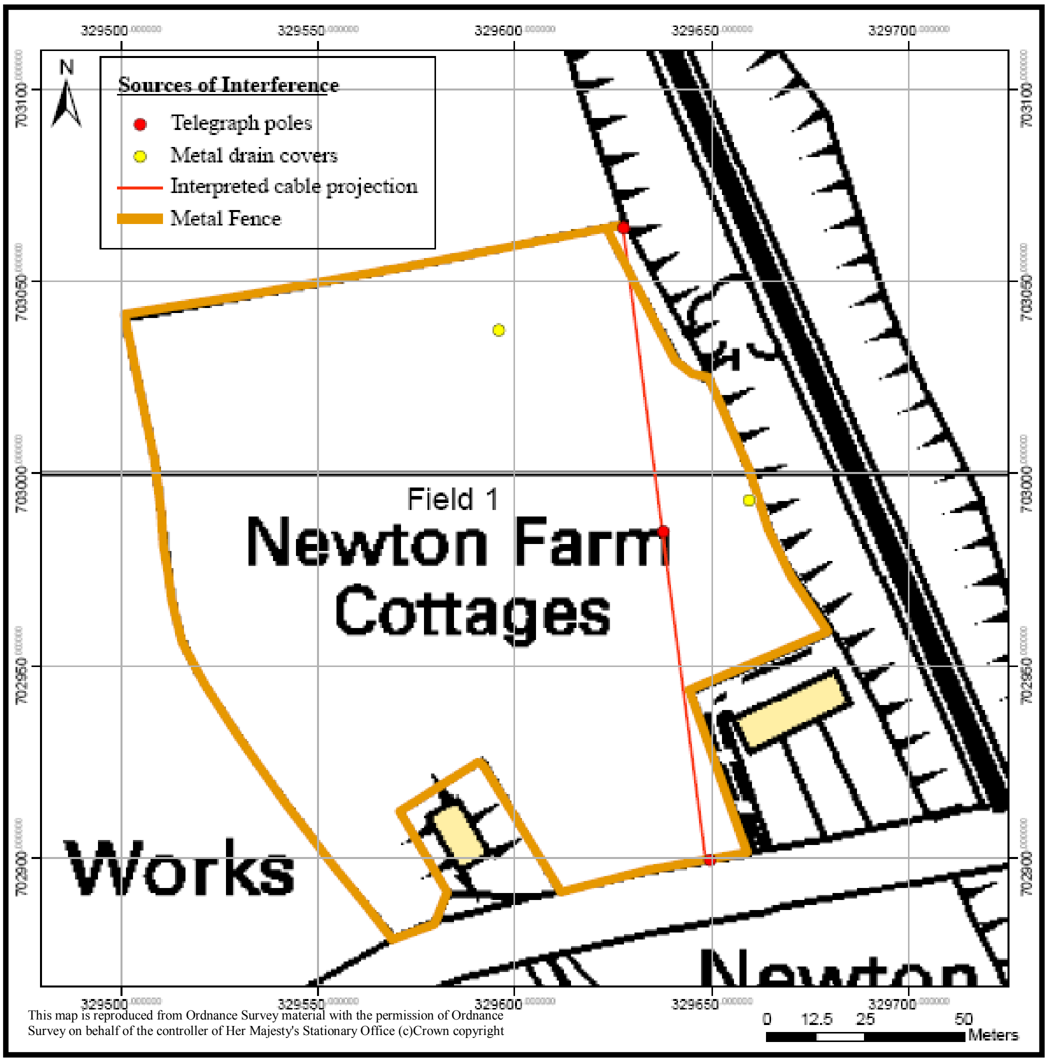

Figure 1.8. Map of Newton farm with possible interference sources displayed.

Figure 1.9. Barbed wire metal fences that surround all three fields.

Figure 1.10. Overhead power cables crossing field 1 trending north-south.

CHAPTER 2: BACKGROUND INFORMATION

2.1 Archaeological Background

There have not been any previous geophysical surveys or archaeological studies performed at Newton Farm, however excavations in the Markinch region have shown that the area has had previous human settlement from as early as the Neolithic. This is represented by the Balfarg/Balbirnie ceremonial complex (Mercer, 1981; Mercer *et al*. 1988; Barclay & Russell-White, 1993). This complex is the only evidence of significant human activity around the Neolithic and Iron Ages in Fife. However, recent small excavations 1 km south of Newton Farm revealed a small number of Iron Age artefacts such as pottery, suggesting the archaeology at Newton Farm could be of a similar age (Manson, *personal communication,* 2009). The series of visible concentric cropmarks caused by the underlying ring ditches are typical of Iron Age fort complexes with further cropmarks interpreted as ceremonial ring ditches and burial barrows (Figure 2.1). Its partially defended nature with little evidence of ring ditches on the west side and the presence of possible ceremonial ring ditches, suggests that the site may have had religious or ritual significance possibly used for religious gatherings. Comparable Iron Age sites can be seen at Mains of Edzell (NGR: 35886 76920) and Brown Caterthun (NGR: 35553 76686) in Angus, both of which show multiple ring ditch enclosures of similar form to those on the Newton Farm site (RCAHMS, 2009).

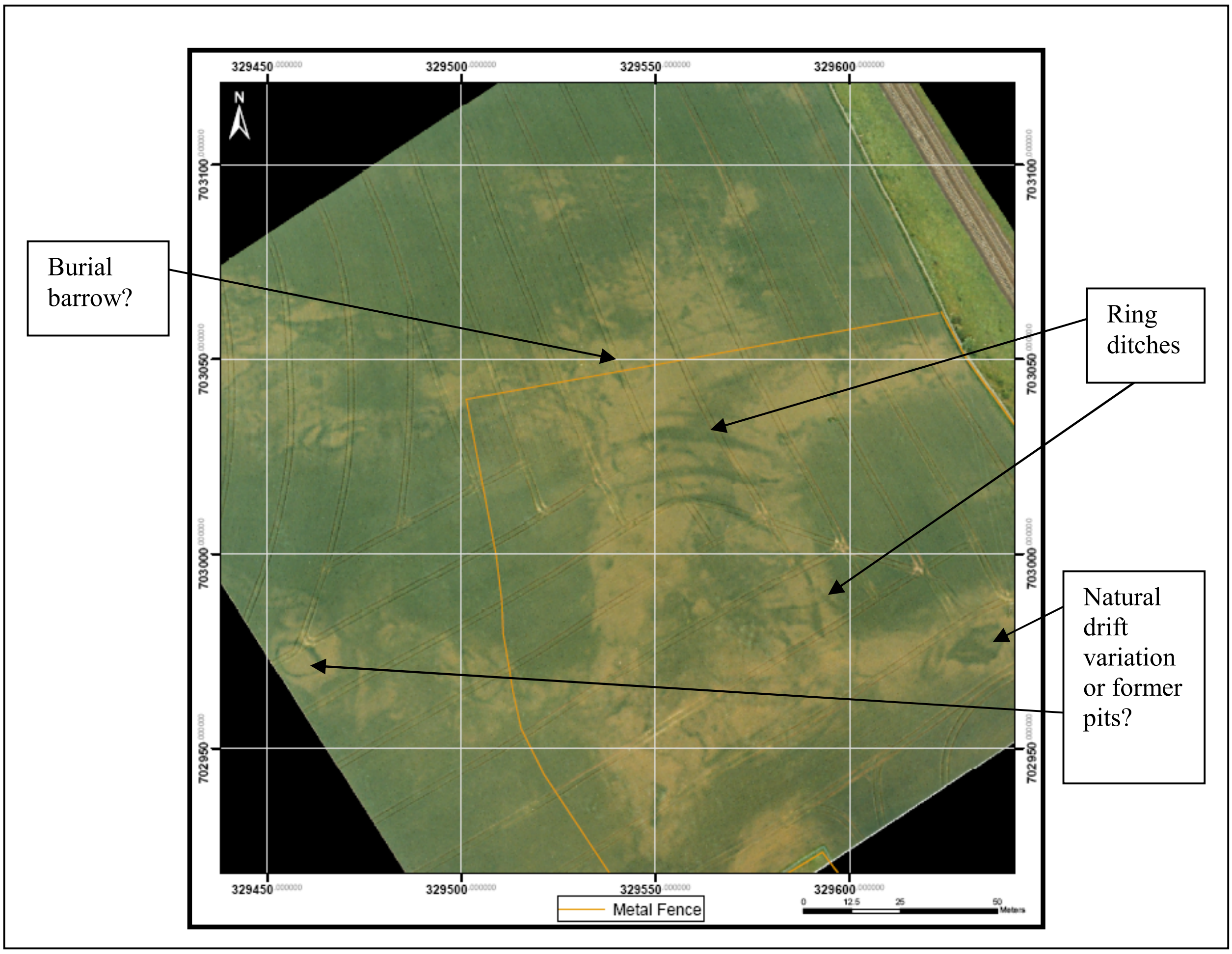

Figure 2.1. Aerial imagery of Newton Farm showing cropmarks with interpretations situated mainly within Field 1 (Aerial imagery supplied by Fife Council).

Cropmarks are only visible under certain conditions. Crops generally grow taller and healthier over subsided features such as ditches whereas solid features such as walls generally cause crops growing above to be lacking in height and density compared to the surrounding crops. These differences in growth are normally caused by variations in soil type and therefore nutrients and water saturation (Renfrew & Bahn, 2001). Ditches generally retain more moisture allowing better vegetation growth, whereas shallow soils over solid features hold less water and may be nutrient poor (Figure 2.2). The aerial photography of Newton Farm only reveals archaeological features caused by an increase in soil moisture attributed to the ring ditches and possible burial barrow.

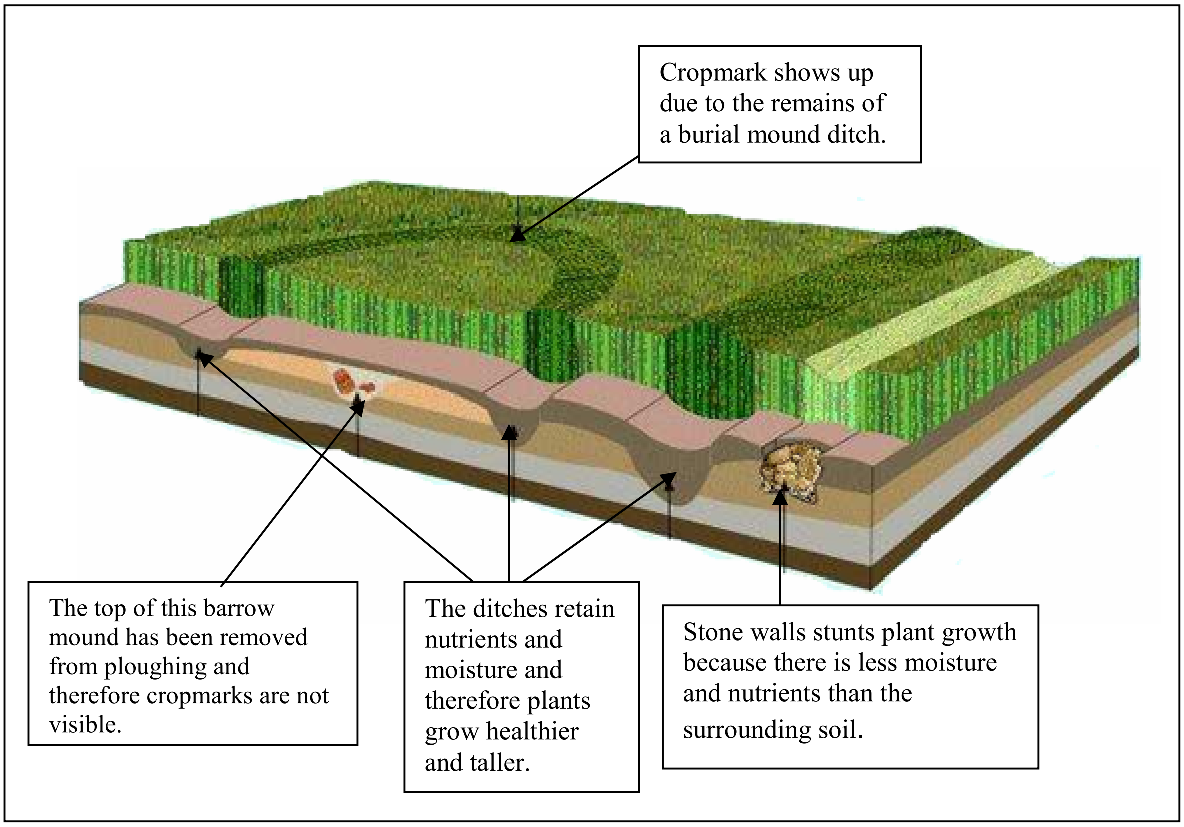

Figure 2.2. The formation of cropmarks (adapted from AARG, 2009).

2.2 Solid Geology

Geophysical response can vary considerably depending on the underlying geology. As drift deposits over the region have considerable depth, it is not possible to view and identify any of the local bedrock beneath Newton Farm or in the vicinity. Research of geological map data suggests that the underlying bedrock is comprised of Carboniferous sedimentary rocks (Figure 2.3). The site sits on the Limestone Coal Formation which consists of mixed sequences of sandstones, mudstones and siltstones with occasional coal horizons, typical in this region of Fife. A geological report carried out near Newton Farm prepared by the BGS suggests that sandstones dominate this part of the Limestone Coal Formation with a general dip to the southwest, consisting of beds commonly 1 to 4 m thick (Dochartaigh, 2002). Mudstone and siltstone beds are generally less than 1 m thick (Dochartaigh, 2002).

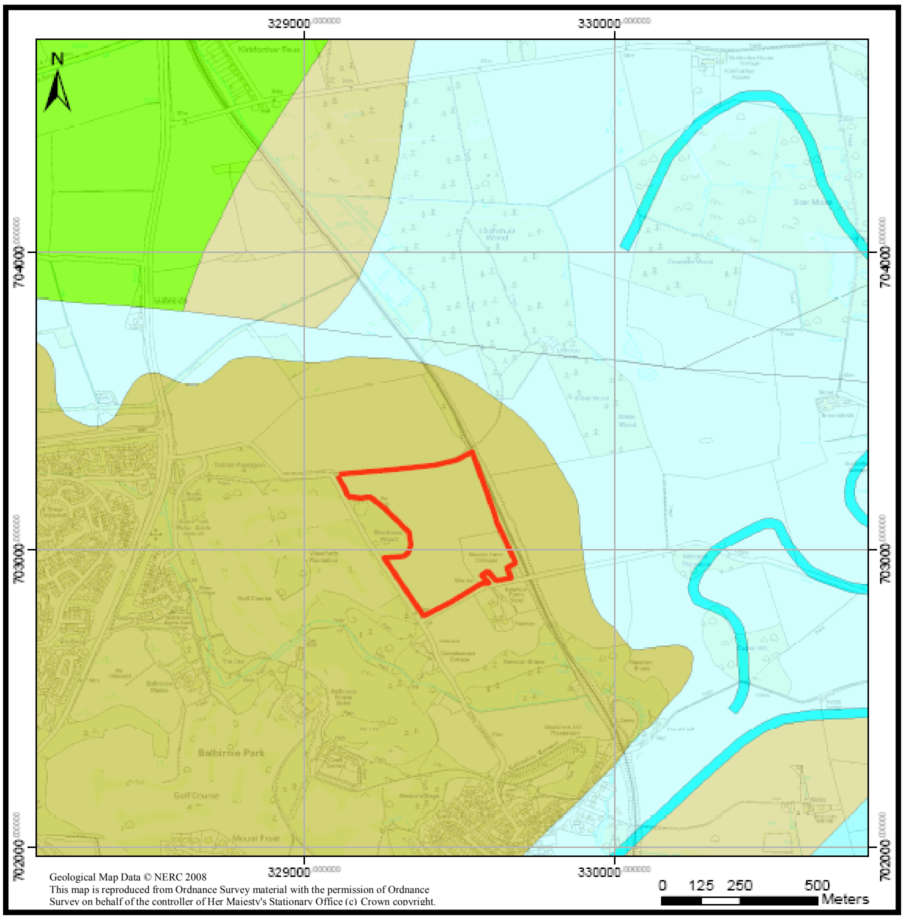

Map Colour	Rock Name	Rock Type
	Limestone Coal Formation	Undivided cyclic sedimentary rocks
	Lower Limestone Formation	Undivided cyclic sedimentary rocks
	Upper Limestone Formation	Undivided cyclic sedimentary rocks
	Dinantian to Westphalian Sills of Lothians and Fife	Dolerite
	Passage Formation	Undivided cyclic sedimentary rocks

Figure 2.3. The solid geology of Newton with site outlined in red (Geology BGS Digimap supplied by Fife Council).

2.3 Drift Geology

Newton Farm sits on up to 1 m of topsoil which has been highly disturbed due to ploughing. The drift geology in the region and below the site consists of glaciofluvial ice-contact deposits with glaciofluvial sheet deposits cutting the extreme northern margin of Field 3 (Figure 2.4). The glaciofluvial deposits consist of varying quantities of gravel, sand and silt. A collection of BGS borehole data within 200 m of Newton Farm was examined and an estimated model of the ground truth below the site of interest was created (Appendices A.1 and A.2). It was estimated from this data that Newton Farm is positioned on glaciofluvial deposits of at least 25 m depth (Appendix A.2). The borehole data reveals the deposits in general are poorly sorted and range from fine-grained sand to gravel with cobbles up to 100 mm in length. The larger clasts have varying compositions, with predominantly sandstone, dolerite, quartzite, coal and occasional granite clasts. This was confirmed during the excavation. All these deposits were likely to have been transported from the northwest and deposited during the last glacial period (Devensian Glaciation).

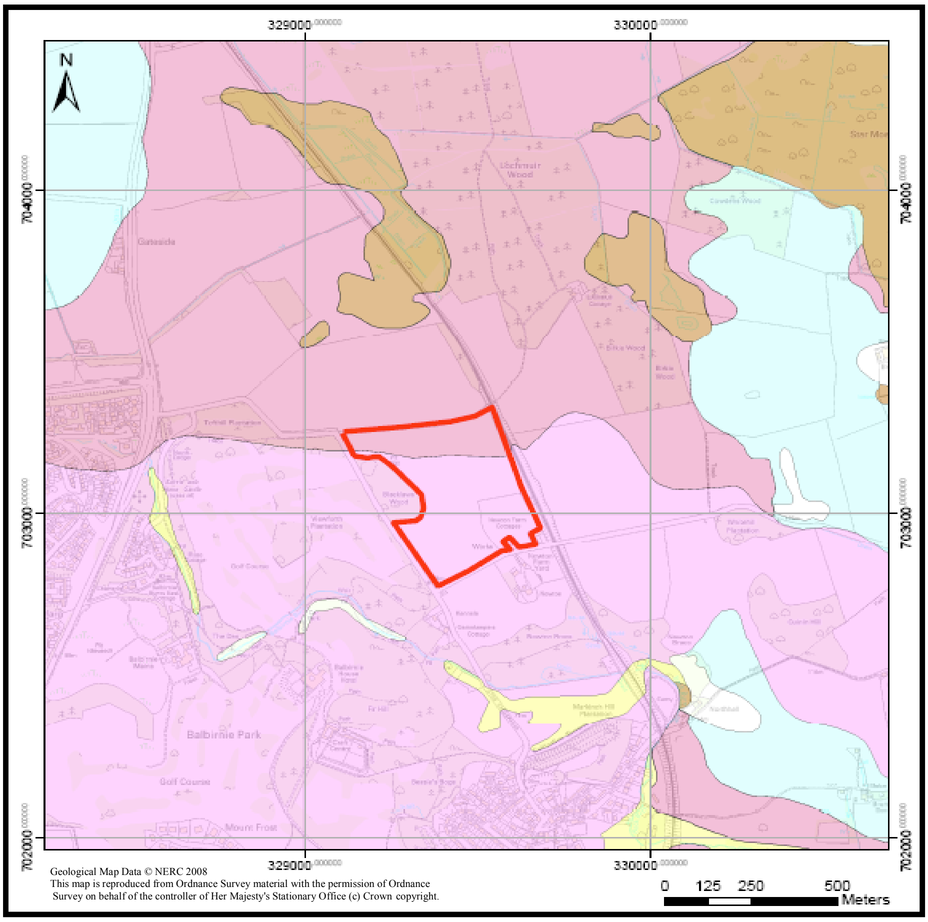

Map Colour	Rock Name	Rock Type
	Peat	Peat
	Alluvium	Sand and gravel
	Glaciofluvial ice-contact deposits	Gravel, sand and silt
	Glaciofluvial sheet deposits	Gravel, sand and silt
	Till	Diamicton

Figure 2.4. The drift geology of Newton with site outlined in red (Geology BGS Digimap supplied by Fife Council).

CHAPTER 3: FIELD SURVEY

3.1 Introduction

Although cropmarks reveal some archaeological features there are in most cases additional buried features that do not create cropmarks. It was hoped that this survey incorporating a range of geophysical techniques would detect additional buried features and help characterise and reveal the nature of the site. These results were also planned to help positioning of the trenches. Finally, it was possible to compare the interpreted geophysical results with the ground truth revealed by excavation.

Geophysics enables understanding of structure and organization within the subsurface of a site over large areas, whereas archaeological excavations can only cover a small area. Geophysics also has the advantage of being able to map subsurface archaeology non-invasively and non-destructively (Gaffney & Gater, 2003). Geophysical techniques have been used successfully to map similar ring ditch complexes in the past (e.g. Lewis, 2003; Mytum & Webster, 2003; Murdie *et al.* 2003; Watters, 2007 and Crane & Poucher, 2009), therefore providing evidence that geophysics could be used be successfully within this investigation.

The following 'key' (Table 3.1) edited by Jones (2008) shows which geophysical methods were most likely to identify specific features likely be present on Newton Farm. It was decided that EM (Electromagnetism), DC (Direct Current) resistivity, magnetometry and magnetic susceptibility could all be of use when surveying Newton Farm (Table 3.1). Equipment availability meant it was not possible to use GPR (Ground Penetrating Radar). Due to the site size and equipment availability it was decided that EM would form a substantial part of the survey with the other methods complementing EM within Field 1. The field survey was carried out from the 01/06/09 -18/06/09.

Table 3.1. Matching survey method to feature type possible on Newton Farm: survey options (from Jones, 2008).

Feature	**Mag area survey**	**Earth Res survey**	**GPR**	**EM (Conductivity)**	**Magnetic Susceptibility**
Areas of occupation	Y	n	N	?	Y
Below artifact scatters	Y	Y	N	?	Y
Large pits (> 2 m diameter)	Y	y	Y	?	N
Smaller pits (<2 m diameter)	Y	?	Y	N	N
Ring gullies (prehistoric)	Y	n	N	?	N
Post-holes (>0.5 m diameter)	Y	N	Y	N	N
Hearths	Y	N	N	n	?
Ditches (>2m width)	Y	Y	N	y	N
Roads/tracks	Y	y	Y	y	N
Robber/bedding trenches	Y	Y	?	?	N
Timber structures	Y	N	?	N	N
Graves	?	Y	?	N	N
Cremations	N	Y	N	N	?

Key:

Y **The technique responds well in most conditions.**
y **The technique can respond well but is best used with other methods.**
? **The technique may work well in some conditions but its use may be questionable; an alternative technique might be preferable.**
n **The technique may work in some conditions but is not usually recommended ; alternative techniques usually preferable.**
N **The technique is probably ineffective or its effectiveness is uncertain.**

3.2 DC Resistivity

Direct Current (DC resistivity) surveys, sometimes referred to as earth resistance surveys, were performed on Field 1. The method used involved carrying out electrical profiling rather than the common twin probe methods used for area surveys in archaeological prospection. This allowed measuring variations in resistivity with depth giving useful input into the geophysical model. Table 3.2 shows the advantages and disadvantages of DC resistivity.

Table 3.2. The advantages and disadvantages of DC resistivity.

Advantages	Disadvantages
Ease of data processing.	Rate of ground coverage is low so survey costs per unit area high.
Good vertical resolution with up to 60 m depth penetration.	Poor lateral resolution.
Multiple array types.	Ground contact needed.
Complements magnetometry.	Effectiveness decreases at low resistivity levels.

Resistivity of the ground is mostly dependent upon the amount and distribution of moisture (Clark, 1996). Resistivity surveys therefore have the ability to identify pits and ditches as they normally retain more moisture than the surrounding soil. Typical resistivity values of ground materials, measured in ohm-metres (Ω/m), can be seen in Figure 3.1. Resistivity is particularly useful because unlike magnetometry it is particularly valuable in areas of high magnetic interference or where ground conditions are not conducive to the development of human related magnetic anomalies (Jones, 2008).

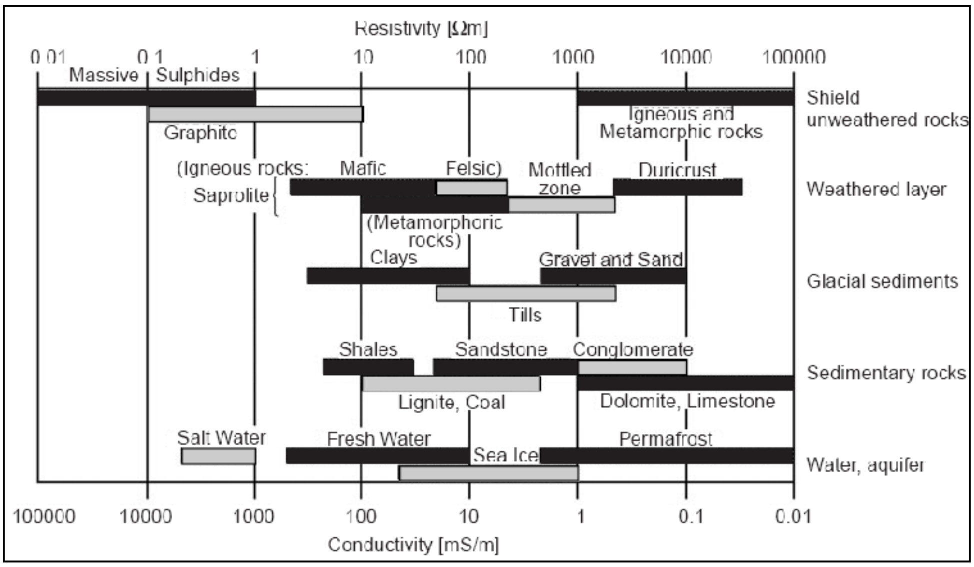

Figure 3.1. The typical resistivity (Ω/m) and conductivity (mS/m) values of ground materials (from Bernstone *et al.* 2000).

The electrodes for resistivity profiling can be set-up in many different configurations, termed 'arrays' (Figure 3.2) with each array having its advantages and disadvantages (Table 3.3). By keeping the voltage and current circuits separate contact resistances between the ground and electrodes do not limit the current flow (Milsom, 2003). The greater the spacing between electrodes the deeper the currents penetrate giving a greater depth of investigation. DC resistivity theory can be viewed in Appendix B.1.1.

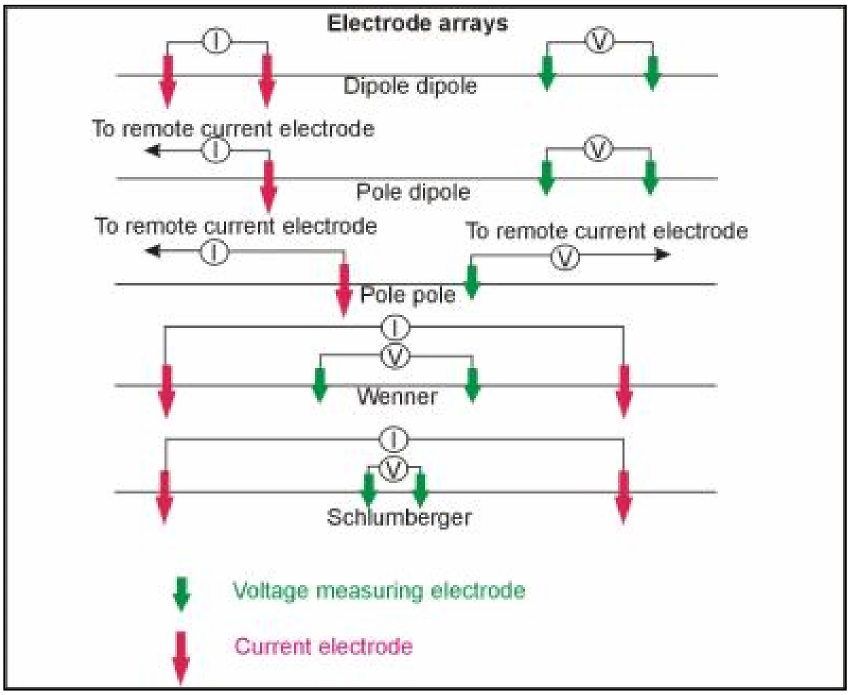

Figure 3.2. Common DC resistivity electrode arrays (Central Federal Lands Highway Division, 2009)

Table 3.3. Suitability of the common DC resisitivity arrays (edited from Reynolds, 1997).

Criteria	Wenner	Schlumberger	Dipole-dipole	Square
Vertical Resolution	Good	Moderate	Poor	Moderate
Depth Penetration	Poor	Moderate	Good	Moderate
Suitability to VES	Moderate	Good	Poor	Unsuitable
Sensitivity to Orientation	Yes	Yes	Moderate	No
Sensitivity to Lateral Inhomogeneties	High	Moderate	Moderate	Low
Labour Intensive	Yes (No*)	Moderate (No*)	Moderate (No*)	Yes
Availability of interpretational aids	Good	Good	Moderate	Poor

*When using a multicore cable and automated electrode array

3.2.1 *Field Procedure*

The ABEM Terrameter 4000 LUND imaging system was used for both resistivity transects. Full specifications can be found in Appendix B.2.1 and ABEM (2010). Due to the time consuming nature of this surveying method two transects cutting across the main features (cropmarks) in Field 1 were used (Figures 3.3a and 3.4). The electrodes were set-up with a spacing of 1 m. The system was then operated using the Wenner (short and long) arrays and performed automatic pre-defined tests which included identifying any faulty electrode connections. While this was in operation a topographic survey was performed using the HiPer Pro Topcon integrated RTK GPS (Figures 3.3b and 3.3c). For full specifications of the HiPer Pro Topcon GPS see Appendix B.3. This survey gave an accurate representation of the topography on which the resistivity results can be plotted. The data was presented using inversion software.

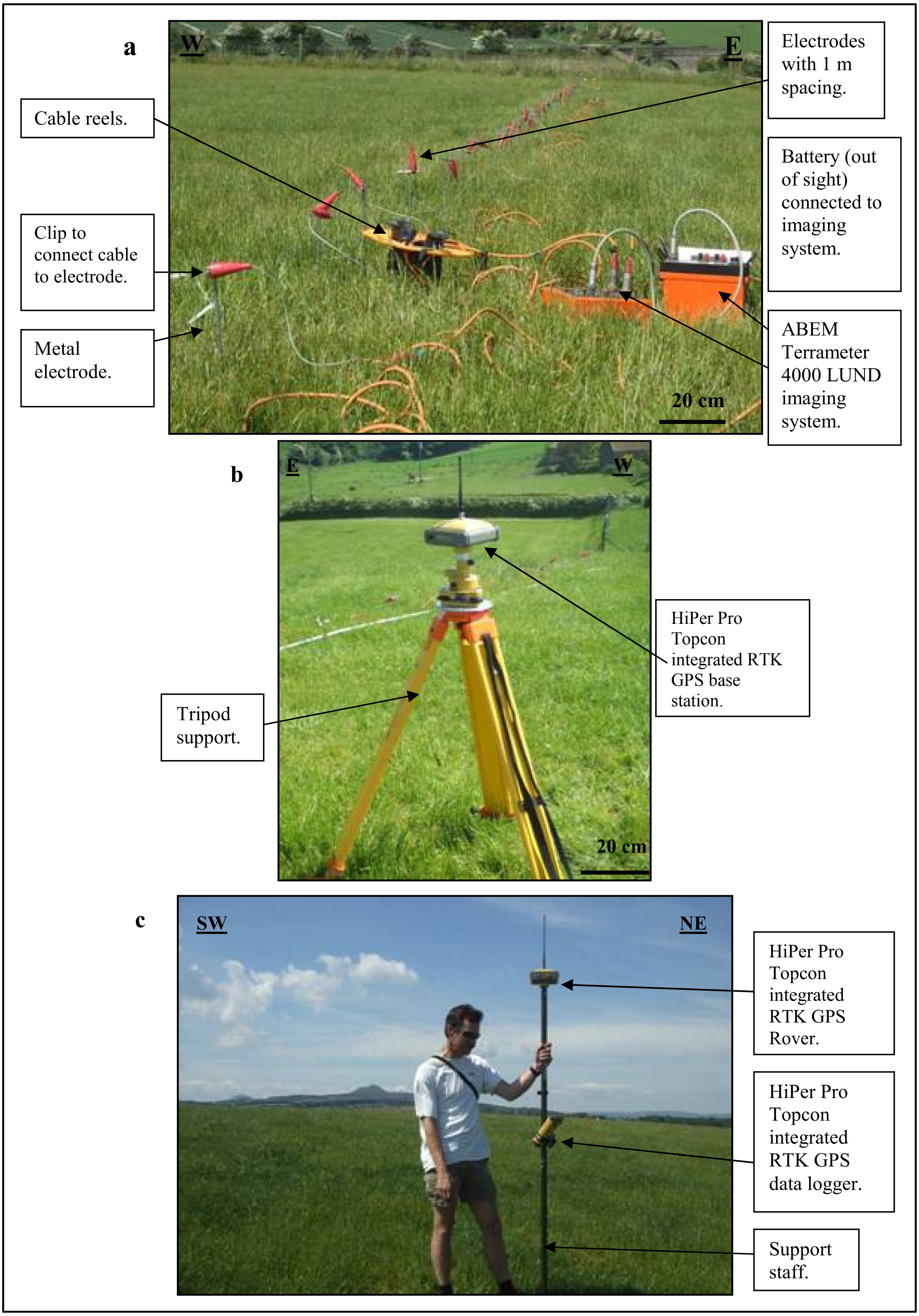

Figure 3.3. The DC Resistivity in operation in the north-south trending transect on Field 1 (**a**). The HiPer Pro Topcon integrated RTK GPS base station used for the topographic and EM surveying of the trenches (**b**). The HiPer Pro Topcon integrated RTK GPS rover in operation used for the topographic survey (person for scale) (**c**).

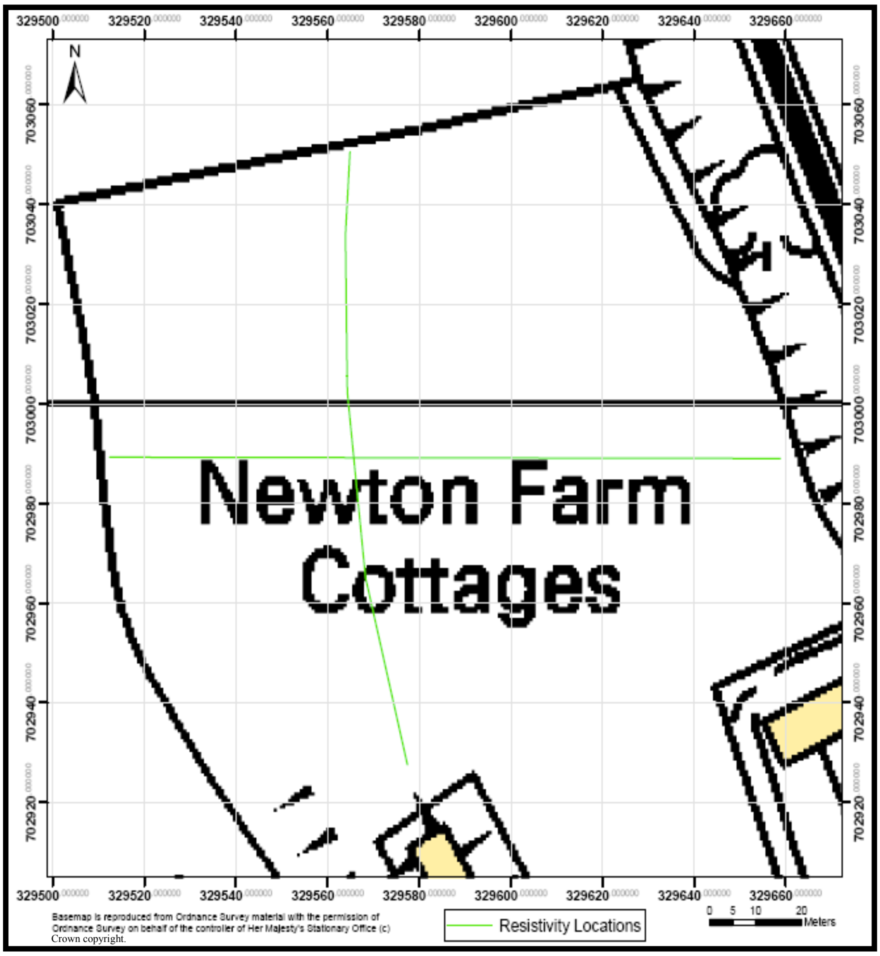

Figure 3.4. Location of the two DC Resistivity transects recorded using the HiPer Pro Topcon integrated RTK GPS.

3.3 Electromagnetism (EM)

Electromagnetism formed a substantial part of this survey. The equipment used for the surveying was FDEM (Frequency Domain Electromagnetism). Table 3.4 shows the advantages and disadvantages of FDEM.

Table 3.4. The advantages and disadvantages of FDEM.

Advantages	**Disadvantages**
High survey productivity with precise measurement of small changes in conductivity.	Measurement of very small secondary field in the presence of primary field.
Direct measure of ground conductivity giving a continuous readout.	Very sensitive to cultural electrical noise.
High lateral resolution.	Limited vertical resolution.
No ground contact needed.	Limited depth of penetration.

EM systems are sensitive to the conductivity (the inverse of resistivity) of the ground. Typical conductivity values of ground materials can be seen in Figure 3.1 measured in milliSiemens per metre (mS/m). Depending on the various parameters most FDEM systems can be used to locate similar features to those detected with DC resistivity. FDEM surveys can represent one of the most useful geophysical techniques in archaeological studies because variations in conductivity are normally related to differences between archaeologically significant lithological sequences and disturbed soils (Bates *et al.* 2007). These surveys are becoming particularly favourable for sites that require large area coverage due to high survey productivity and are commonly used on land where connection with the ground surface is variable or where contact resistance is high e.g. sand (Gaffney & Gater, 2003), making it an appropriate survey option for Newton Farm. EM is useful for this survey as it can detect remnants of mounds, in-filled fortifications, buried stone structures, pits, ditches and metallic artifacts (Gaffney & Gater, 2003). It must be noted that large inter-site variability of the EM response is common, with geology and soils being the main influence of this variability (Jones, 2008). For theory on FDEM view Appendix B.1.2.

3.3.1 *Field Procedure*

The Geonics EM31 and the Geonics EM38 were used for surveying the site. Both systems measure ground conductivity but the EM38 can also measure the magnetic susceptibility of the soil. The EM31 has better depth penetration than the EM38 due to its larger inter-coil spacing. Care was taken to follow the same set procedure at the beginning of each day and checks were made during surveys at the specified calibration points, one in each field (NGR: 329632 702901, 329342 702843 and 329523 703060), to ensure accurate and consistent data collection. The line separation with both the EM31 and EM38 during each survey was also kept consistent. Due to sensitivity of the equipment, all metallic items (e.g. watches, mobile phones, etc) were removed. Field conditions such as previous rainfall and ground conditions were also noted to ensure consistency with the data collection. The recorded data was uploaded to *Geomar 'Trackmaker'* software on computer which converted the data to 'xyz' format readable in *Microsoft Excel*. The data was then presented using *Golden Software, Inc. 'Surfer V. 7.02*' for analysis and the final presentation was displayed using *ArcView GIS* (Chapter 4).

3.3.1.1 *EM31 Survey*

The EM31 has a coil separation of 3.66 m and an operating frequency of 9.8 kHz. In vertical dipole mode, the mode used for this survey, the effective depth of exploration is around 6 m (Geonics Limited, 2005 and Appendix B.2.2). The EM31 was attached to an Allegro CX data logger connected to a Garmin Differential Geographical Positioning System (DGPS) (Figures 3.5a and 3.5b). Using the DGPS with the data logger gives the ability to track and record conductivity values simultaneously whilst traversing the site. Data was recorded and stored using the *Geomar 'Trackmaker 31'* software. The set-up procedure for the EM31 followed Young's (1998) guidelines and can be viewed in Appendix B.2.2.

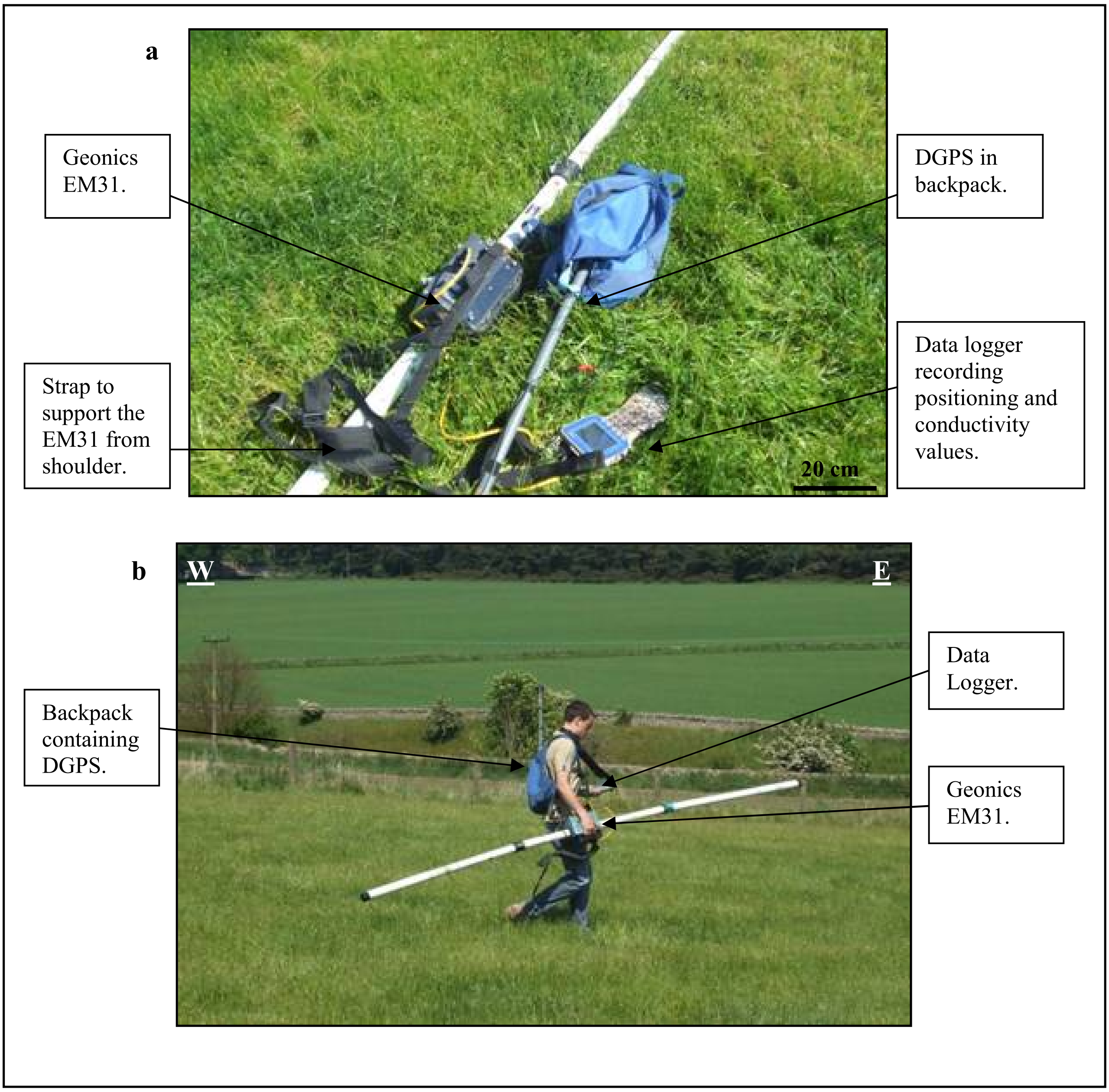

Figure 3.5. The Geonics EM31 equipment (**a**) and the Geonics EM31 during surveying on Field 1 (person for scale) (**b**).

In all three fields the EM31 transects were carried out with a line separation of around 3 m using a zigzag traverse. Although Field 1 is of primary importance it was useful to extend the survey to Field 2 and Field 3 to achieve an overall characterisation of the site to detect any changes in general ground conditions and boundaries of any archaeological features. The traverses performed with the EM31 can be seen in Figures 3.6, 3.7 and 3.8.

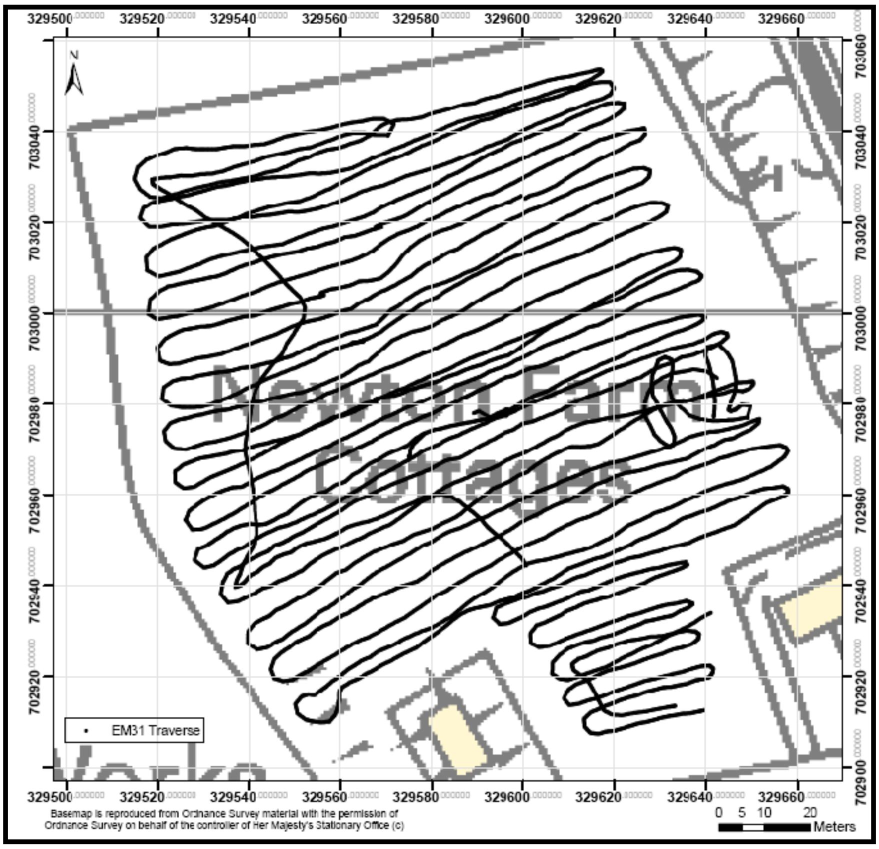

Figure 3.6. The SW-NE traverse performed on Field 1 with the Geonics EM31.

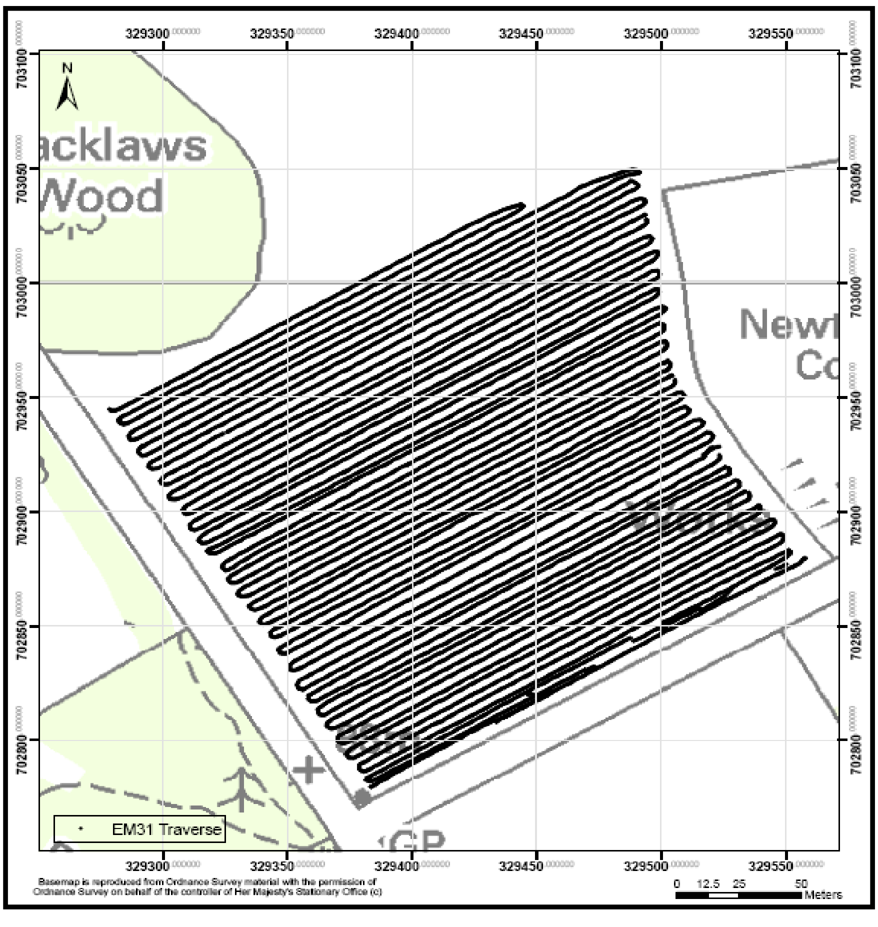

Figure 3.7. The SW-NE traverse performed on Field 2 with the Geonics EM31.

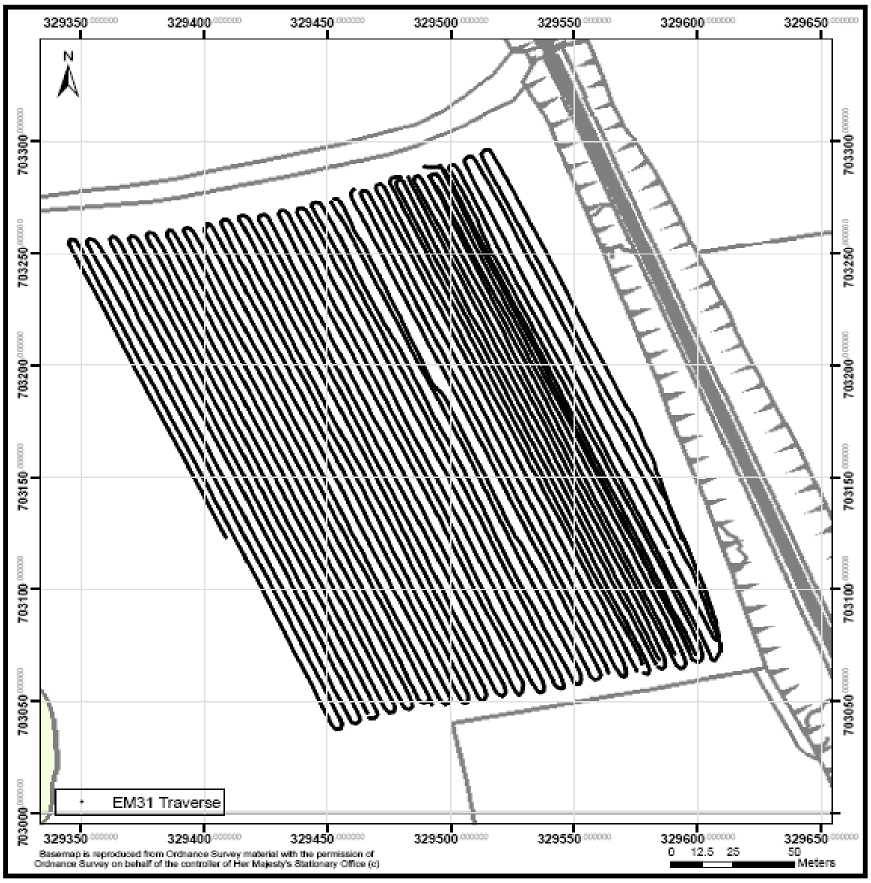

Figure 3.8. The NW-SE traverse performed on Field 3 with the Geonics EM31.

3.3.1.2 *EM38 Survey*

The Geonics EM38 has a coil separation of 1 m and an operating frequency of 14.6 kHz (Geonics Limited, 2005). The EM38 can provide both measurement of ground conductivity (quad-phase) and magnetic susceptibility (in-phase). These measurements can be performed within two depth ranges, 1.5 m in the vertical dipole mode and 0.75 m in the horizontal dipole mode (Figure 3.9) (Geonics Limited, 2009). Full specifications of the Geonics EM38 can be seen in Appendix B.2.3. The additional equipment used was the same as that for the Geonics EM31 (Figure 3.11). Data was recorded and stored using *Geomar 'Trackmaker 38'* software. The set-up procedure followed can be viewed in Appendix B.2.3.

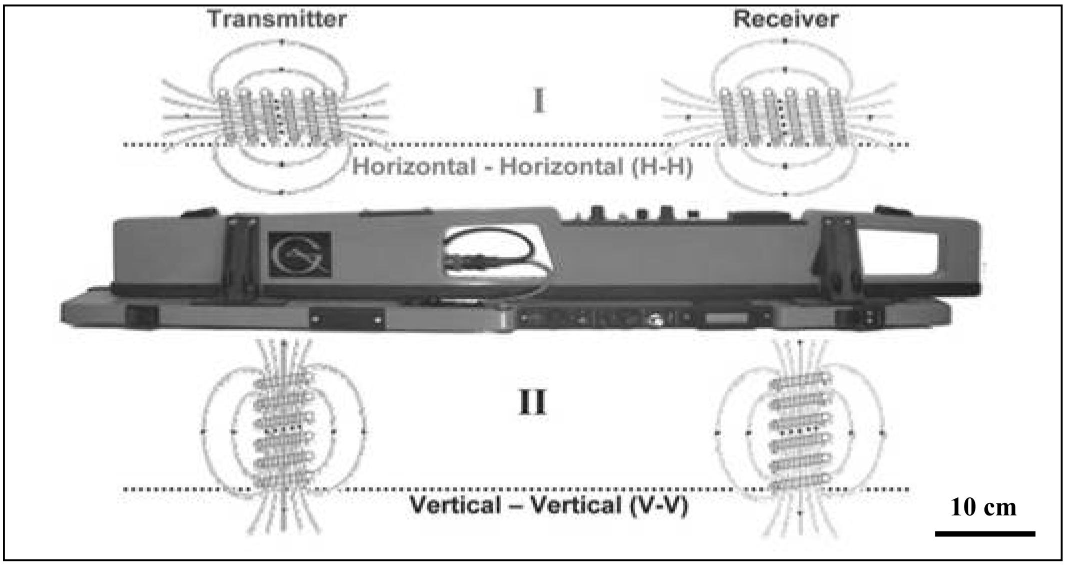

Figure 3.9. Transmitter and receiver dipole orientations (horizontal and vertical) of the EM38 (instruments are oriented parallel to the surface). The loops of wire form a solenoid and a dipole is created when current passes through the wire (Abdu *et al.* 2007).

3.3.1.2.1 *EM38 - Vertical Dipole Mode - Quad-phase (Conductivity)*

Surveying ground conductivity to a depth of about 1.5 m (vertical mode) was performed on all three fields and transects were carried out with a line separation of about 1 m using the zigzag traverse (Figure 3.10). The traverses performed with the EM38 in vertical dipole mode can be seen in Figures 3.11 - 3.13. A small percentage of data is missing from Field 3 (Figure 3.13) due to equipment malfunction.

Figure 3.10 The Geonics EM38 in vertical dipole mode on Field 1 (person for scale).

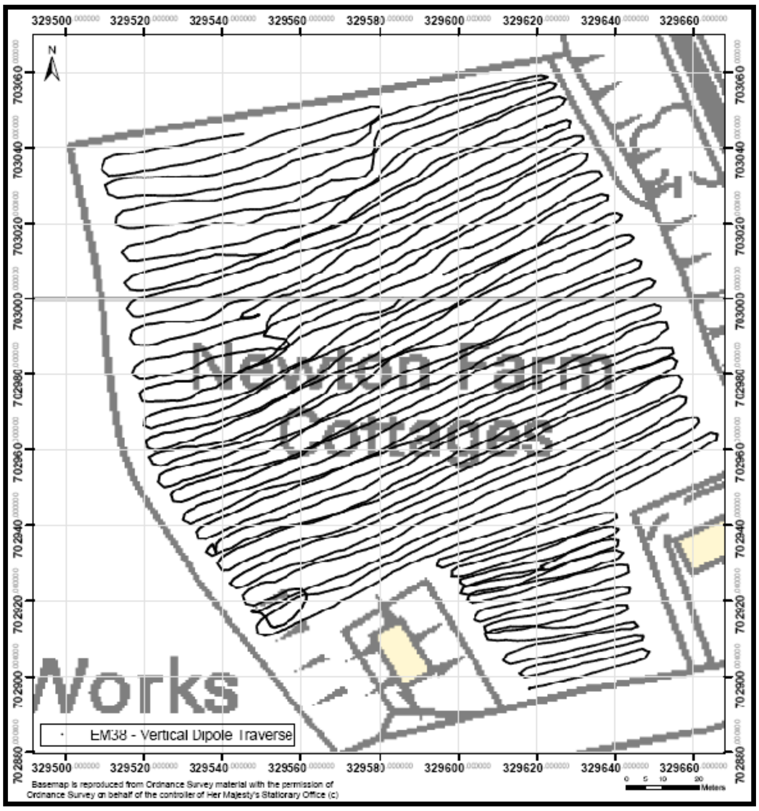

Figure 3.11. The SW-NE traverse performed on Field 1 with the Geonics EM38 in vertical dipole mode quad-phase.

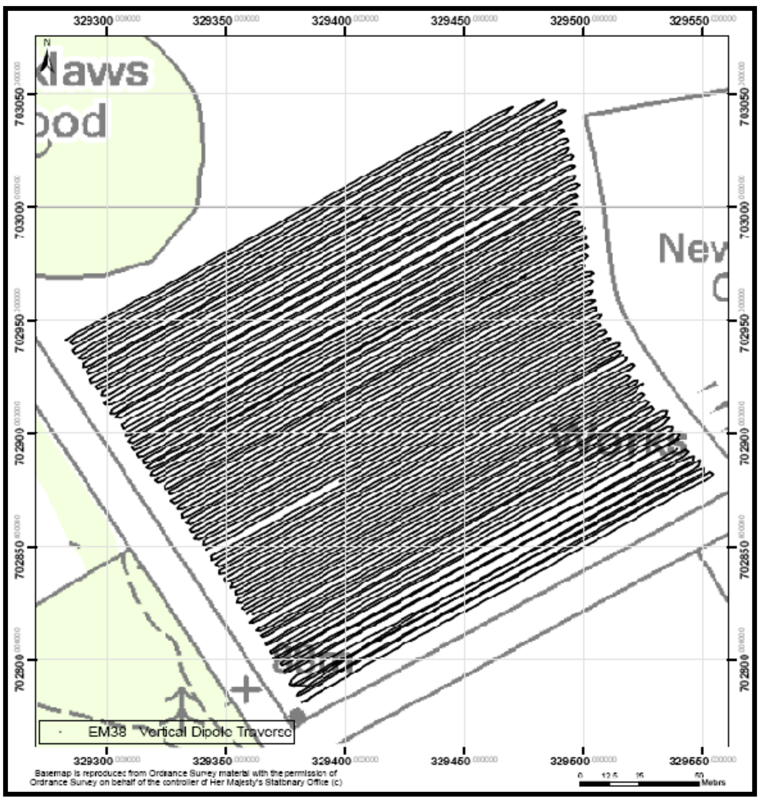

Figure 3.12. The SW-NE traverse performed on Field 2 with the Geonics EM38 in vertical dipole mode quad-phase.

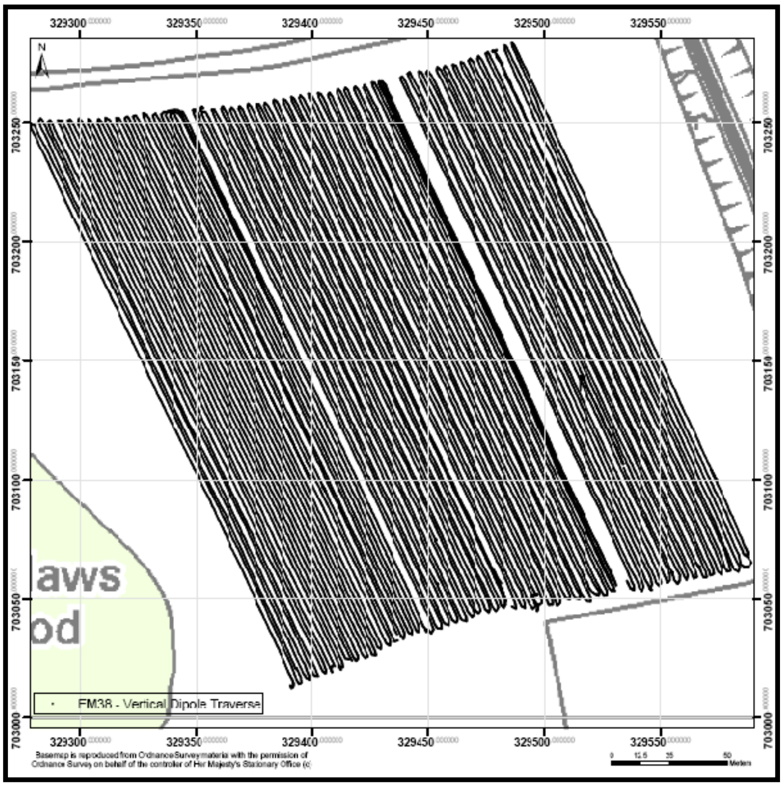

Figure 3.13. The SE-NW traverse performed on Field 3 with the Geonics EM38 in vertical dipole mode quad-phase. An average of the surrounding values will be taken where data is missing.

After removal of the topsoil during excavation (~40-50 cm depth) the trenches were surveyed to gain a clearer understanding of the subsurface features and consider the effect the topsoil may have had in the data collected. Line spacing was kept to about 30 cm to allow for a more in depth evaluation. To ensure the GPS readings were as accurate as possible the EM38 was connected to the HiPer Pro Topcon integrated RTK GPS (Figure 3.14) allowing up to 2 cm horizontal and 4 cm vertical accuracy in location measurements (Topcon Positioning, 2010).

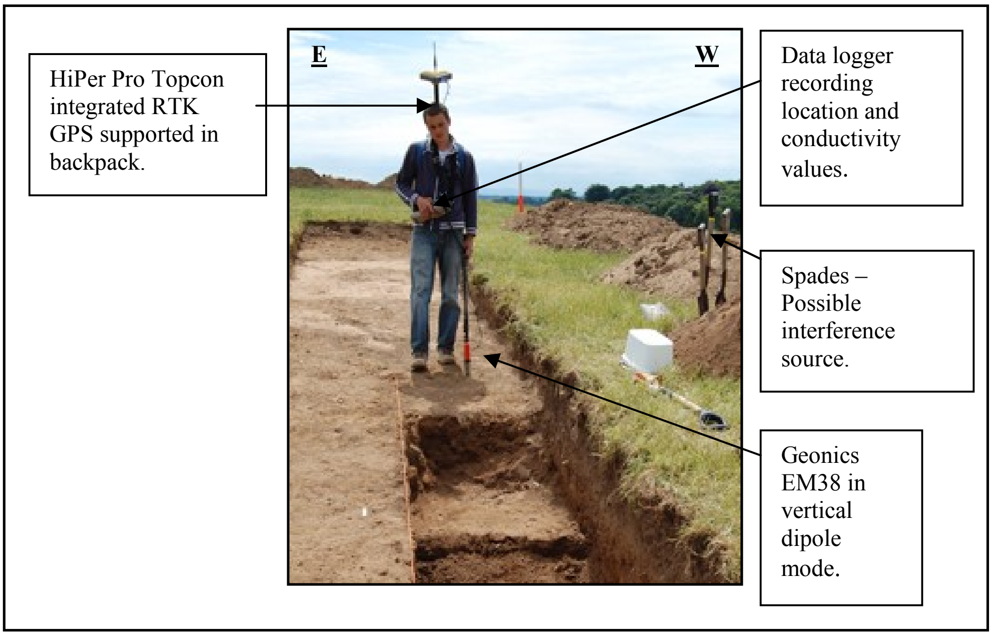

Figure 3.14. Surveying with the Geonics EM38 attached to the HiPer Pro Topcon with the topsoil removed (person for scale).

3.3.1.2.2 *EM38 - Horizontal Dipole Mode - Quad-phase (Conductivity)*

Surveying of ground conductivity to a depth of about 0.75 m (horizontal mode) was performed on Field 1 for detection of any shallow archaeological features. Surveying was performed in a NE-SW direction with line spacing of about 1 m (Figure 3.15).

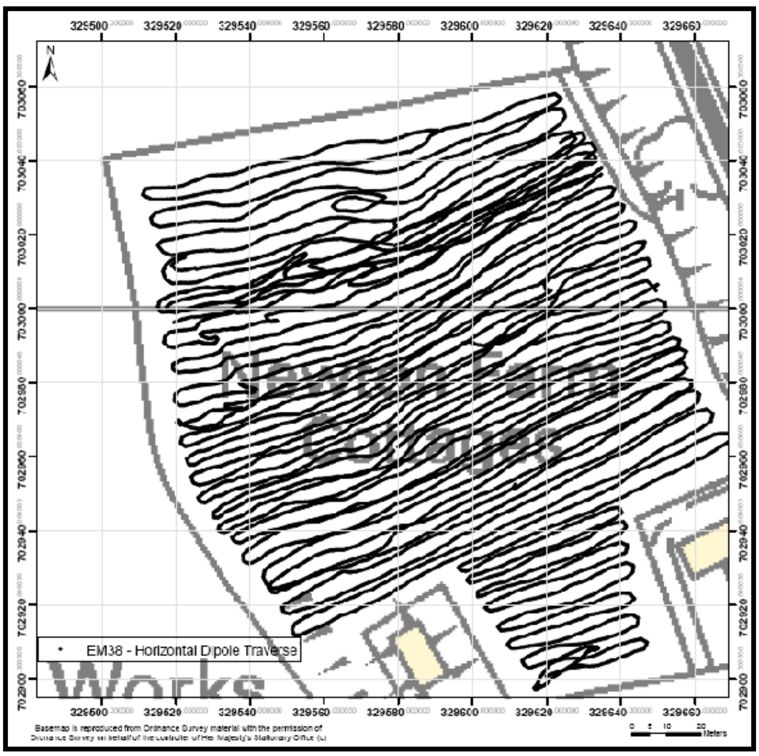

Figure 3.15. The NE-SW traverse performed on Field 1 with the Geonics EM38 in horizontal dipole mode quad-phase.

3.3.1.2.3 *EM38 – Vertical Dipole Mode – In-phase (Magnetic Susceptibility)*

As an extension to the EM38 survey, a further survey measuring magnetic susceptibility (in-phase) of the upper half metre of the soil was performed on Field 1 using the EM38 in vertical dipole mode (in-phase). This was used to locate areas of previous human activity (Section 3.5). Surveying was performed in a NE-SW direction with a line spacing of about 1 m (Figure 3.16).

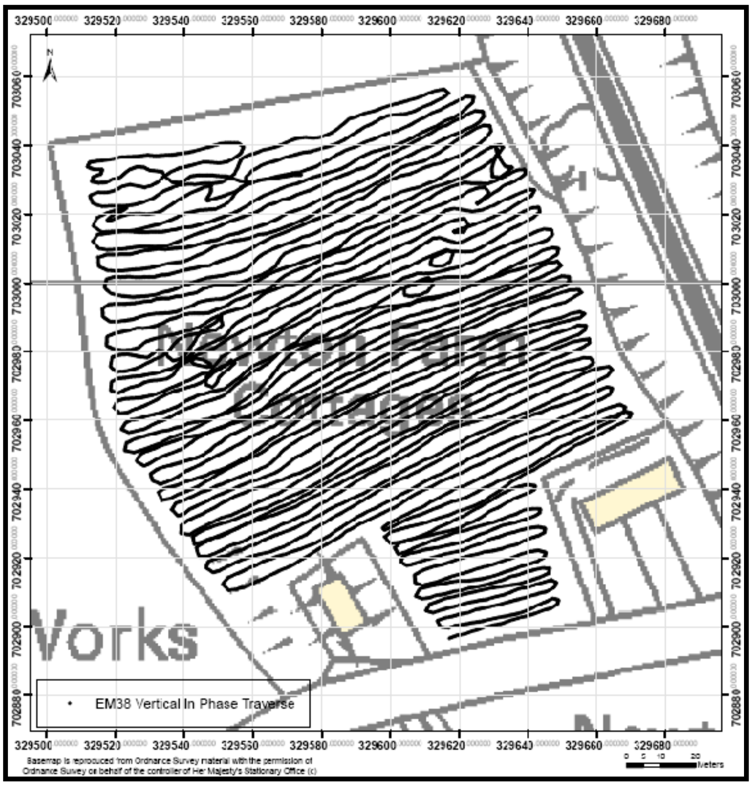

Figure 3.16. The NE-SW traverse performed on Field 1 with the Geonics EM38 in vertical dipole mode in-phase.

3. 4 Magnetometry (Gradiometry)

Magnetometer surveys have the advantage of being able to offer fast ground coverage and respond well to sites that have experienced previous human activity. In theory, magnetometer surveys detect variations in magnetic susceptibility associated with differences in rock and mineral type (Clark, 1996). This means that the underlying geology has a significant influence on the data collected. There is often a large degree of local variation and magnetic response within drift deposits which is usually dependent on the magnetic mineralogy of the parent soil geology (Jones, 2008). This was therefore taken into consideration when interpreting results. Survey effectiveness depends upon the absolute magnetic susceptibility of the soil and how it differentiates with the soil underneath (Clark, 1996). The basis for magnetometer surveys is to detect weakly magnetised iron oxides in the soil. Ditches, pits and kilns can have high concentrations of these oxides and act like a magnet, producing anomalies in the Earth's magnetic field (Gaffney & Gater, 2003). Magnetometry is commonly measured in nanoteslas (nT) and the depth of penetration is dependent on the magnetic strength of the material being measured, e.g. highly ferrous materials can be detected much deeper than weakly ferrous materials. Theory for the proton precession magnetometer can viewed in Appendix B.1.3.

3.4.1 *Field Procedure*

A GEM GSM-19T proton precession magnetometer was used for the survey (Figure 3.17). This magnetometer has a sensitivity for magnetic fields and magnetic gradients of 0.01 nT and an accuracy of ± 1 nT over the full operating range (Giscogeo, 2006 and Appendix B.2.4). The distance between the two sensors was set at 56 cm and the bottom sensor was set constant at a distance of 112 cm from the ground (Figure 3.17). The equipment was set up to measure magnetic gradient (gradiometry) to provide better resolution of small, near-surface objects.

Figure 3.17. The GEM GSM-19T Proton Precession Magnetometer measuring magnetic gradient in operation on Field 1 (person for scale).

Due to the sensitivity of the equipment all magnetic objects were removed from clothing. It was decided that 4 grids of 50 m x 50 m was the most appropriate strategy for surveying, thus covering the areas of primary importance in Field 1. All recordings were taken walking in one direction (south to north) to avoid any form of striping to the results (spatial aliasing). Station spacing and line interval spacing was measured using a tape measure to 2 m. The magnetometer was held vertically with the sensors facing north at all times during the survey to ensure consistent data collection. The starting/station point (0, 0) at NGR: 329540 702932 was recorded with a handheld ‘Garmin GPS Map 60Cx’. Tape measures were then set up from this point to form a 50 m x 50 m grid with recordings taken every 2 m in a south to north direction (Figures 3.18 and 3.19). Surveying was performed on a parallel traverse so that once 50 m had been covered in the south to north direction, the line 2 m to the east was then covered in a south to north direction. The tape measure readings were used to perform the individual magnetometer sampling intervals to make any error in the original GPS reading relative.

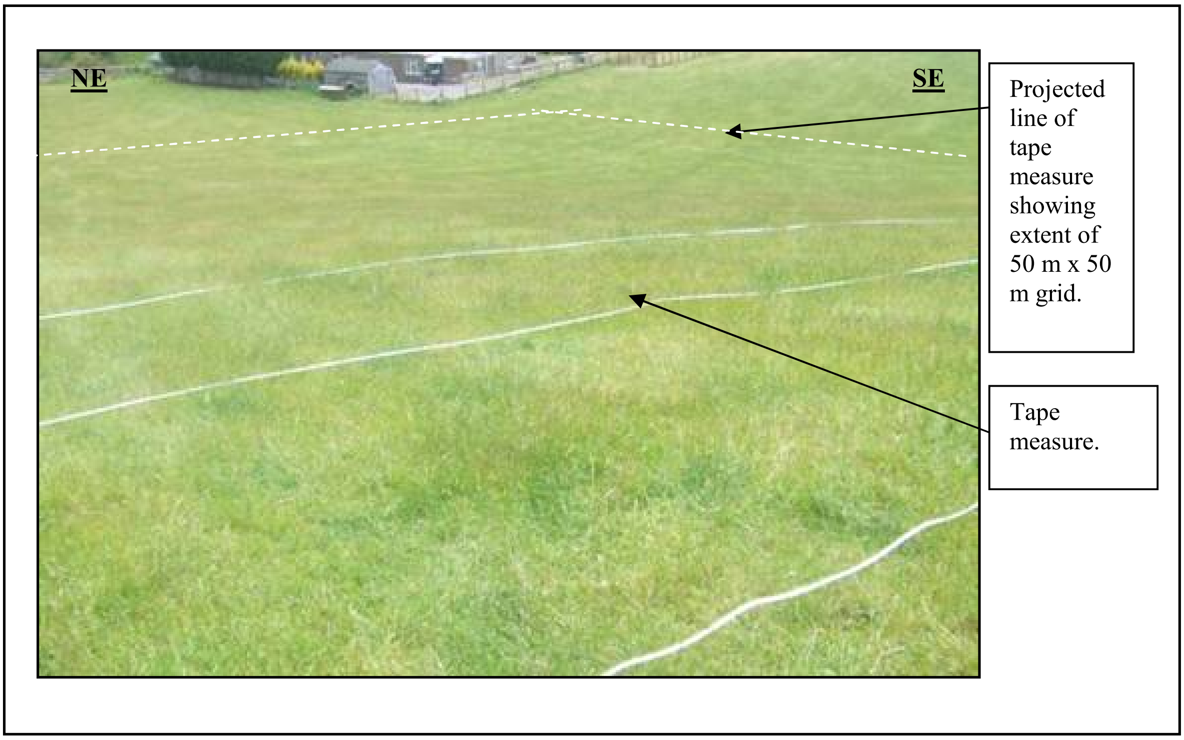

Figure 3.18. Grid 2, the southeastern 50 m x 50 m grid used for the magnetometer survey with 2 m spacing between each tape measure.

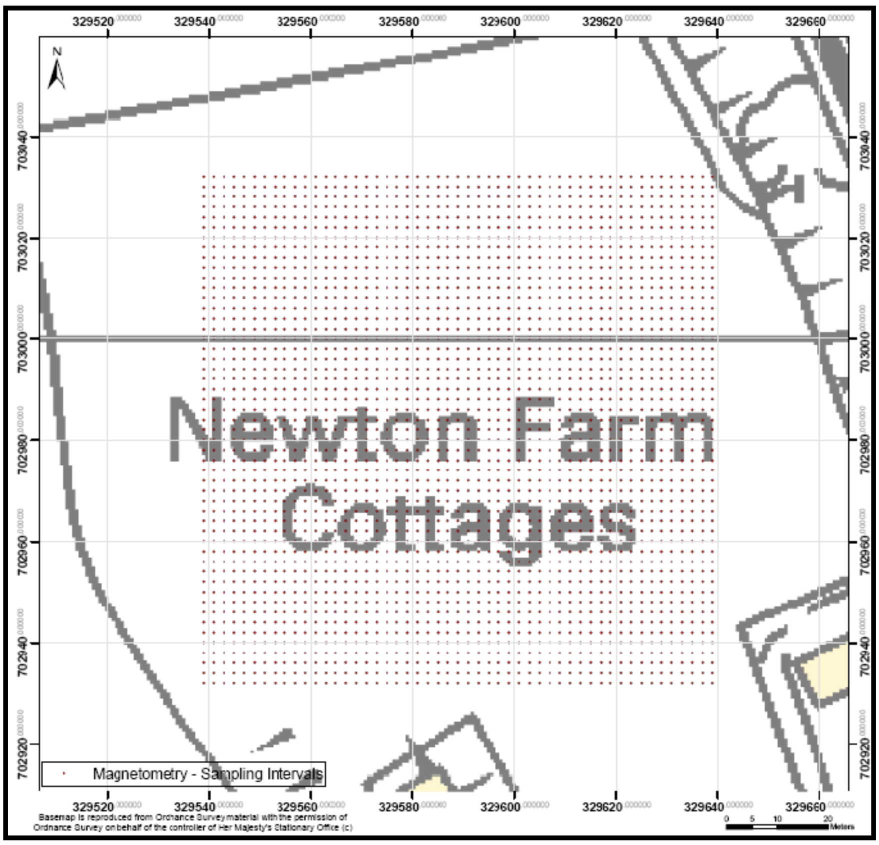

Figure 3.19. The magnetometer sampling intervals on Field 1.

3.5 Topsoil Magnetic Susceptibility

The property of topsoil magnetic susceptibility enhancement was first discovered through work by Le Borgne (1955, 1960). Long-lived and large settlements tend to produce significant anomalous areas within magnetic susceptibility (χ). Archaeology therefore can often result in localised concentrations of soils with enhanced magnetic susceptibility, mainly due to the alteration of ferrous minerals. The enhanced levels of magnetic susceptibility are normally a result of disturbance of the overlying features or strata by ploughing, animals (e.g. burrowing) and other natural techniques (Gaffney & Gater, 2003). Despite using this method for detecting previous human occupation as well as defining limits in the topsoil, it doesn't need significant archaeological remnants to be successful (Clark, 1996). Theory on magnetic susceptibility enhancement in soils can be viewed in Appendix B.1.4.

3.5.1 *Field Procedure*

A total of 43 samples were taken over Field 1. The grid reference was taken at the starting point (NGR: 329551, 702906) with a handheld 'Garmin GPS Map 60Cx' and then using tape measures, samples were taken with a station spacing and line spacing of around 20 m (Figure 3.20). As the HiPer Pro Topcon integrated RTK GPS was not responding at the time of surveying, the 'Garmin GPS Map 60Cx' was used to note the grid references at every sample point for clarification of location. Samples were collected using a soil auger retrieving soil consistently to a depth of 45 cm.

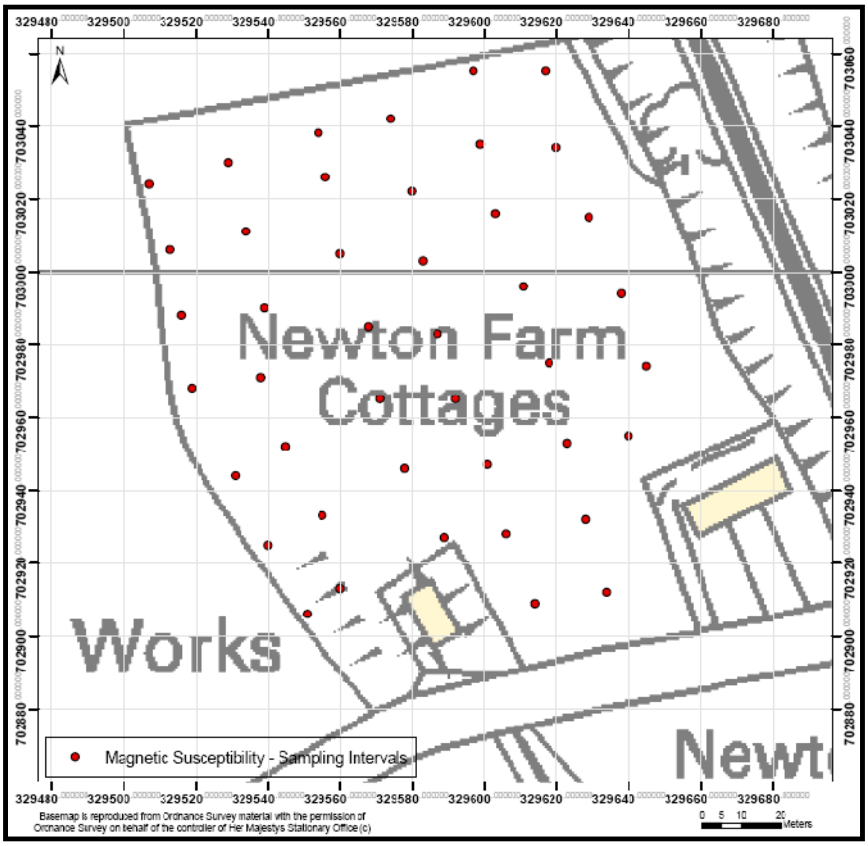

Figure 3.20. Soil sampling locations for magnetic susceptibility.

3.5.2. *Analytical (Lab) Procedure*

All 43 soil samples were dried slowly in an oven at a constant temperature of 37 ^{o}C. When dry the samples were lightly crushed and 8-10 g of each sample was then placed and secured in a sample pot. Using the Bartington MS2 magnetic susceptibility meter, three types of magnetic susceptibility were measured: the volume susceptibility (k, dimensionless in SI units), mass specific susceptibility (X_{lf} and X_{hf}, $10^{-8}m^3kg^{-1}$) and frequency dependent susceptibility (X_{fd}, %). The Bartington MS2 magnetic susceptibility meter is a dual-frequency sensor that measures single samples whilst a magnetic field is applied (Bartington, 2009). For each sample two readings (one repeat) were taken to ensure accuracy, for first the low frequency (LF) and then the high frequency units (HF). Low frequency susceptibility provides information relating to the total concentration of ferromagnetic minerals, the main interest for this survey.

High frequency susceptibility is a function of the antiferromagnetic and paramagnetic mineral (e.g. haematite and pyrite respectively) components of the soil (Walden *et al.* 1999). Measurements displayed on the meter were volume susceptibility readings converted by dividing the average of the two readings by the weight of the sample to calculate the mass specific susceptibility (X_{lf} and X_{hf}). Full specifications of the Bartington magnetic susceptibility system can be viewed in Appendix B.2.5.

3.6 Survey Modelling

The objective of this study was to use a range of different geophysical techniques to help try and understand the size and nature of the archaeological settlement present on Newton Farm in more detail. The concentric shaped cropmarks mark the likely locations of ring ditches. The crops forming the concentric ring patterns appear greener and healthier than the surrounding crops suggesting that they are growing in soil that retains more moisture and/or nutrients. The investigation was initiated on the basis that the soil within these ring ditches is likely to be finer-grained, have higher clay content and show compositionally different mineralogy to the surrounding soils, therefore causing differing geophysical signatures.

Using typical resistivity values of ground materials (Table 3.5) it was possible to create geological and geophysical models to aid with the survey and geophysical interpretation (Figure 5.21). As ground conditions were dry it was assumed the ditches would be predominantly filled with dry silts rather than saturated silts which would have shown a much higher conductivity.

Table 3.5. Typical resistivity and converted conductivity values of the materials likely on or surrounding Newton Farm (adapted from Reynolds, 1997)

Material	Nominal Resisitivity Values (Ω/m).	Converted Conductivity Values (mS/m)
Clays	$1\text{-}10^2$	10-1000
Alluvium and sand	$10\text{-}8 \times 10^2$	1-1.25
Soil (40% clay)	8	125
Soil (20% clay)	33	30.3
Top soil	250-1700	0.6-4.0
Clay (very dry)	50-150	6.6-20.0
Gravel (dry)	1400	0.7
Gravel (saturated)	100	10.0
Quaternary/ Recent sands	50-100	10-20
Dry sandy soil	80-1050	0.1-12.5
Wet sands	20-150	6.6-50
Sand clay/clayey sand	30-215	4.7-33.3
Sand and gravel	30-225	4.4-33.3
Sand clay/clayey sand	30-215	4.7-33.3
Sand and gravel	30-225	4.4-33.3

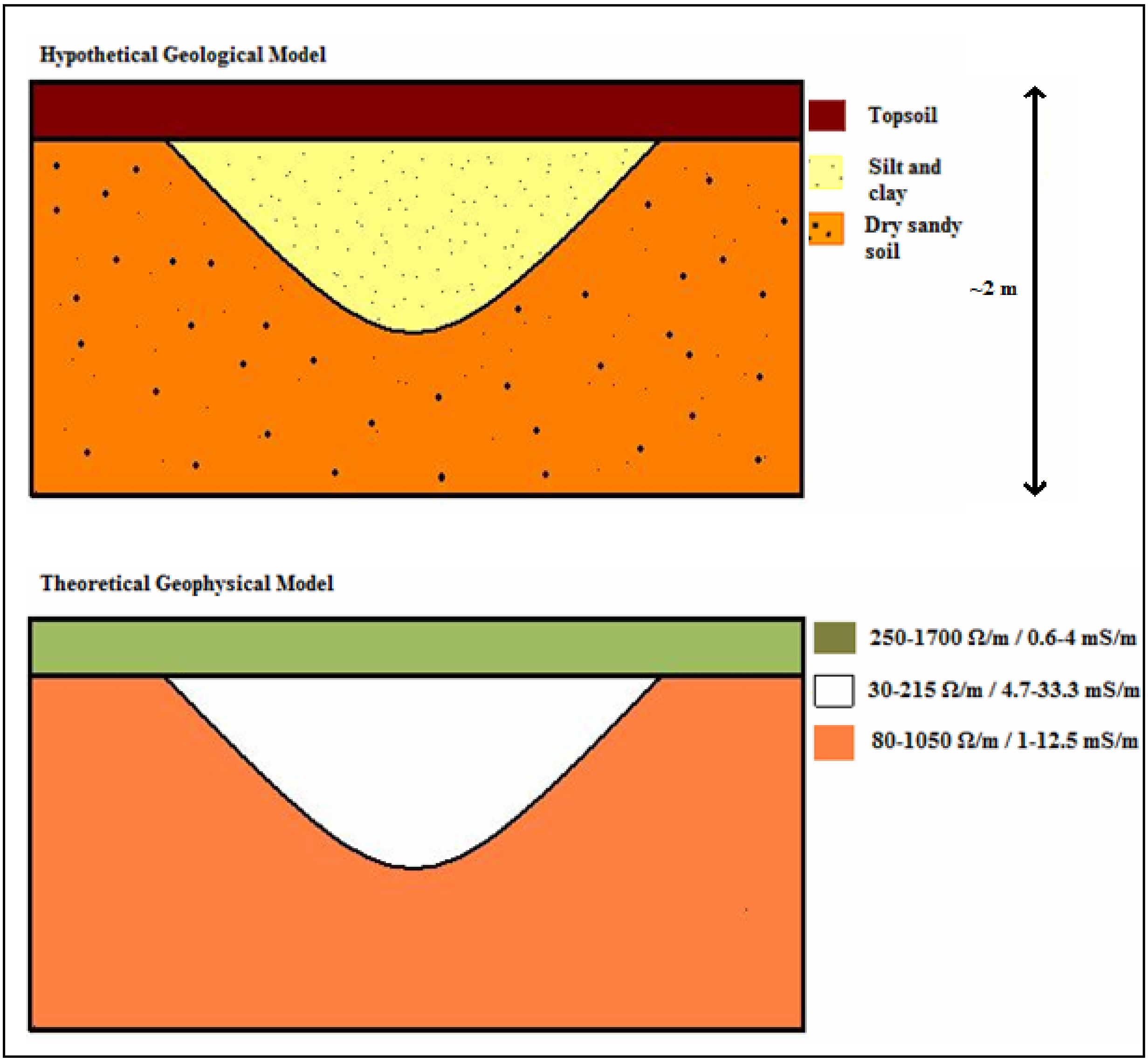

Figure 3.21. Geological and geophysical models for the ring ditches (resistivity values converted to conductivity on geophysical model). Note: Model only shows depth to 2 m however borehole data suggests that the sandy soil will continue to a depth of at least 20 m.

CHAPTER 4: SURVEY RESULTS AND INTERPRETATION

The following chapter presents and interprets the geophysical data collected within the field area. During the data processing stage it was evident that due to very minor conductivity changes with the EM31 and EM38 over the whole field area it was not possible to use a consistent colour ramp interval range to display the data. By using different interval ranges for each survey it was possible to display the very subtle changes of conductivity within each field that might have gone amiss if using the same default colour interval range. It is important to note that there are often similarities in resistivity ranges of different materials, therefore making interpretation subjective. The interpreted and analysed geophysical anomalies represent the subsurface physical properties and not the actual geological or archaeological feature itself (Hewson *et al.* 2005; Watters, 2007). The only information on the size and structure of any archaeological features can be on the evidence provided by excavation.

4.1 DC Resistivity

4.1.1 *Limitations*

Whilst performing DC resistivity it is crucial that the internal resistance of the potential measuring circuit is significantly higher than the ground resistance between the potential electrodes (Reynolds, 1997). As Reynolds (1997) notes, one of the most common sources of field problems occurs due to very high electrode contact resistance. This is likely to occur in dry sands and gravels. Although Newton Farm is situated on sandy soils, the soil was not dry enough to cause any significant problems and the system informed the user if any problems did occur.

4.1.2 *Results*

The DC resistivity data retrieved are displayed as 2D inverted models (‘geoelectric’ cross-sections or pseudosections) measured in ohm-metres (Ω/m) (Figures 4.1 and 4.2). These models show the thickness and resistivities of the geoelectric units. The geological and geophysical models (Section 3.5) were used to help make interpretations on the underlying geology and archaeological structures. As the resistivity profiles only display data in the vertical dimension, it was hoped that the EM31 and EM38 surveys would fill in the ‘gaps’ around this data (Section 4.2), to form a complete survey of Newton Farm.

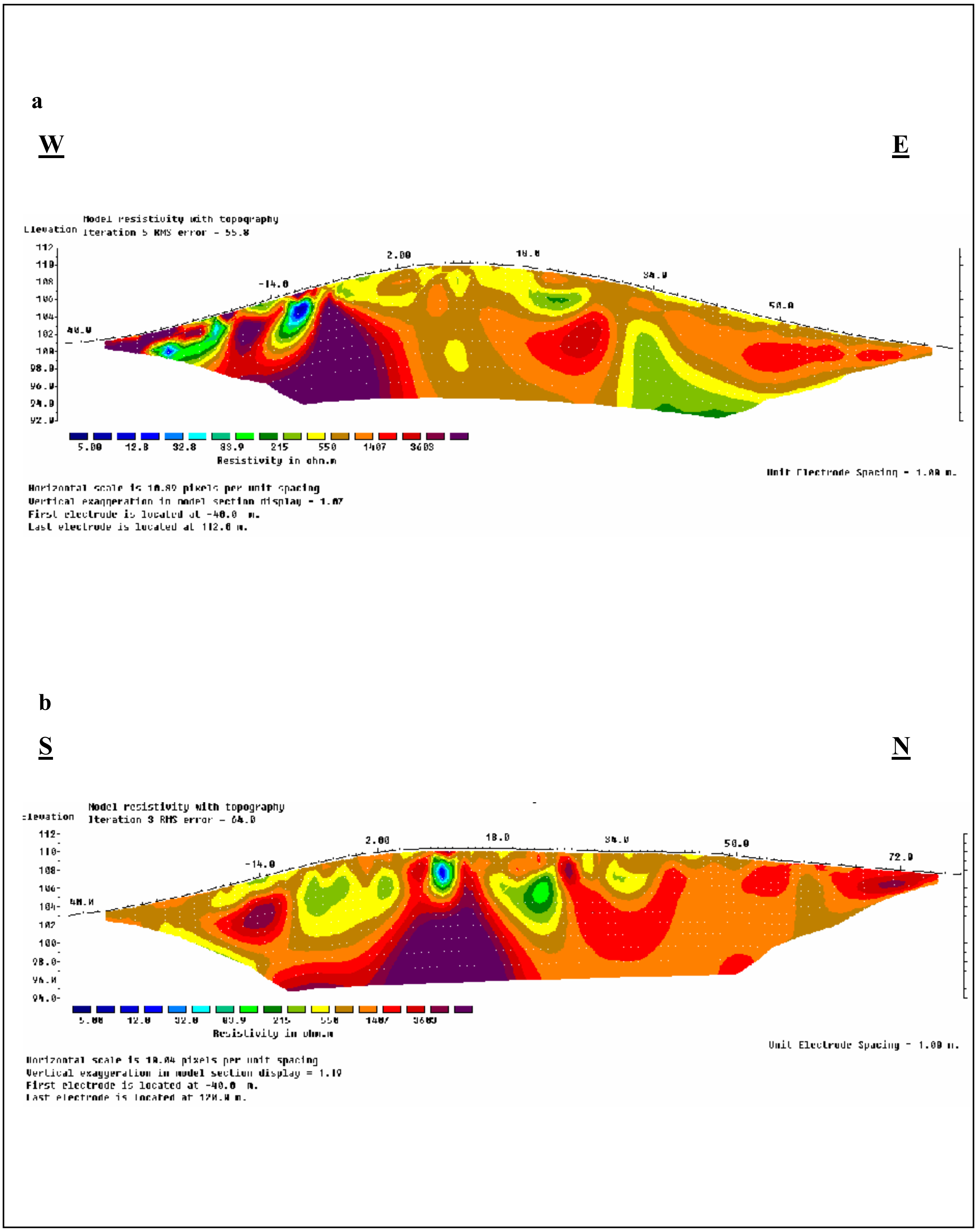

Figure 4.1. DC resistivity results presented for the west-east transect (**a**) and the south-north transect (**b**).

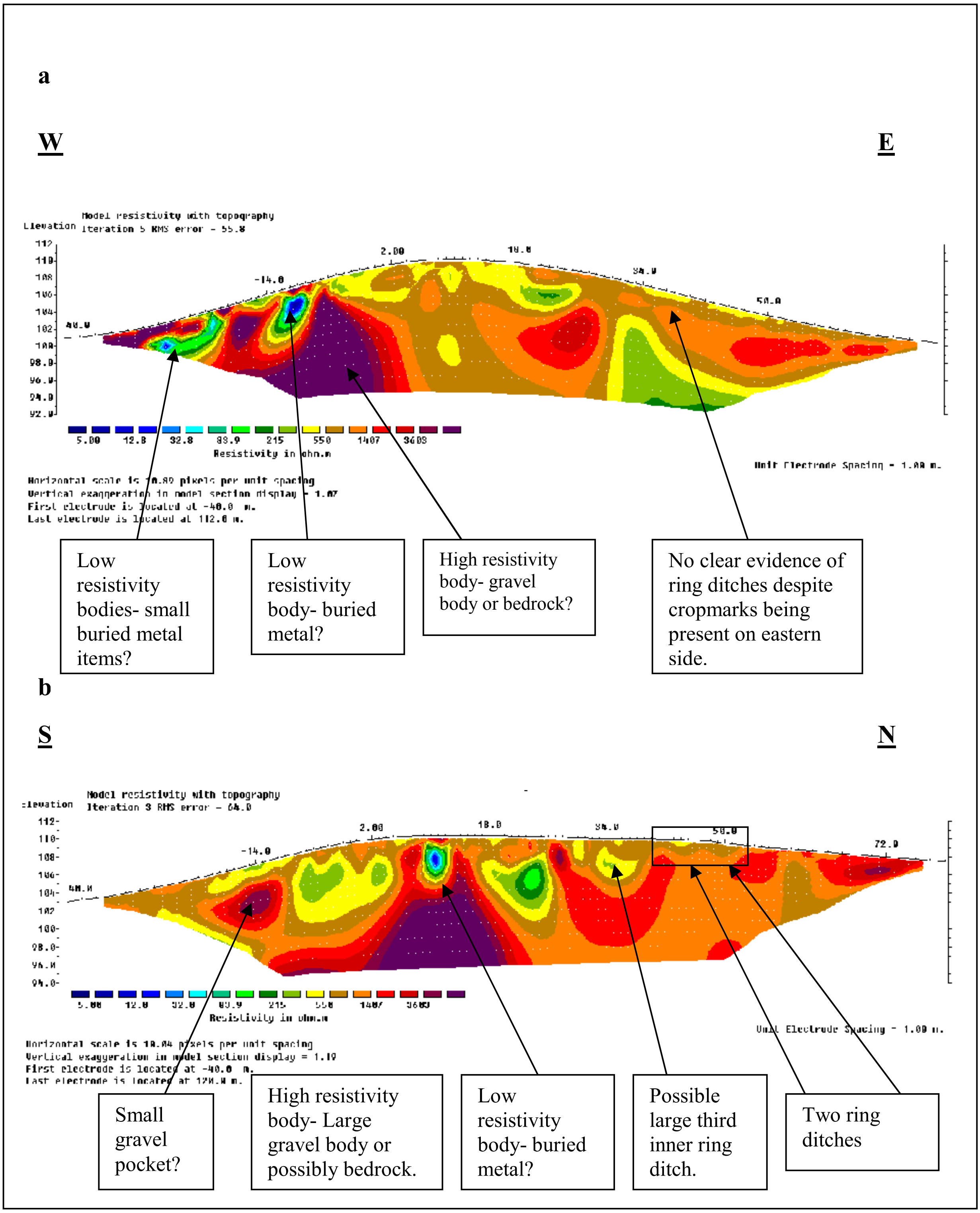

Figure 4.2. Analysis of DC resistivity results for the west-east transect (**a**) and the south-north transect (**b**).

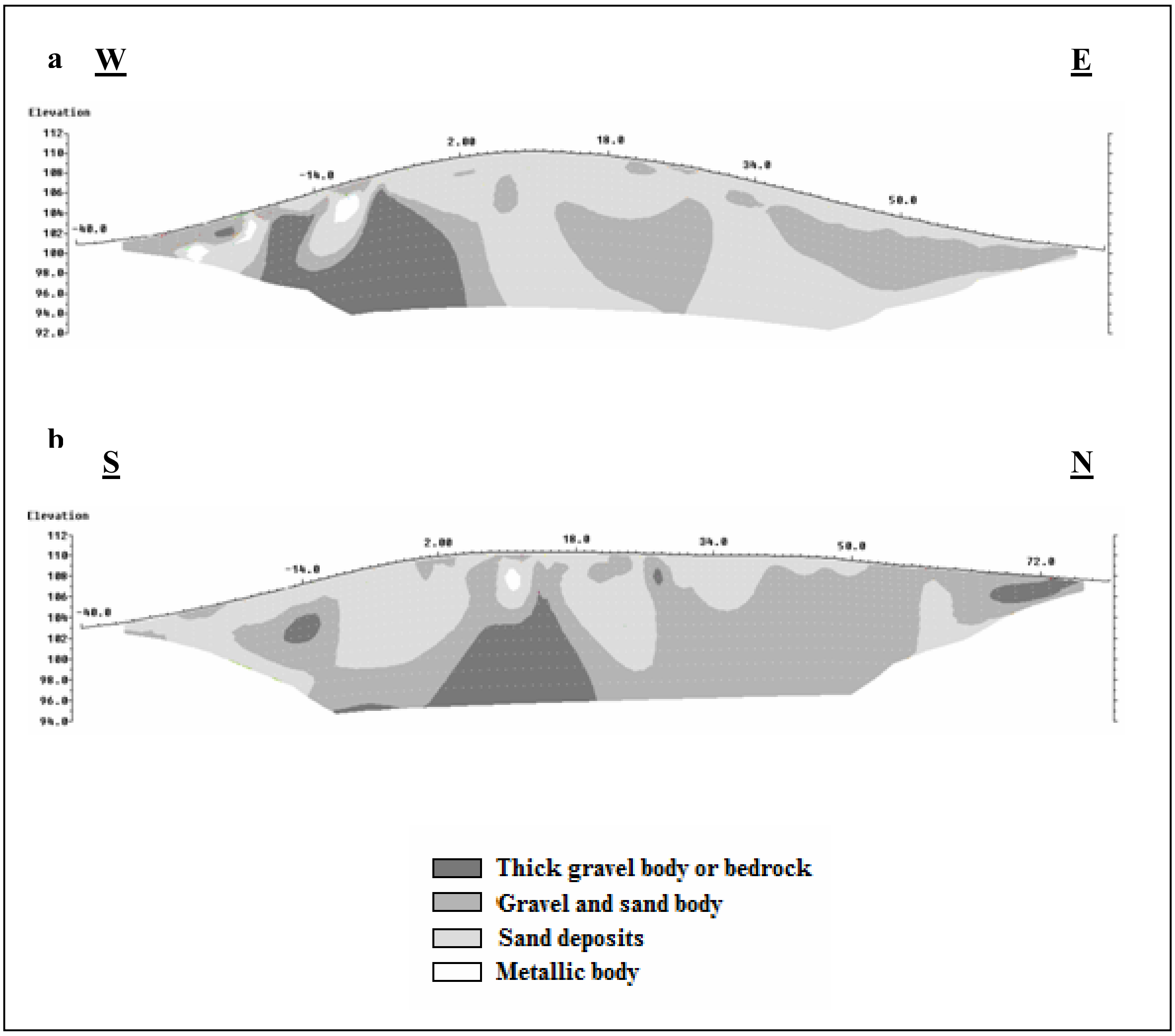

Figure 4.3. Subjective interpretation for the DC resistivity west-east transect (**a**) and the south-north transect (**b**). In reality the boundaries of each unit are unlikely to be as sharp and would merge into each other but they are represented as simple as possible for aid with interpretation.

4.1.3 *Discussion*

The 1 m electrode separation allowed interpretation of geological variations and archaeological features up to 10 m depth within the subsurface. Despite both transects showing very complex subsurface geological variations, the resistivity changes near the ground surface were very subtle and it is hard to identify many of the ring ditches despite both DC resistivity transects cutting across the cropmarks created by the presence of the ring ditches (Figure 4.4). Two ring ditches were identified on Figure 4.2b on the northern side at 40-52 m showing a resistivity around 500 Ω/m (~2 mS/m), a much higher resistivity value than predicted in the geological model (Section 3.5).

This suggests the ditch infill is composed of much lower conductivity sediment than predicted in the models, possibly because it was dry and/or similar in composition and grain size to the surrounding sediment. In both transects small highly conductive/low resistivity (>28.5 mS/m / <35 Ω/m) bodies were visible (displayed in white in Figure 4.3), some of which were identified in the magnetometry survey (Section 4.3.3) allowing these to be interpreted as metallic bodies.

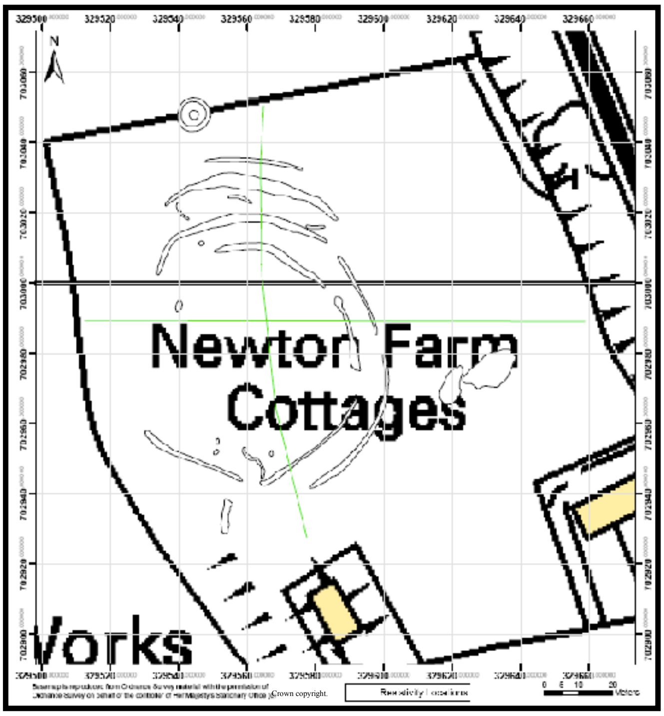

Figure 4.4. Location of the two DC resistivity transects (green) in comparison with the cropmarks (black).

4.2 Electromagnetism

4.2.1 *Limitations*

Frequency domain electromagnetism (FDEM) methods are extremely sensitive to noise sources, e.g. metal fences. To avoid this problem both the EM31 and EM38 were operated away from any potential noise sources (Figure 1.8).

4.2.2 *EM31 Results*

All the EM31 results are displayed using the same colour ramp and conductivity colour interval ranges measured in milliSiemens per metre (mS/m) to simplify the interpretation process. Using the original geophysical model (Section 3.5), the ring ditches should have been identifiable by increased conductivity values (12.5-33.3 mS/m / 215-1050 Ω/m) coloured in purple or white. The model suggests surrounding soils, i.e. soil unrelated to the archaeology, were likely to show lower conductivity values (0.6-12.5 mS/m / 215-250 Ω/m) coloured in shades of green.

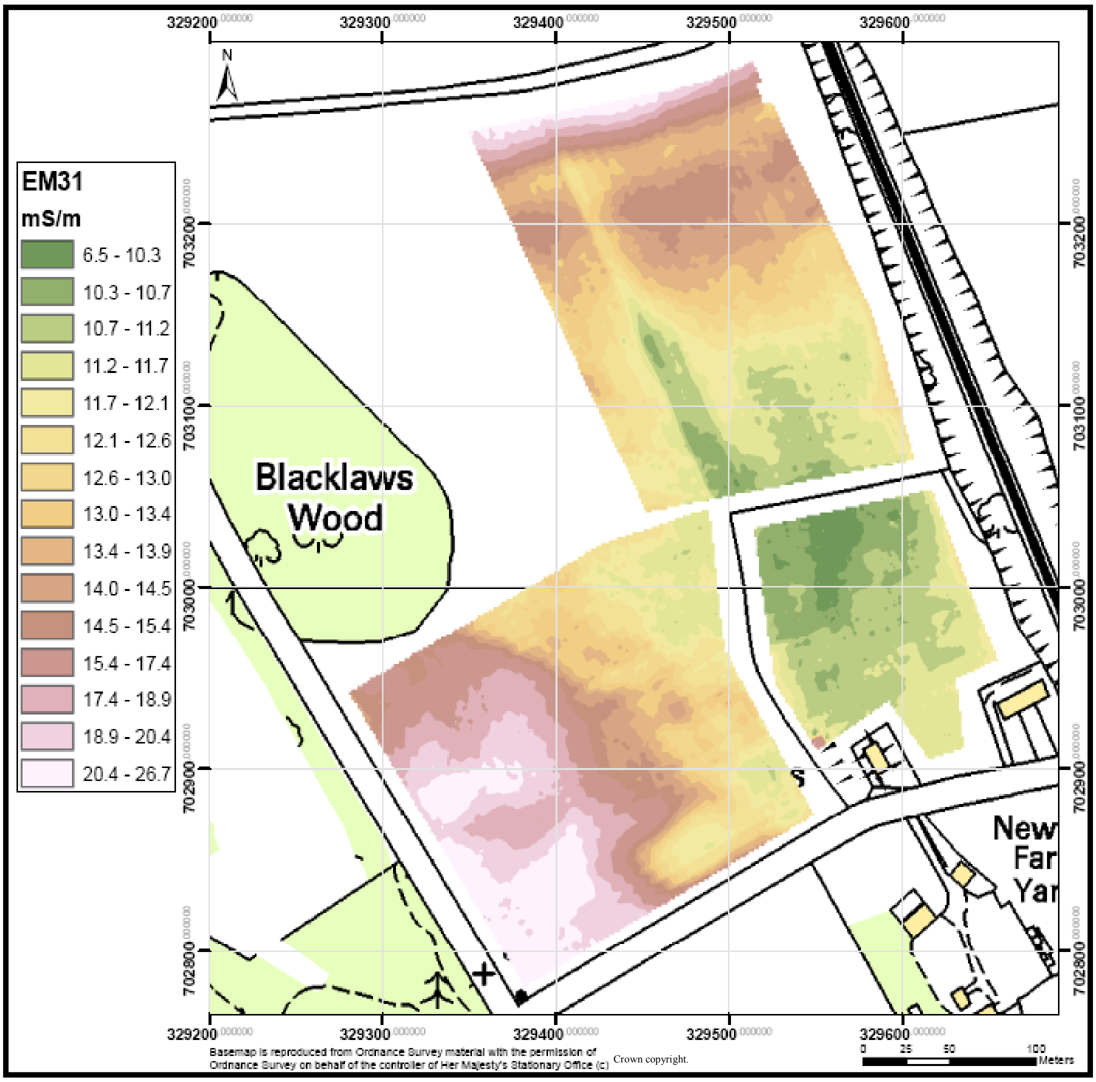

Figure 4.5. Final presentation of conductivity results using the Geonics EM31 on Newton Farm.

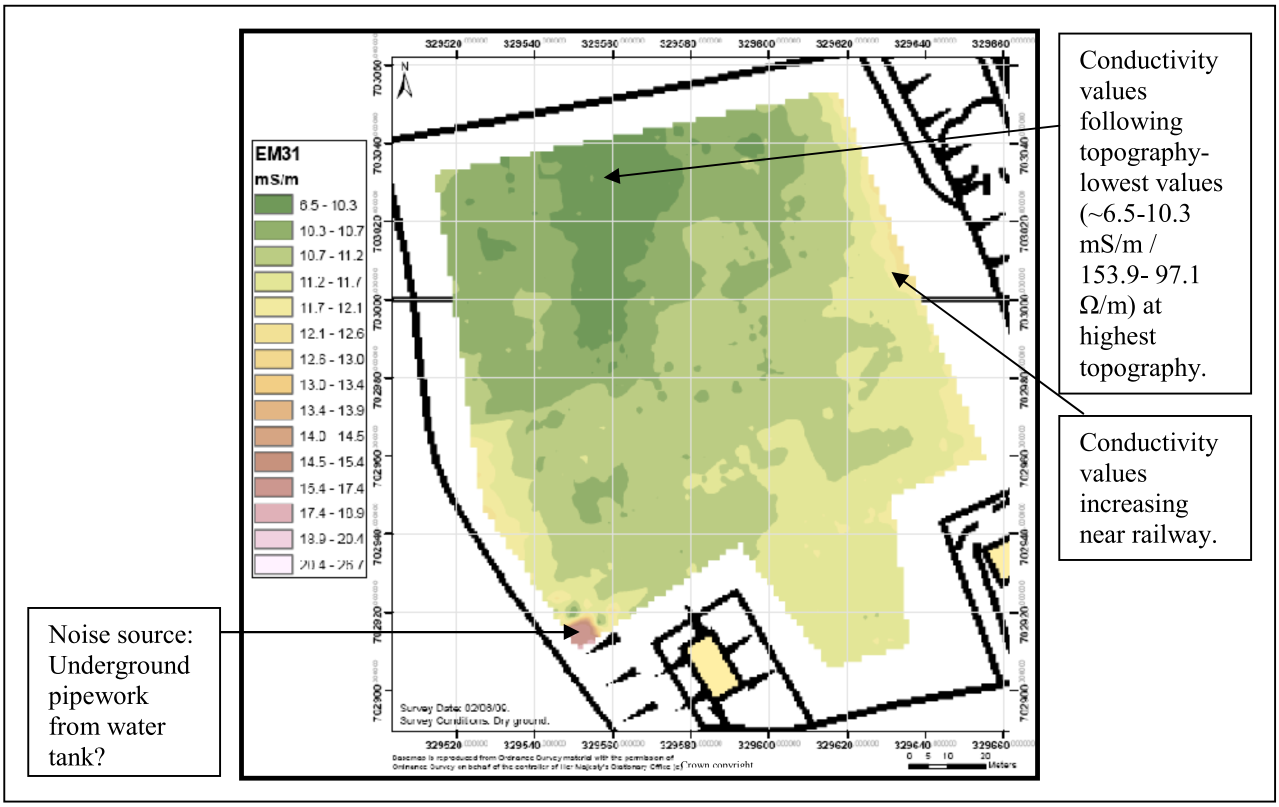

Figure 4.6. Final presentation and analysis of conductivity results using the Geonics EM31 on Field 1.

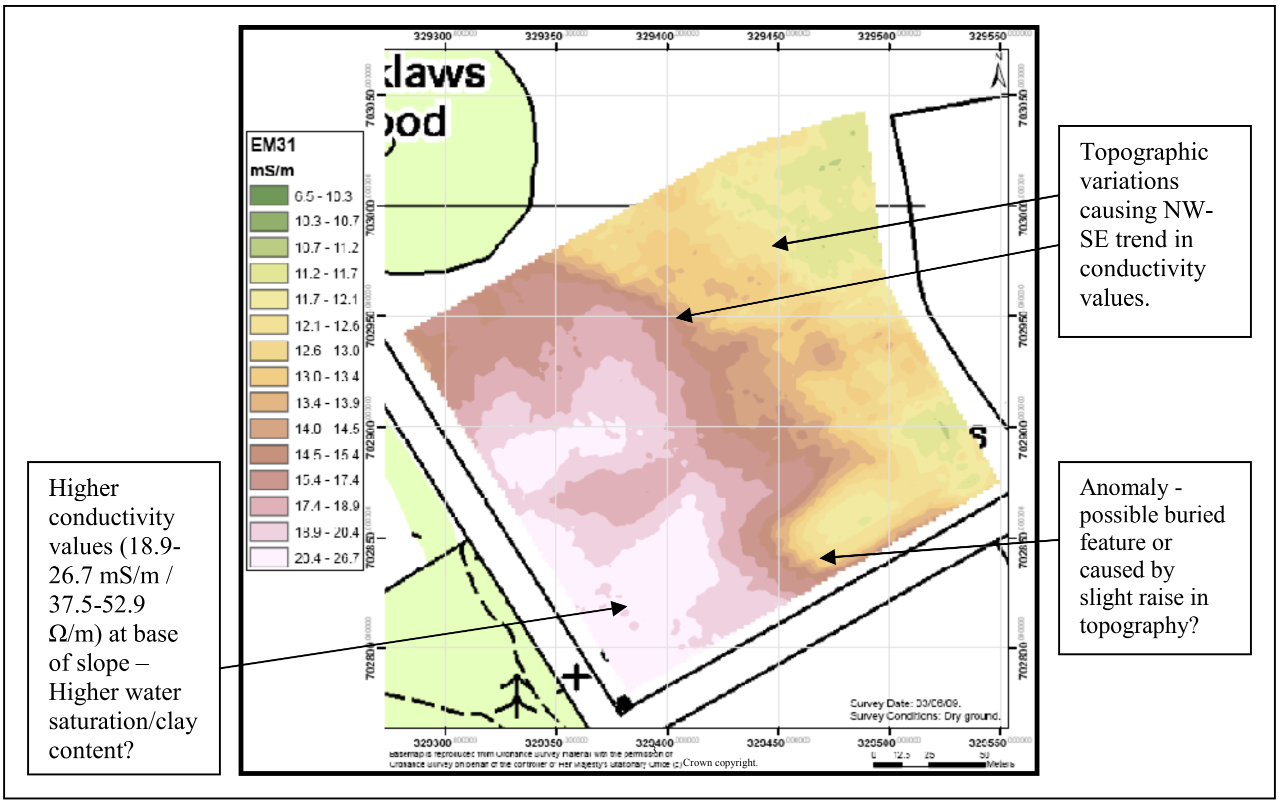

Figure 4.7. Final presentation and analysis of conductivity results using the Geonics EM31 on Field 2.

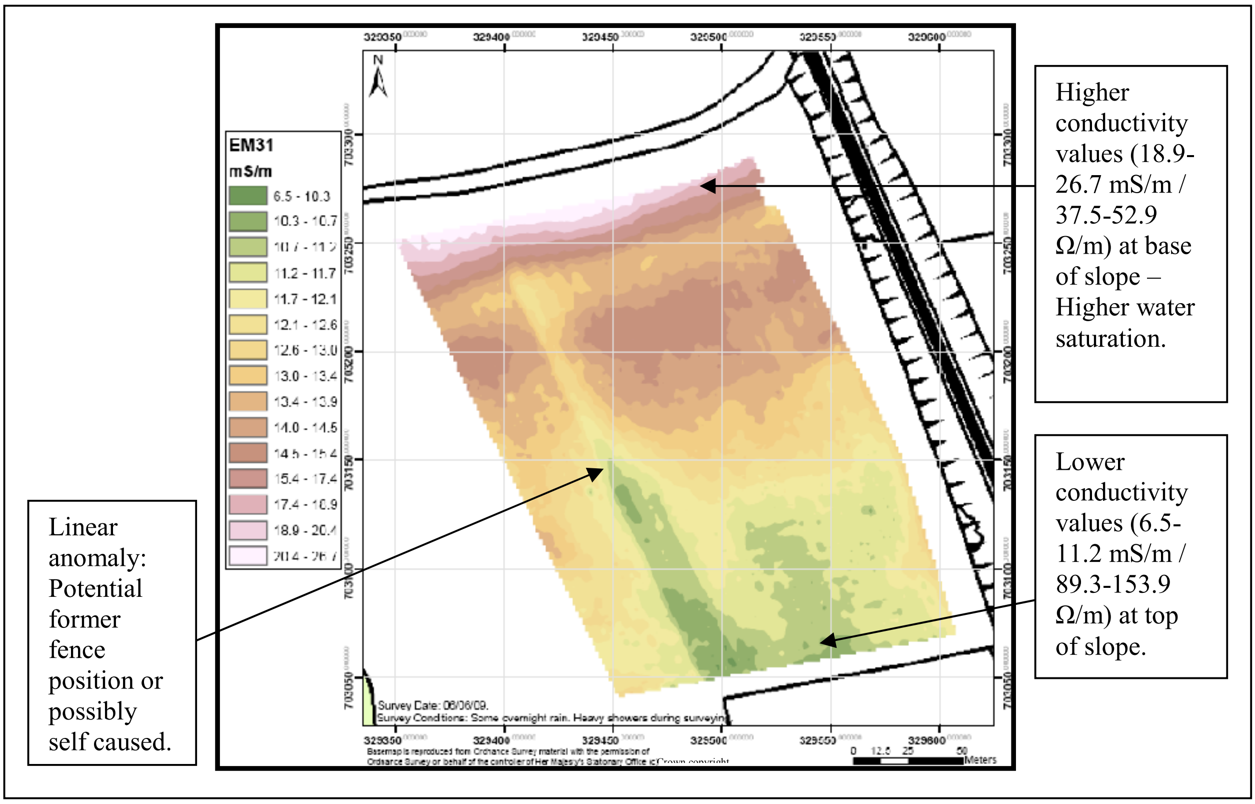

Figure 4.8. Final presentation and analysis of conductivity results using the Geonics EM31 on Field 3.

4.2.2.1 *Discussion*

The EM31 was used to define the overall ground conditions of Newton Farm and to detect any deeper archaeological structures within the site. Analysis of the data (Figures 4.5-4.8) shows that the EM31 failed to allow for any interpretations of archaeological structures within the site relating to the cropmarks, suggesting the archaeological features may be less deep, within 3 m of the ground surface. Alternatively, the archaeological structures may be less significant than first thought, therefore making detection much harder. A distinct linear anomaly on Field 3 (Figure 4.8), following the trend of the current fence bounding Field 1, could be interpreted as a former fence line. Field 1 also showed a very high conductivity anomaly (18.9-26.7 mS/m / 37.5-52.9 Ω/m) in the southwest corner of the site next to the water tank. It is likely that this is a noise source caused by buried pipes or metal relating to the water tank.

Analysis of Figure 4.9 shows that there is a relationship between ground conductivity and topography, for example, the highest conductivity values (20.4-26.7 mS/m / 37.5-49.2 Ω/m) were seen in areas of lowest topography. This is likely to be due to higher ground water saturation and higher clay content because of water and weathered soil travelling downslope aided by the presence of furrows. Soil samples from various areas of the site would need to be analysed to confirm this statement.

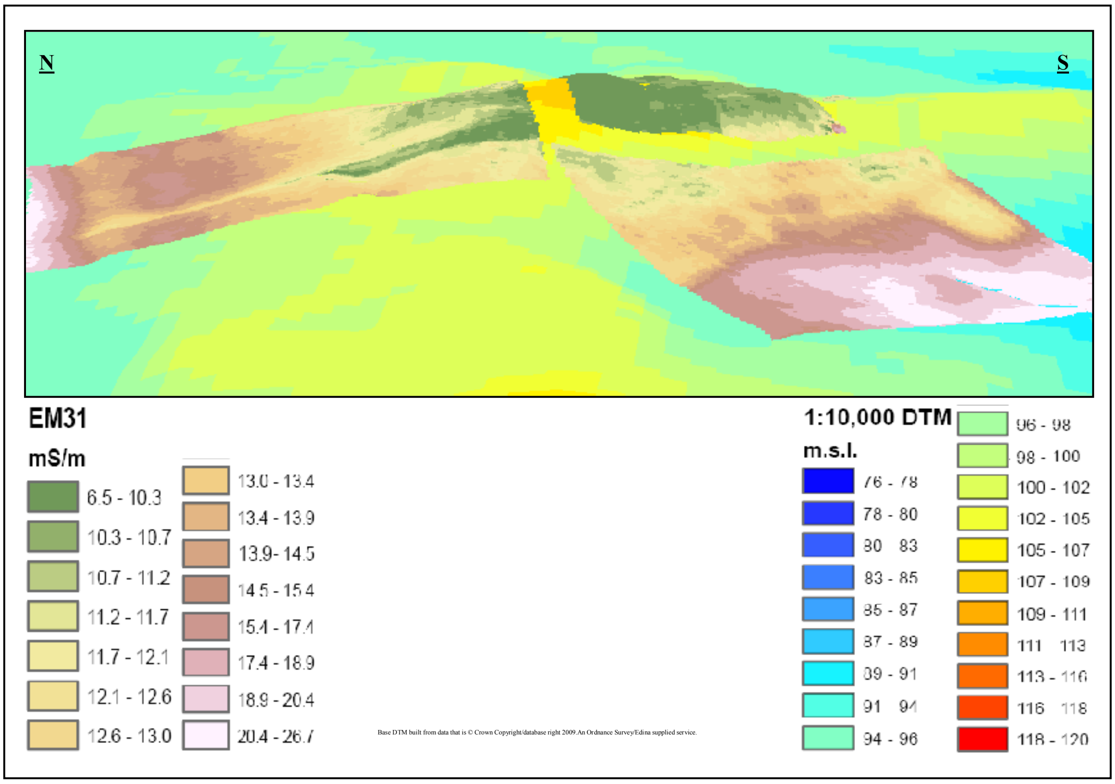

Figure 4.9. The EM31 survey displayed over a 1:10,000 DTM (Digital Terrain Model) showing the relationship between ground conductivity and topography on Newton Farm created in ArcScene.

It was planned to display the EM31 conductivity survey with the two DC resistivity profiles simultaneously by converting the EM31 conductivity values to resistivity values (Ω/m). This might have been useful to interpret any subsurface archaeological structures in the vertical dimension. However, the location of the resistivity transects passed through no areas of significant geophysical variation on the EM31 results for this comparison to be of any use (Figure 4.10).

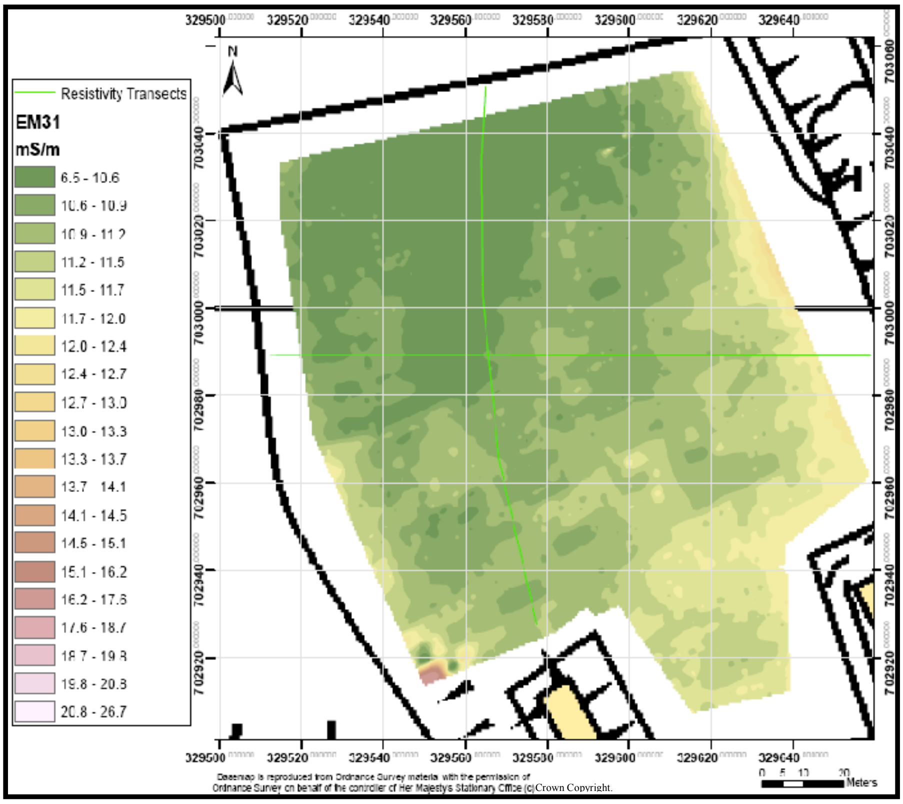

Figure 4.10. The two DC Resistivity transects (green) shown in their position relative to the EM31 survey on Field 1. Neither resistivity transect passes through any significant geophysical variation.

4.2.3 *EM38 - Vertical Dipole Mode (Quad-phase) Results*

The EM38 vertical dipole mode (quad-phase) results for each field are displayed using the same colour ramp and conductivity colour interval ranges in milliSiemens per metre (mS/m) to simplify the interpretation process. Like the EM31, the original geophysical model was used as an aid for interpretation (Section 3.5).

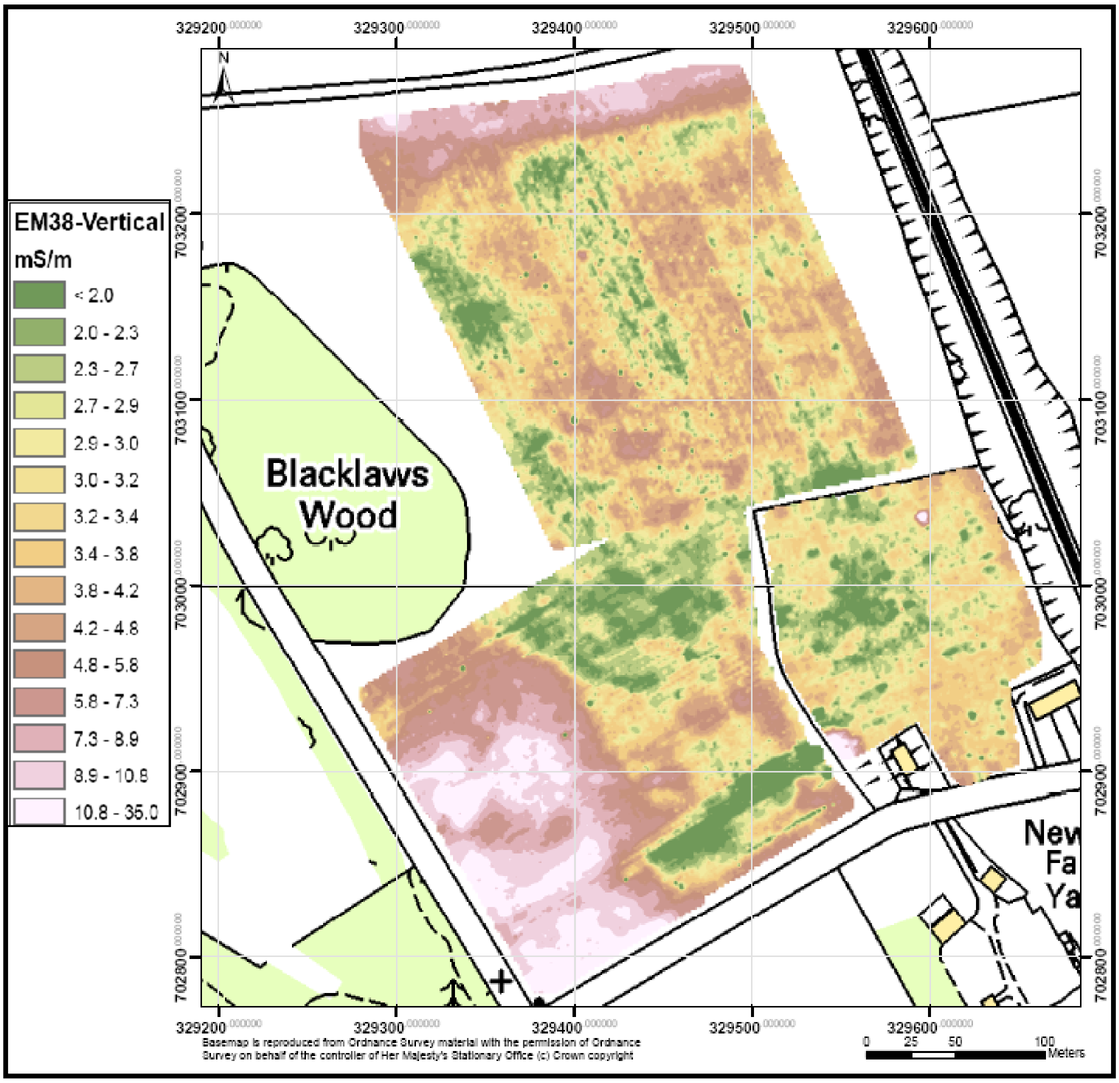

Figure 4.11. Final presentation of conductivity results using the Geonics EM38 in vertical dipole mode on Newton Farm.

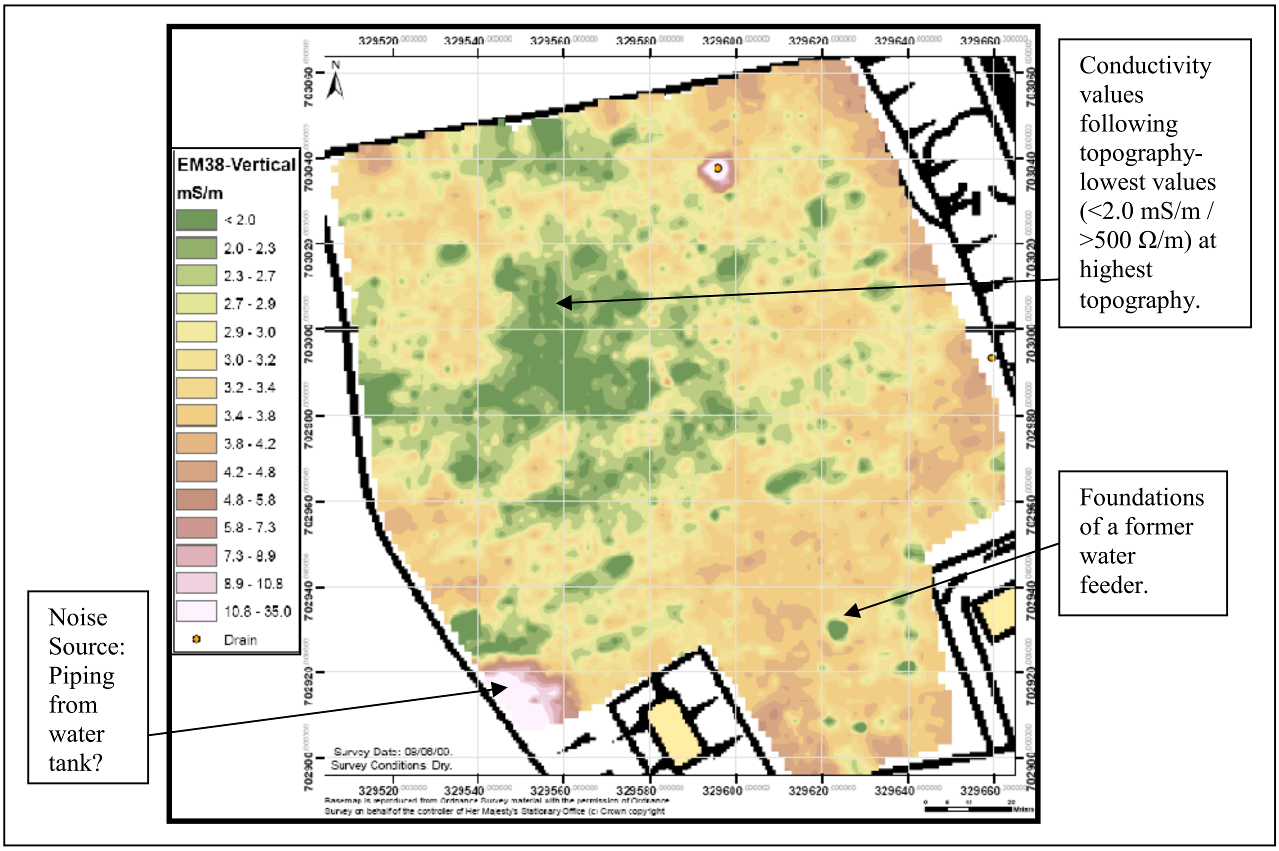

Figure 4.12. Final presentation and analysis of conductivity results using the Geonics EM38 in vertical dipole mode on Field 1.

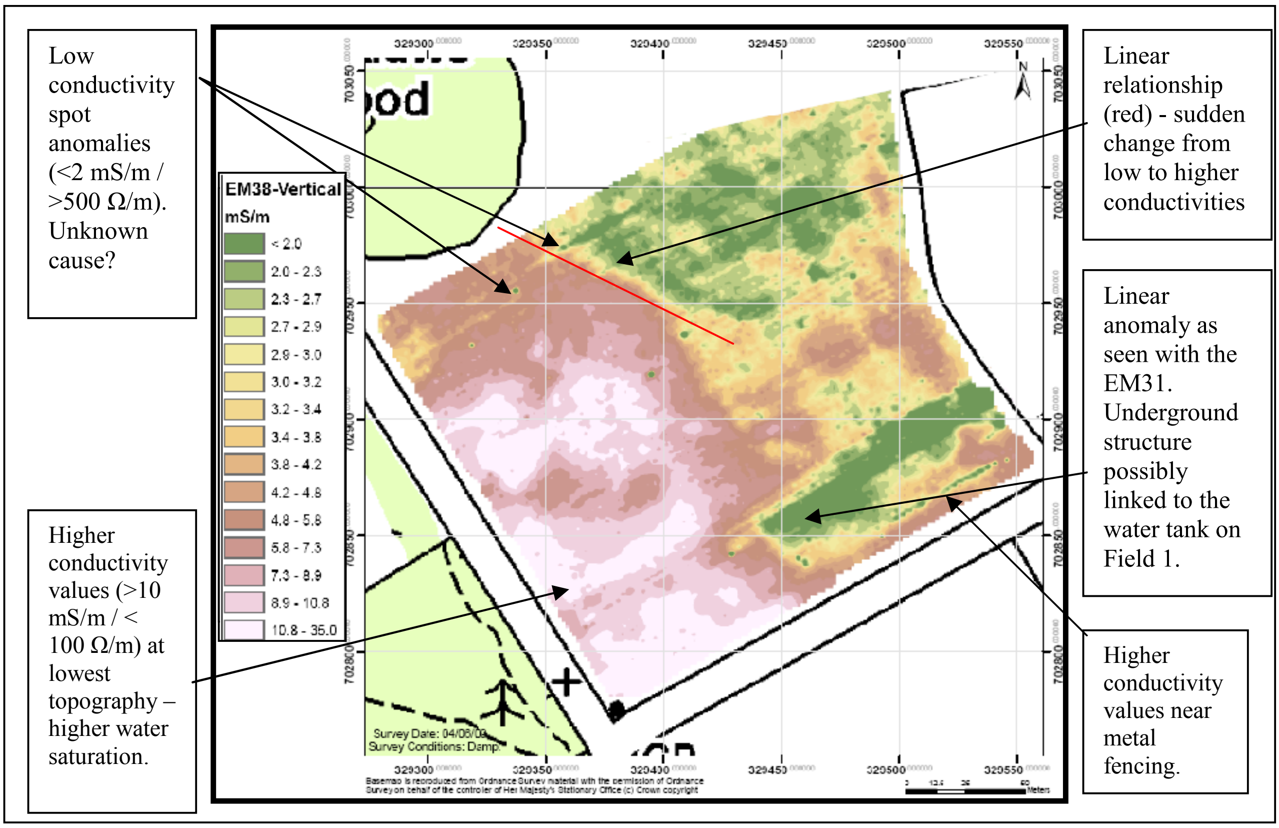

Figure 4.13. Final presentation and analysis of conductivity results using the Geonics EM38 in vertical dipole mode on Field 2.

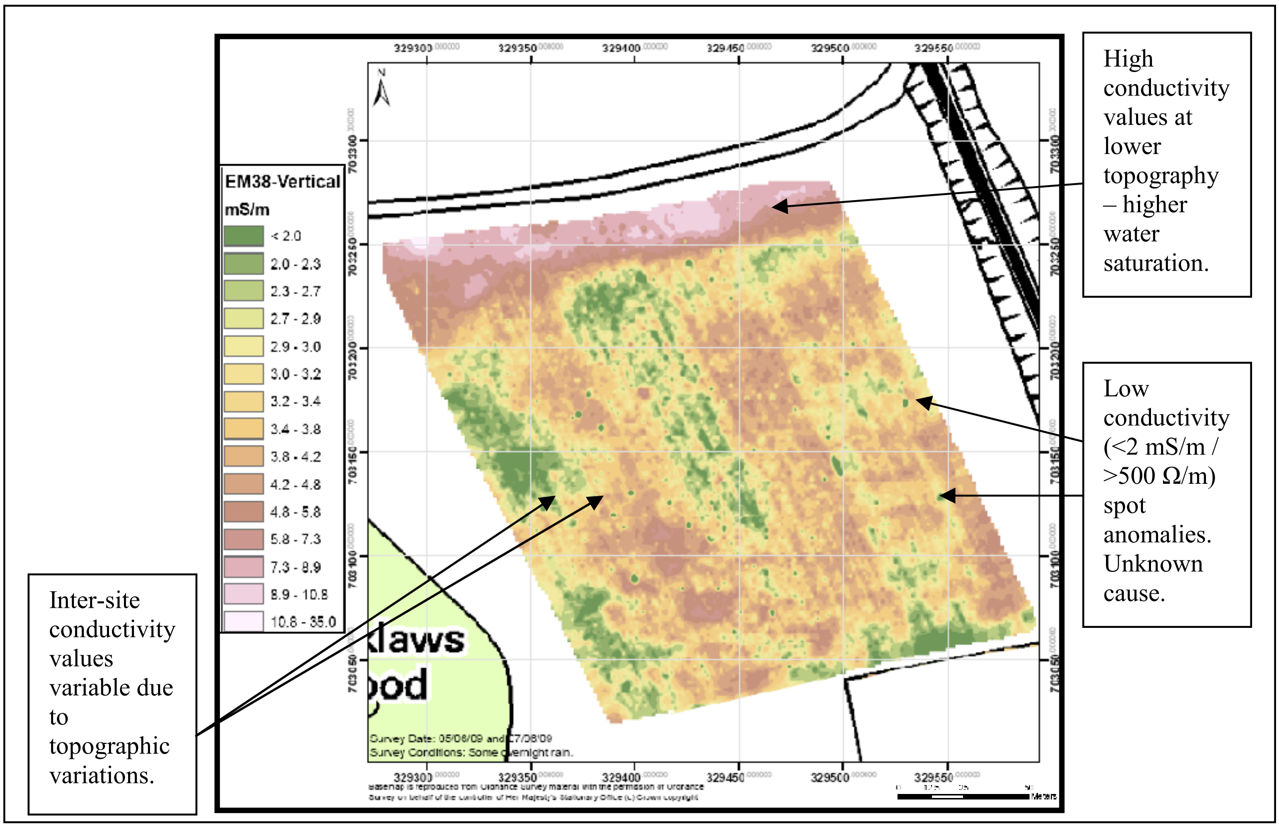

Figure 4.14. Final presentation and analysis of conductivity results using the Geonics EM38 in vertical dipole mode on Field 3.

4.2.3.1 *Discussion*

The EM38 survey, like the EM31 survey, showed a relationship between ground conductivity and topography with the highest conductivity values seen in areas with the lowest topography (Figure 4.11). This again was linked to higher water saturation being present in areas with lower topography. It was not possible to interpret significant archaeological features and the underground features causing the cropmarks were unnoticeable. On Field 1 an unusual low conductivity spot anomaly (<2 mS/m / >500 Ω/m) was seen at GR: 329623 702933 which marks the position of a former animal water feeder confirmed by aerial imagery (Figure 1.3). However this does not explain the existence of several low conductivity spot anomalies occurring throughout all three fields (Figures 4.12, 4.13 and 4.14). At present the cause of these spot anomalies is unknown. On Field 2 there were two significant geophysical variations present (Figure 4.13). The first is highlighted with a red line marking a sudden change from higher conductivity values (~10 mS/m / 100 Ω/m) to lower conductivity values (~2 mS/m / 500 Ω/m) from west to east. This could be due to topographic variations however as these changes occurred over such a short distance (~ 5 m) it could be due to changes in the physical properties of the ground. It had been suggested before surveying that there used to be a historic road passing Field 2 running towards the water tank (Manson, *Personal Communication*, 2009). This anomaly is trending in the same direction and could therefore be a signature from this former road/track. More surveying and excavation would be needed to confirm this. The second anomaly on Field 2 is linear trending southwest-northeast running towards the water tank (NGR: 329450 702950 – 329540 703010). This is likely to be related to the anomaly in Field 1 at NGR: 329550 702910 assumed to be a noise source from the water tank. It is possible there are underground foundations or piping below this part of Field 2 forming this linear anomaly displayed with both the EM31 and EM38. As both the EM31 and EM38 failed to recognize significant features it again suggests there may be few archaeological features.

4.2.4 *EM38- Horizontal Dipole Mode (Quad-phase) Results*

The EM38 horizontal dipole mode (quad-phase) results are displayed in milliSiemens per metre (mS/m) (Figure 4.15). The EM38 was operated in horizontal dipole mode on Field 1 only. Due to the horizontal dipole mode having a maximum vertical depth resolution of 0.75 m, it is unlikely the original geophysical model is valid, nevertheless the survey was performed in the hope to reveal shallow, subtle archaeological features.

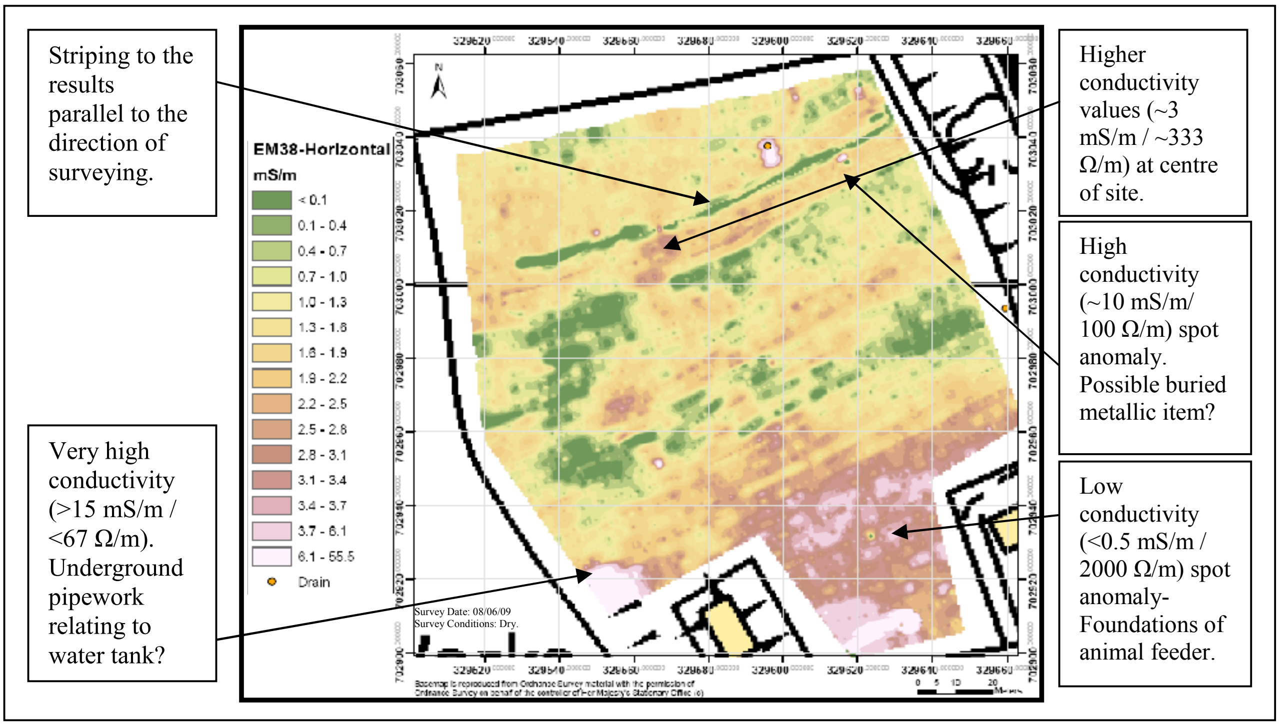

Figure 4.15. Final presentation and analysis of conductivity results using the Geonics EM38 in horizontal dipole mode (quad-phase) on Field 1.

4.2.4.1 *Discussion*

Analysis of the presented data (Figure 4.15) shows that the EM38 failed to detect any significant archaeological structures within the site relating to the cropmarks, which again could suggest the archaeological features may be more limited than first thought. Alternatively, the topsoil could be of considerable depth and of low conductivity therefore ‘masking’ the true conductivity values below. Spot anomalies of higher conductivity values than the surrounding area (~6-10 mS/m / 100-166 Ω/m) present at NGR: 329567 702952 and 329617 703036 possibly represent small buried metallic items. As with the other EM surveys, there was a large noise source in the southwest of Field 1 (NGR: 329555 702915) and it can be assumed this is caused by the nearby water tank. Conductivity values to the south of Field 1 (around NGR: 32963 70293) were higher (~2-6 mS/m / 100-500 Ω/m) than those to the north of the site. This part of the field is on flat land and therefore likely to have higher water saturation and thus show higher soil conductivity.

After surveying conductivity with both the EM31 and EM38, it could be suggested that the reason for limited archaeological features interpreted was due to the 'masking' effect produced from the topsoil. A further survey was performed after the topsoil was removed during excavation to help prove this hypothesis.

4.2.5 *EM38 – Vertical Dipole Mode (In-phase) Results*

The EM38 vertical dipole mode in-phase results on Field 1 (Figure 4.16) should correspond with the soil samples measured for magnetic susceptibility within the lab (Section 4.4). For final presentation of results, the data output was measured in mS/m and then converted into ppm (parts per million), assuming that 1 mS/m is equal to 29 ppm (Geonics Limited, 2005).

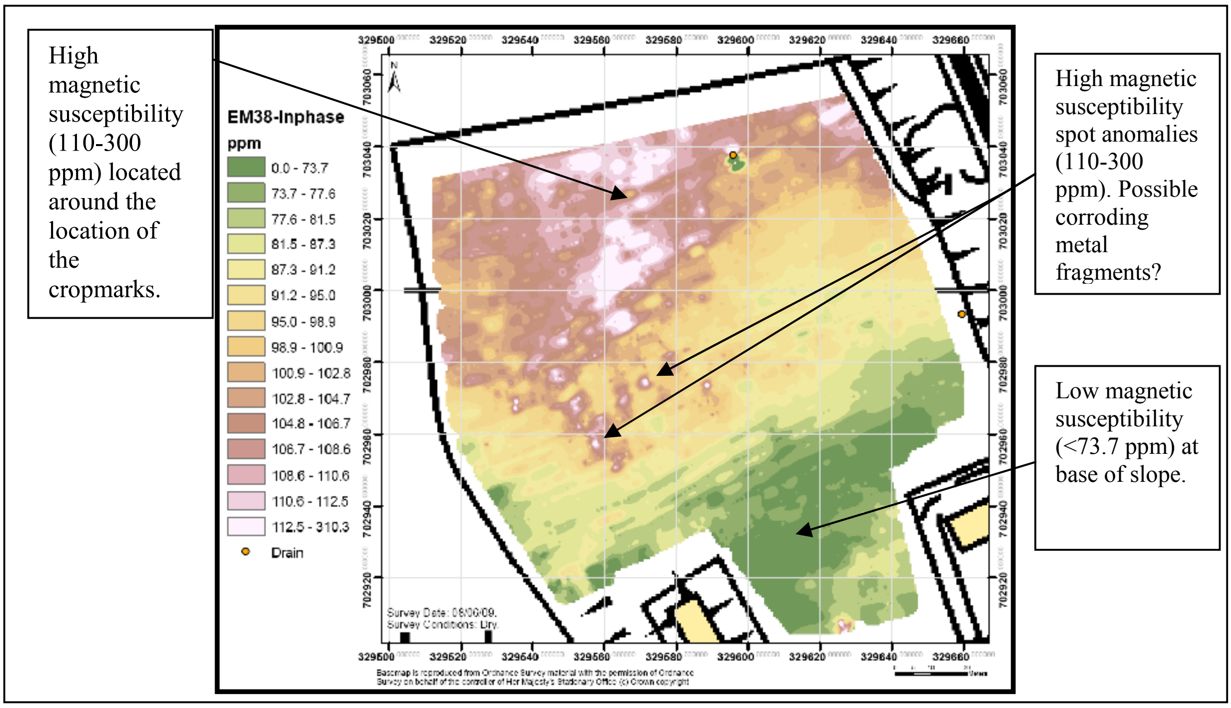

Figure 4.16. Final presentation and analysis of magnetic susceptibility results using the Geonics EM38 in vertical dipole mode (in-phase) on Field 1.

4.2.5.1 *Discussion*

Magnetic susceptibility increased upslope and values greater than 100 ppm were seen around NGR: 329560 703000, suggesting that previous human activity was greatest around this location. There were several high magnetic susceptibility (>110 ppm) spot anomalies, e.g. NGR: 329590 702973, which are likely to represent some form of underground metal fragments or localised increase in magnetic particles. Due to lack of experience with the EM38 in in-phase mode, it was uncertain how reliable these results are and it is suggested the later magnetic susceptibility test may be more accurate (Section 4.4). It does however provide a useful comparison.

4.3 Magnetometry (Gradiometry)

4.3.1 *Limitations*

As the GEM GSM-19T proton precession magnetometer only measures total fields it can be difficult to interpret large anomalies in which the direction of the resultant field changes rapidly from place to place (Milsom, 2003). It is also sensitive to electrical noise so surveying was carried out away from possible interference sources (Figure 1.8). Finally, as the system does not contain an integrated GPS, the first station point was recorded using a 'Garmin GPS Map 60Cx' and a tape measure was used from then on ensuring any error in the original measurement remained relative throughout the survey. Despite careful measurement it is likely that there could have been some inaccuracy in the sampling locations.

4.3.2 *Magnetometry Results*

The data displayed is the magnetic gradient measured in nanoteslas per metre (nT/m) (Figure 4.17). Any significant increases in magnetic gradient to the surrounding values were possible areas of interest relating to archaeology.

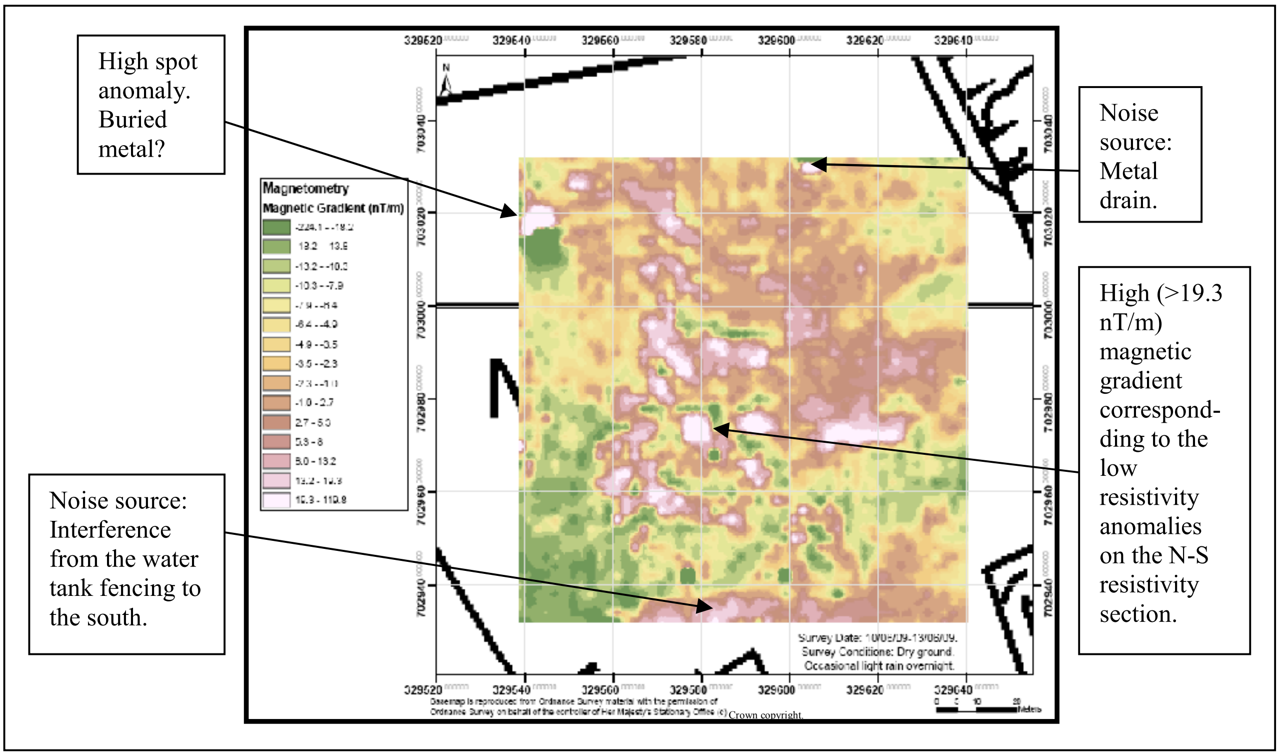

Figure 4.17. Final presentation and analysis of the magnetometry results on Field 1 displaying the magnetic gradient (nT/m) using the GEM GSM-19T proton precession magnetometer.

4.3.3 *Discussion*

The magnetometer survey proved more successful than the EM surveys and detected changes within ground conditions throughout Field 1. Values of magnetic gradient increased towards the top of the hill near areas where the cropmarks are present but the features forming the cropmarks can not be interpreted with the data (Figure 4.18). A strong magnetic gradient anomaly occurred at NGR: 329541 700019 which is interpreted as buried metal. Two other high values of magnetic gradient occurred at NGR: 329580 702973 and 329590 702973, the latter being identified on the N-S resistivity section (Section 4.1.3), suggesting the interpretation of this being a metallic body is correct.

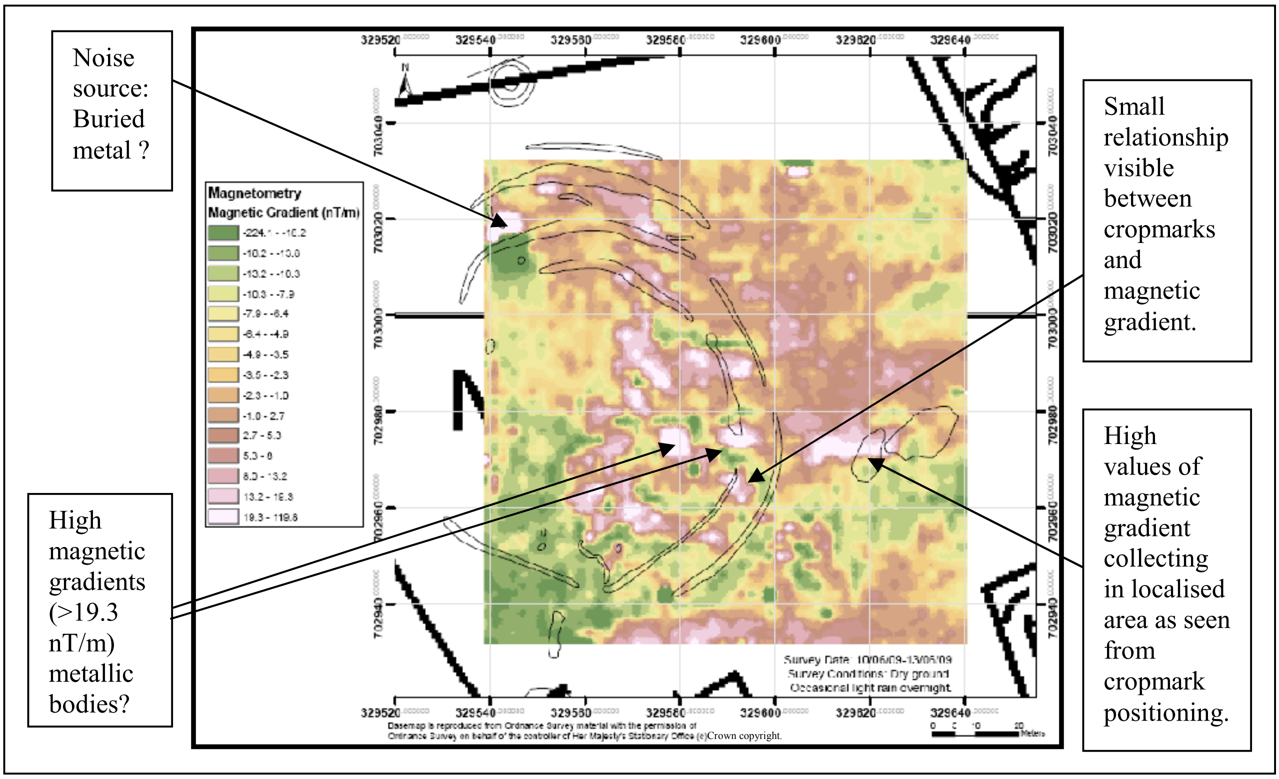

Figure 4.18. Magnetometry results as presented in Figure 4.17 with the cropmark locations in black for comparison on Field 1.

4.4 Magnetic Susceptibility

4.4.1 *Limitations*

Soil samples were collected on a sampling interval range of every 20 m. This meant that values of magnetic susceptibility between these sampling interval points is unknown and can only be averaged using a contour map. Magnetic susceptibility within soils can vary considerably over short distances and therefore frequent sampling interval ranges are more accurate but for locating areas of previous human activity this sampling interval range should be satisfactory.

4.4.2 *Magnetic Susceptibility Results*

The results are displayed using the same colour ramp as for electromagnetism and magnetometry simplifying data interpretation. The data displayed is the low frequency (LF) magnetic susceptibility measured in $10^{-8}m^3kg^{-1}$ (Figure 4.19). LF magnetic susceptibility was the main focus because as this most likely reflects past human activity. Any values of high magnetic susceptibility (>15 x $10^{-8}m^3kg^{-1}$) could represent locations of previous human activity. High frequency (HF) and frequency dependent magnetic susceptibility can be viewed in Appendices B.5 and B.6.

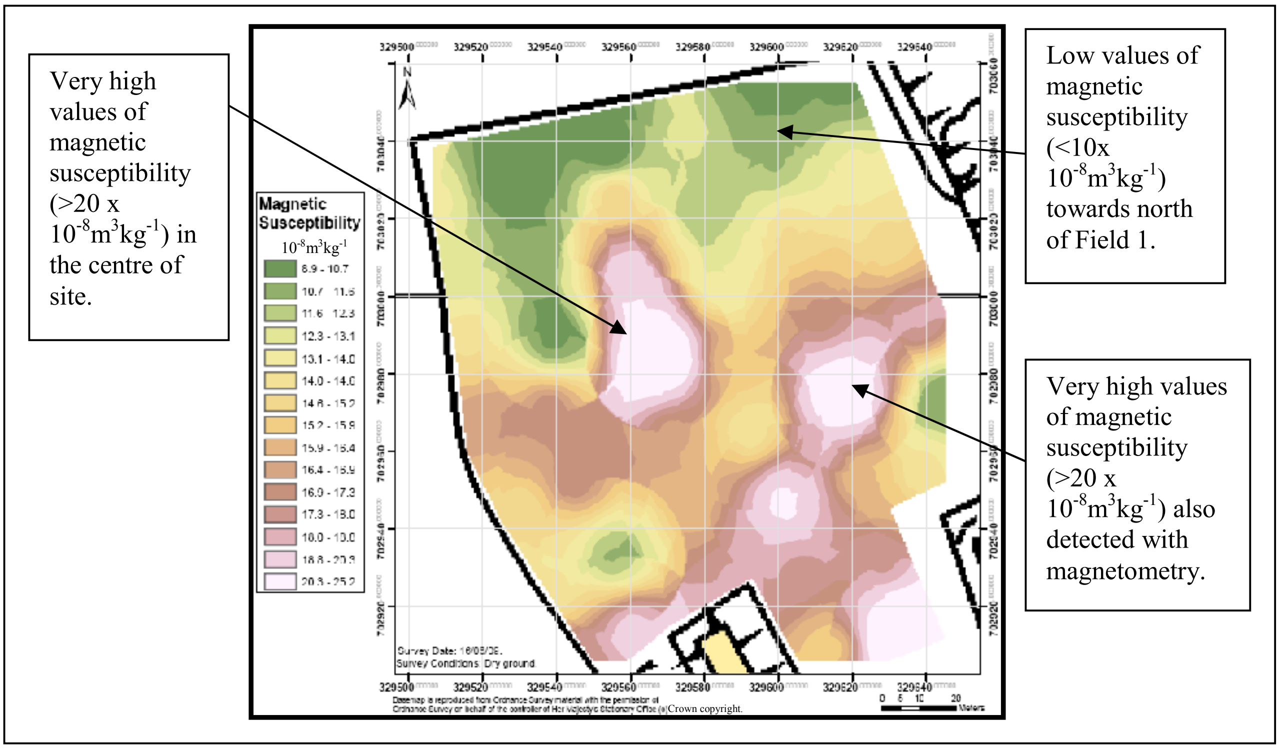

Figure 4.19. Final presentation and analysis of the magnetic susceptibility results on Field 1 displaying the low frequency magnetic susceptibility measured using the Bartington MS2 meter.

4.4.3 *Discussion*

The magnetic susceptibility survey detected changes within the ground conditions throughout Field 1. As expected, values of magnetic susceptibility were higher (> 14 x $10^{-8}m^3kg^{-1}$) in areas where the cropmarks are present (Figure 4.20) due to the ring ditches acting as a ‘sink’ for magnetic particles to accumulate. A very high magnetic susceptibility value (>20 x $10^{-8}m^3kg^{-1}$) occurred in the centre of the cropmarks (NGR: 329564 702980) and due to its positioning can be interpreted as a possible archaeological feature or area of previous human activity. This area was therefore targeted during excavation. As detected with magnetometry, there was a significant increase in magnetic susceptibility of the soil around NGR: 329620 702975 suggesting there is either some metallic material present or the area is, like the ring ditches, acting as a 'sink' collecting magnetic particles.

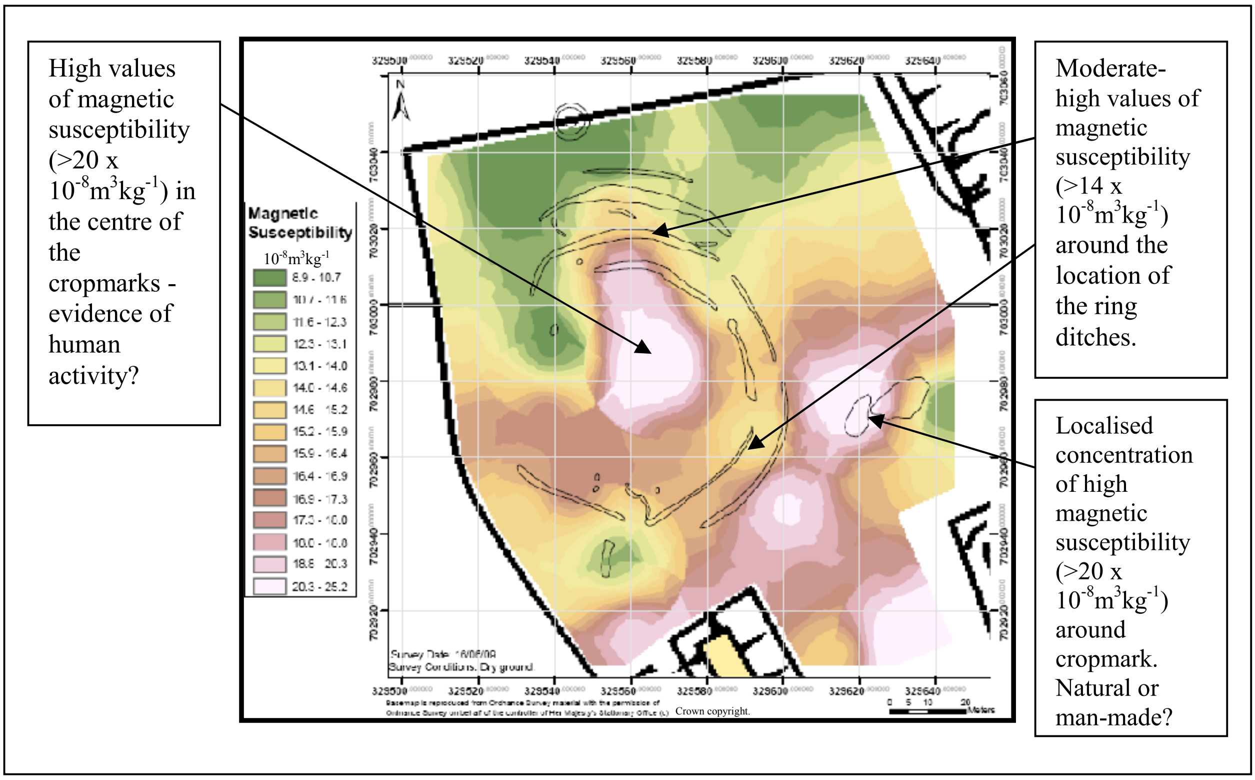

Figure 4.20. Magnetic susceptibility results as presented in Figure 4.19 with the cropmark locations in black for comparison on Field 1.

CHAPTER 5: GROUND TRUTH – EXCAVATION

5.1 Introduction

Both the geophysical survey and the cropmark locations were used as an aid for positioning the trenches (Figure 5.1). Excavation was carried out between the dates 19/06/09-21/06/09. The excavation enabled a comparison of the ground truth with the geophysical data collected and helped explain why interpretation and recognition of subsurface archaeology was limited.

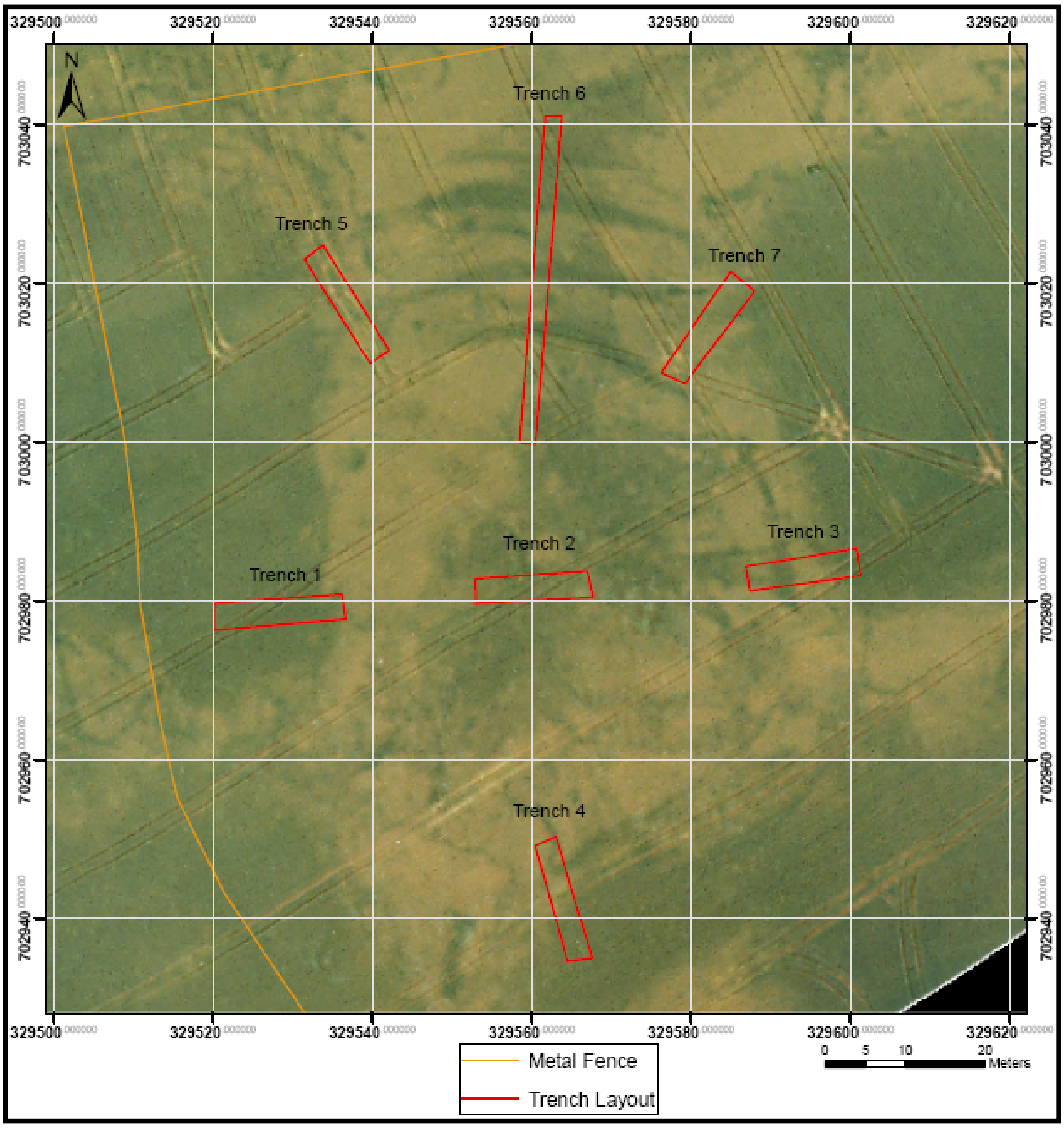

Figure 5.1. The location of the trenches recorded using the HiPer Pro Topcon RTK GPS.

The top 50 cm of soil was removed and the new surface was allowed to dry before targeting the archaeological features located by the presence of darker coloured soil (Figure 5.2).

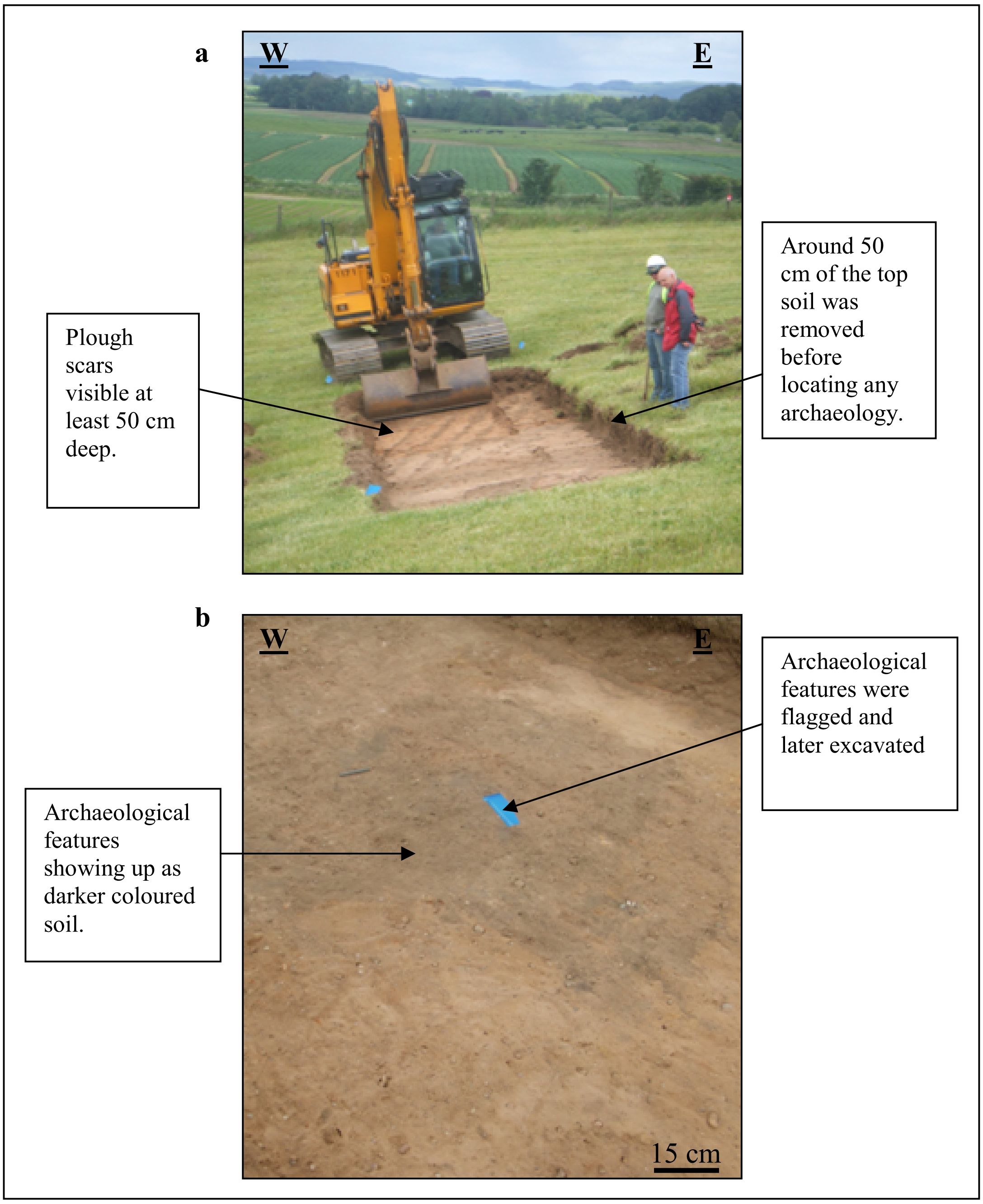

Figure 5.2. Digging of the trenches in progress (person for scale) (**a**) and an archaeological feature flagged recognized due to colour contrast in the soil (**b**).

5.2 EM38 Survey of Trenches

After removal of the topsoil, the Geonics EM38 was set-up in vertical dipole mode (quad-phase) to survey the trenches to ascertain the effect the topsoil may have had in limiting detection of any significant archaeological features (Figure 5.3). The far western trench (Trench 1) was incomplete and could not be surveyed. The results from each individual trench can be viewed in Appendix B.4.

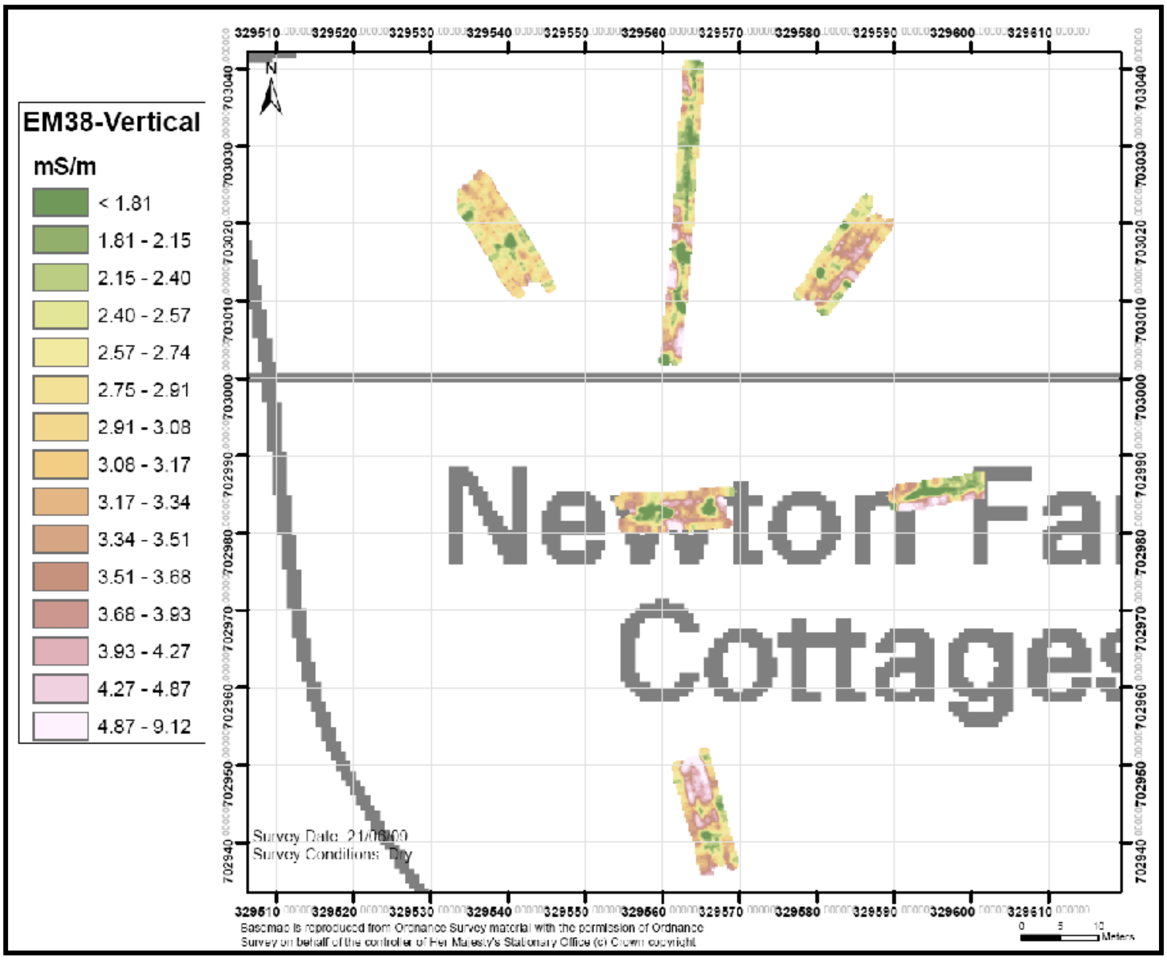

Figure 5.3. EM38 vertical dipole mode (quad-phase) survey over the trenches after removal of ~50 cm of topsoil.

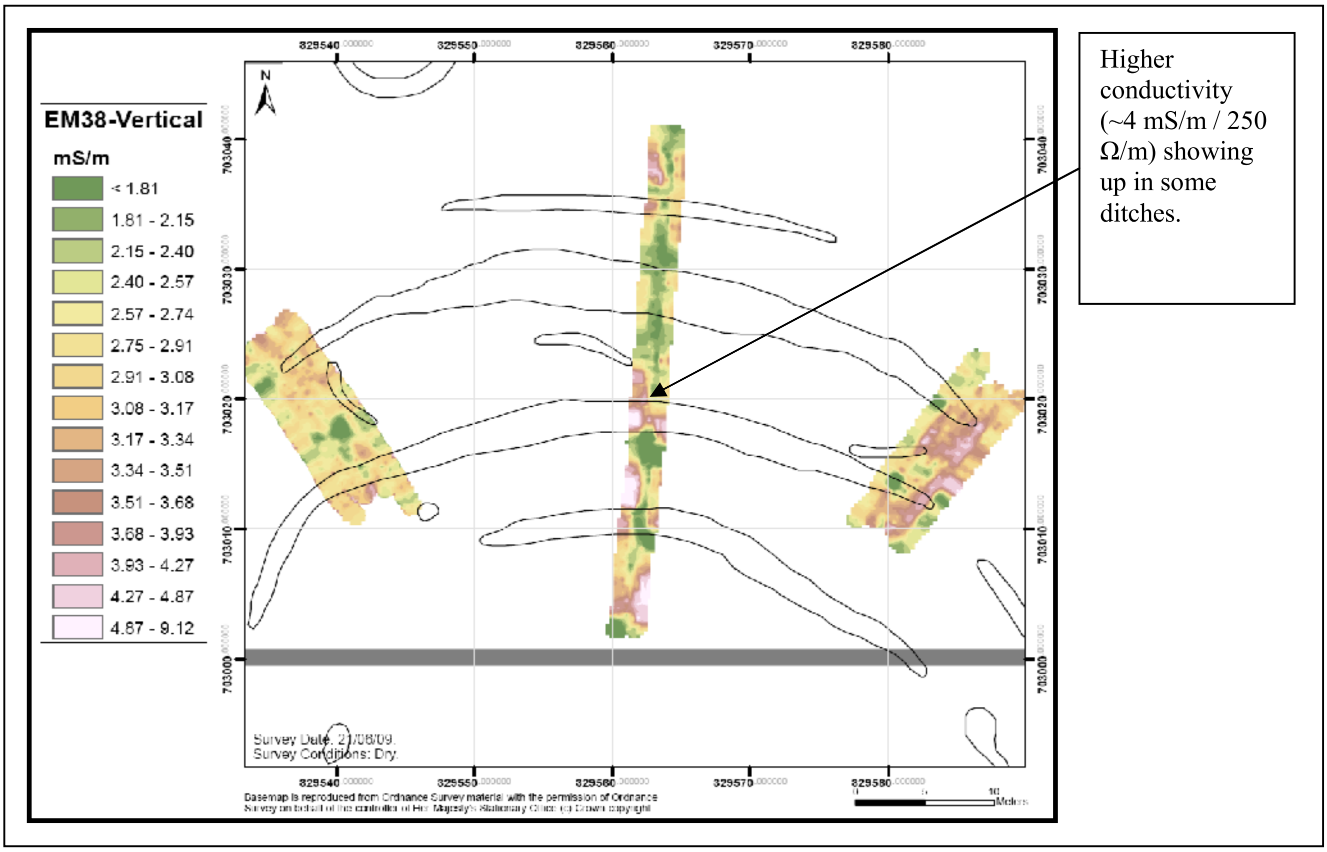

Figure 5.4. EM38 vertical dipole mode (quad-phase) survey over the northern trenches after removal of ~50 cm of topsoil with cropmark annotation.

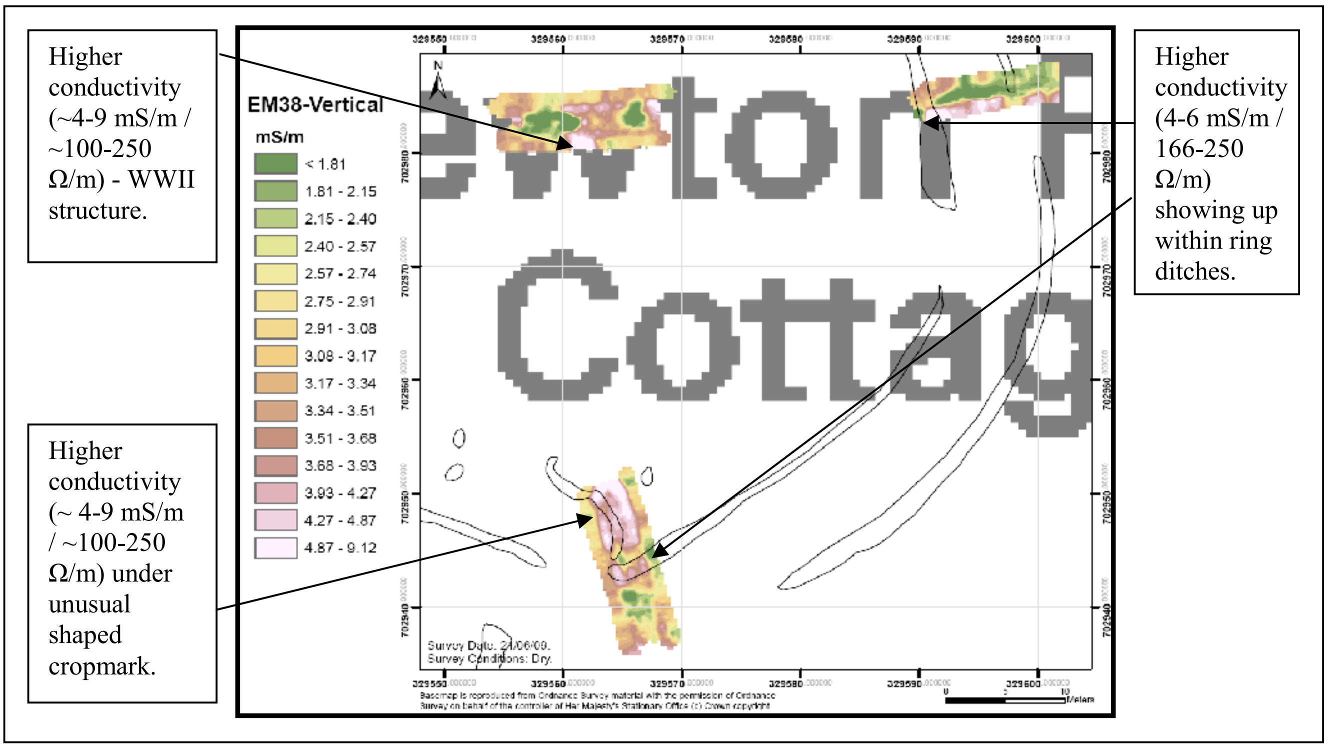

Figure 5.5. EM38 vertical dipole mode (quad-phase) survey over the southern trenches after removal of ~50 cm of topsoil with cropmark annotation.

5.3 Ditch Infill Analysis

During excavation it became apparent that the archaeology present was extremely limited and the features such as ditches were hard to recognize with the naked eye due to similarity in the sediment type and distribution (Figure 5.6). More imagery of the excavation can be viewed in Appendix C.4.

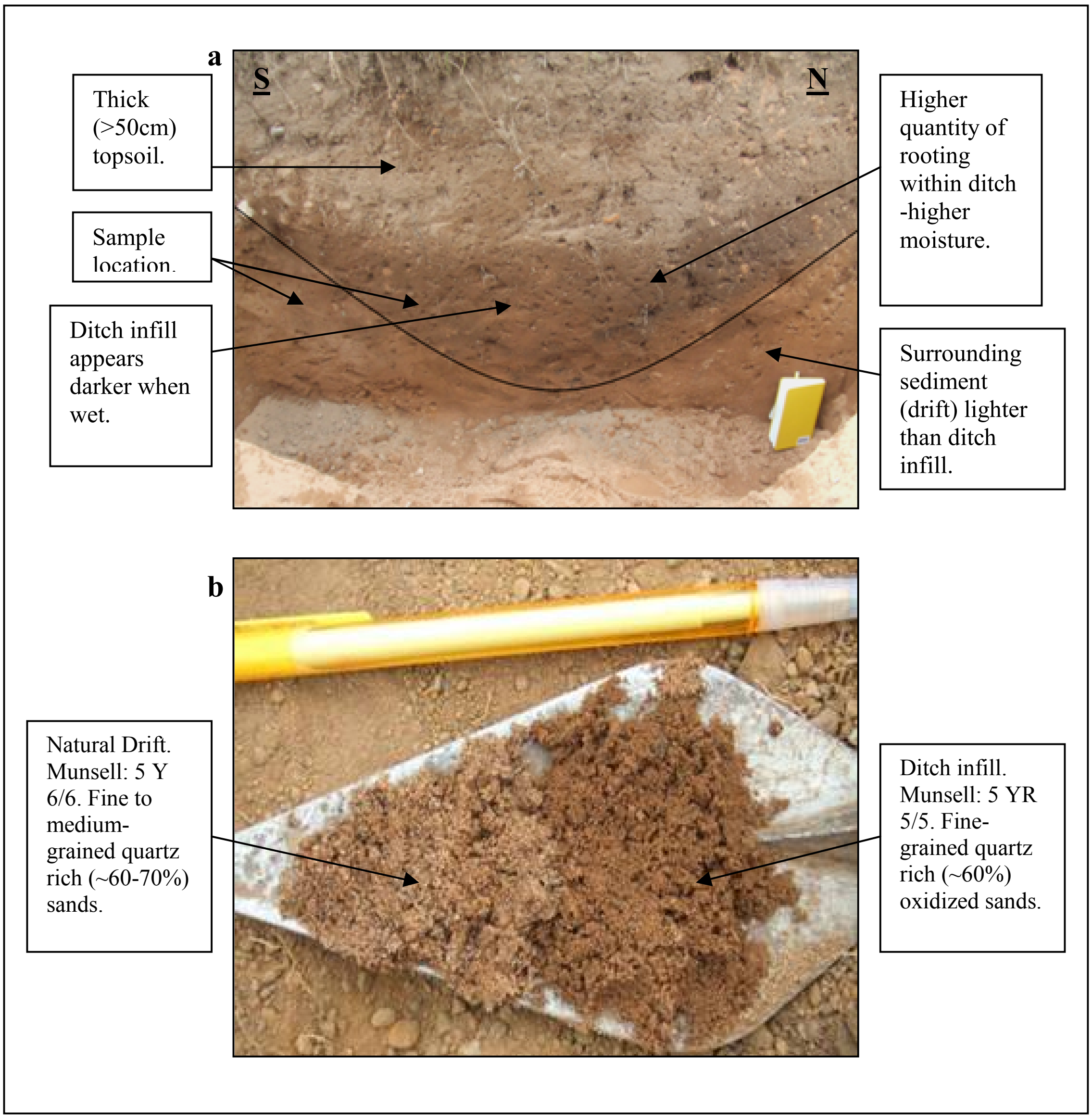

Figure 5.6. Ditch 2 within Trench 6 with an added line to differentiate between the infill and surrounding sediment (**a**) and a trowel showing the contrast in sediment colour when wet (**b**) (Notebook and pencil for scale). Note: sediment in both images has been sprayed with water.

Samples were taken from both the ditch infill and surrounding sediment at the same vertical level (Figure 5.6a and Appendix C) from two of the targeted ditches within Trench 6 (NGR: 329560 703020). As Trench 6 showed the only recognizable ring ditches, samples could only be taken for later laboratory analysis from this location. It was only possible to recognize a significant difference in colour between the two types of soil when wet (Figure 5.6b). Likewise, in the field the composition and grain size were estimated to be very similar (~350 μm average grain size, moderately to well-sorted and ~60% quartz, ~30% feldspar, ~10% lithics). Subsequent XRF, XRD and grain size analysis has shown that the differences between the ditch infill and surrounding sediments were small (Tables 5.1 and 5.2). Mineral and element composition showed little difference between the ditch infill and surrounding sediment with both containing quartz, diopside, anorthite, orthoclase and haematite. Grain size analysis showed that the ditch infill soil has a marginal increase in mean grain size and standard deviation of the grain sizes than the surrounding sediment (Table 5.2). Full XRF, XRD and grain size analysis results can be viewed in Appendix C.

Table 5.1. XRF results for the major elements (%) for sediment within two ditches and the neighbouring sediment outside the ditch for Trench 6 using X-Lab Polarised Energy Dispersive Spectrometer.

Element	SiO_2	Al_2O_3	Fe_2O_3	K_2O	Na_2O	MgO	TiO	P_2O_5	CaO	ClO_2	SO_3
Dimension	%	%	%	%	%	%	%	%	%	%	%
Ditch 2 (Infill)	32.61	3.43	1.89	1.24	0.50	0.25	0.26	0.08	0.20	0.04	< 0.01
Left of Ditch 2	34.23	3.41	1.89	1.43	0.58	0.30	0.21	0.01	0.20	0.04	< 0.01
Ditch 5 (Infill)	35.26	3.10	1.64	1.18	0.49	0.12	0.22	0.08	0.14	0.04	< 0.01
Left of Ditch 5	34.30	3.42	1.76	1.28	0.56	0.27	0.24	0.01	0.13	0.04	< 0.01

Table 5.2. Grain size results using the Coulter LS230 for two ditches sampled for Trench 6.

Third Cycle Measurement	Ditch 2	Left of Ditch 2	Ditch 5	Left of Ditch 5
From (μm)	0.375	0.375	0.375	0.375
To (μm)	2000	2000	2000	2000
Mean (μm)	587	447.7	540.8	371.9
Median (μm)	423.7	301.6	404.1	258.6
Mean/Median Ratio	1.385	1.484	1.338	1.438
Mode (μm)	390.9	429.2	356.1	356.1
S.D. (μm)	519	458.1	479.1	419.2

5.4. Archaeology

Prior to the geophysical survey it was expected that the ring ditches would be interpreted clearly on the presented geophysical data and identified during excavation. As already noted, the ring ditches were barely identifiable and small fragments of bone, flint and charcoal (Figure 5.7) were the only artefacts found which could have been from the Iron Age but realistically could be from any time period.

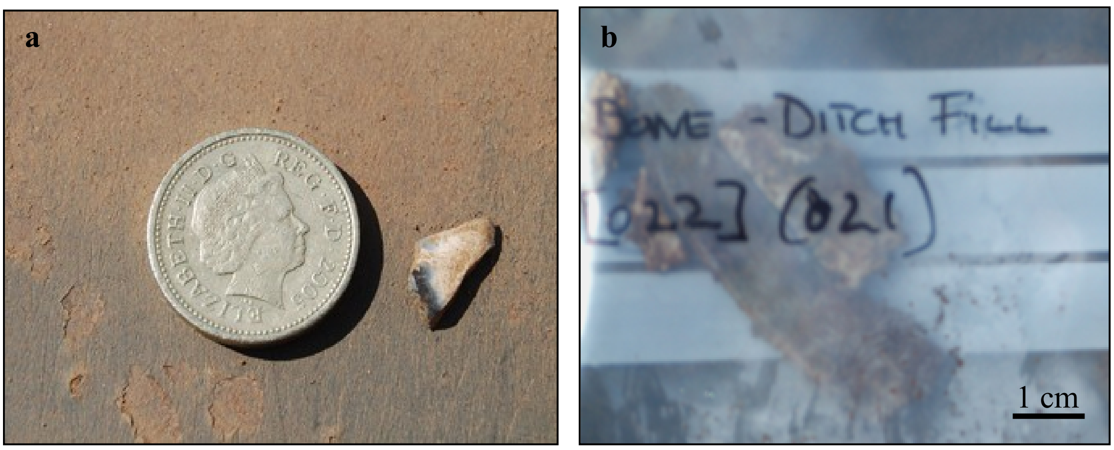

Figure 5.7. A small piece of flint (coin for scale) (**a**) and bone within sample bag (**b**) discovered within the ditch infill.

A relatively modern feature was discovered which dated to the 1940's. Positioned in the centre trench (Trench 2) were the remains of a WWII structure, thought to be a spot light / look out point (Figure 5.8). This structure was able to be dated due to the presence of a metal patent tag related to a barbed wired barricade dated to 1940 (Appendix D.1). Further imagery from the excavation can be viewed in Appendix C.4.

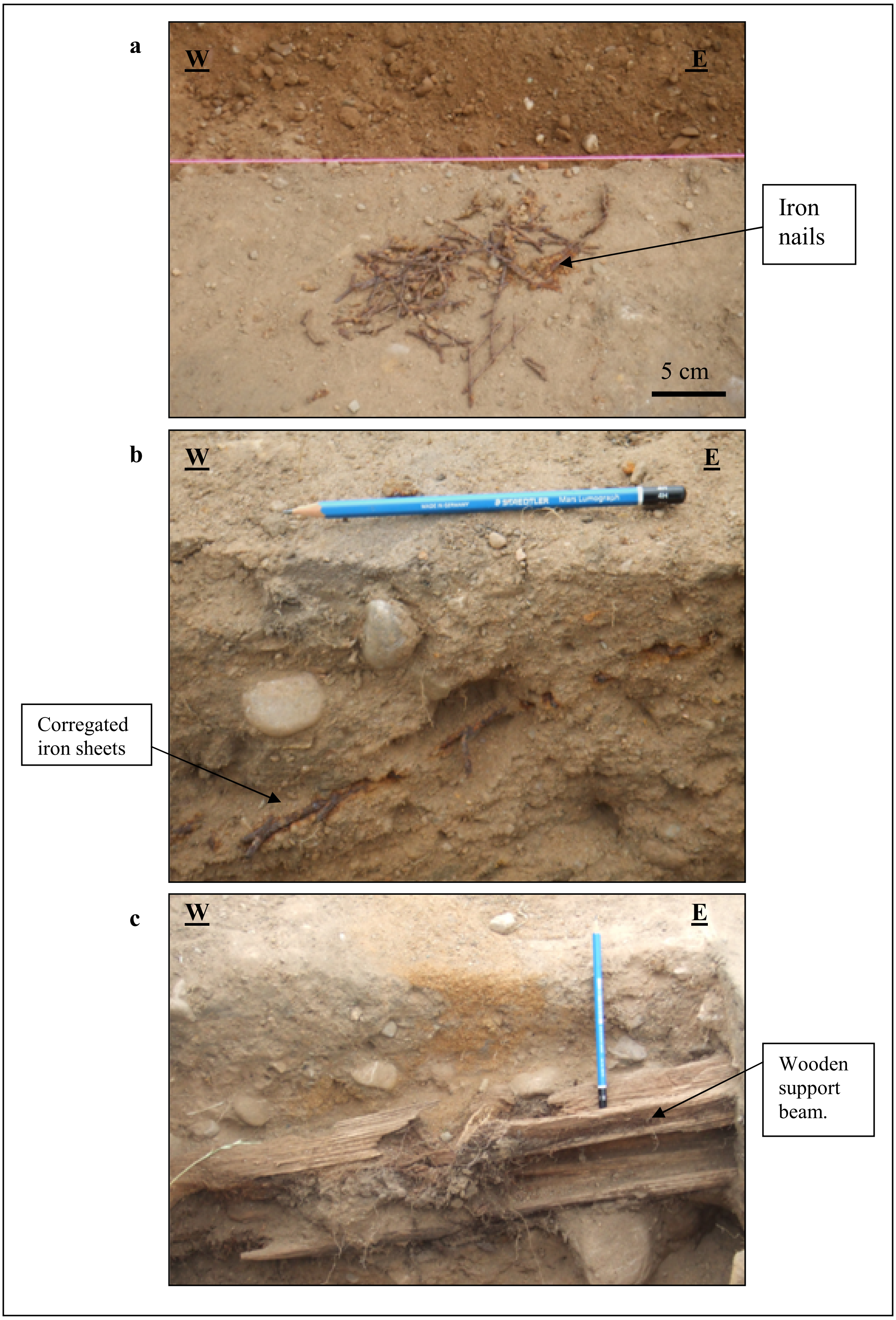

Figure 5.8. Remains of a WWII look out point. Iron nails (**a**), iron sheeting (**b**) and wooden support beams (**c**) discovered whilst excavating the centre trench (pencil for scale).

5.5 Final Model

Despite borehole data giving prior knowledge of the nature of the soil, excavation enabled the geophysical results to be compared with the ground truth from the site itself. The original models showed an expected variation in geophysical response between the ditch infill and surrounding sediment due to contrasting sediment distribution. Subsequent to the geophysical surveying and excavation, the original models were rejected after showing insignificant variations in geology and geophysical response from the ring ditches. Therefore a final geological and geophysical model of the ring ditches and the subsurface on Newton Farm was constructed (Figure 5.9). These models were used as an aid for further interpretation of the results but due to similarities in geophysical signatures between the ditches and surrounding sediment, interpretation of archaeological features was challenging, as recognized from the final model.

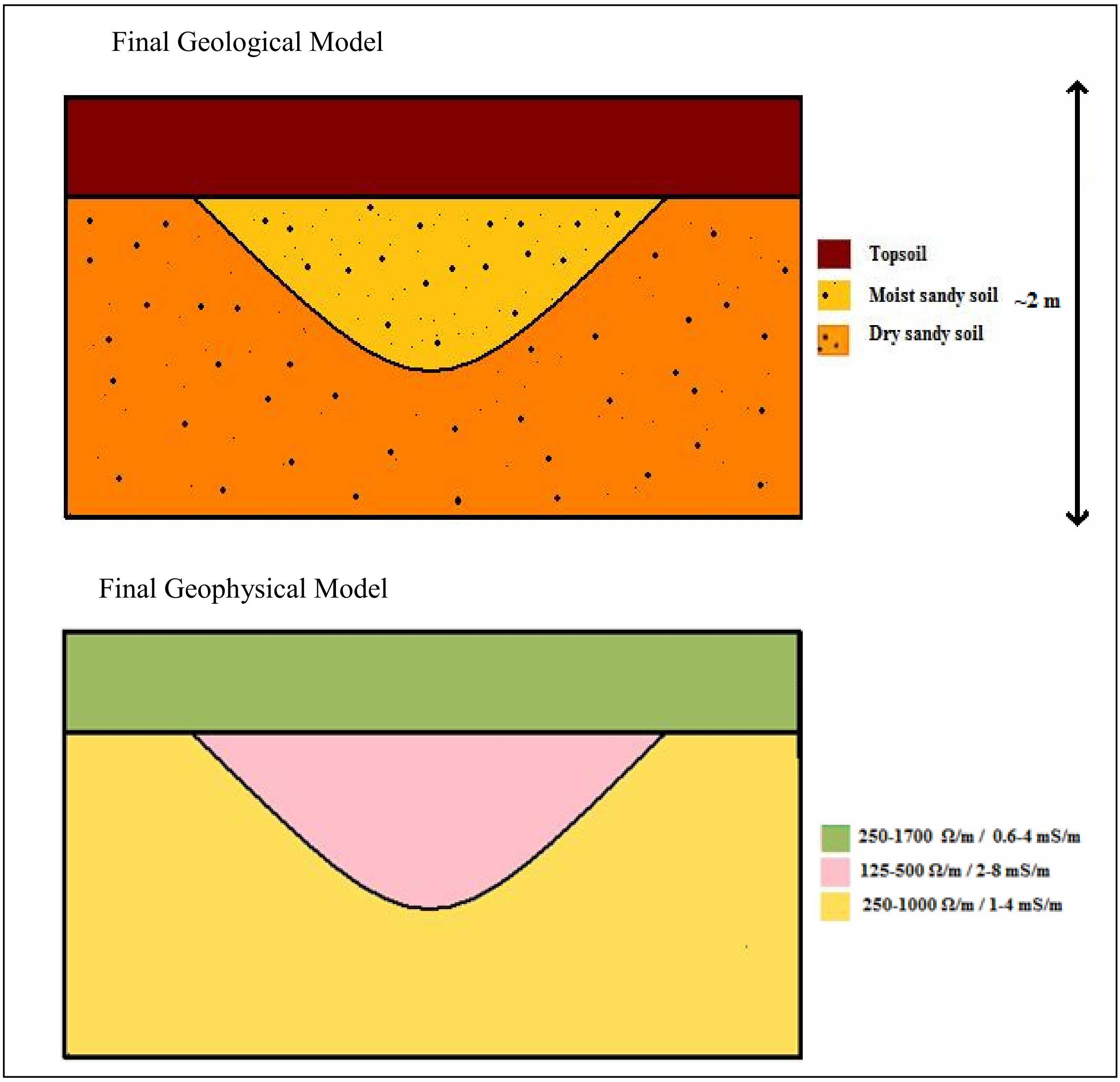

Figure 5.9. Final models of the ring ditches adjusted to ground truth and further surveying after removal of the topsoil from the trenches during excavation. Note topsoil thickness.

CHAPTER 6: DISCUSSION

The aim of this chapter is to form an overall discussion of the results obtained during this investigation in order to try and explain why the geophysical survey was of limited success in allowing interpretation of subsurface archaeology.

6.1 Geophysical Survey

Both DC resistivity and electromagnetism provided limited interpretation of archaeology and although magnetometry and magnetic susceptibility were slightly more successful in detecting some form of underground disturbance and human activity (e.g. NGR: 329580 702973 and 329590 702973), the evidence of a significant previous human settlement is far from convincing.

Ground truth showed there was very little difference in composition and grain size between the ditch infill and surrounding sediment therefore causing insignificant variations in geophysical response. There is also a substantial thickness of topsoil (~50 cm) that has undergone centuries of ploughing with evidence of plough scars at least 50 cm deep (Figure 5.2), suggesting that not only the tops of any archaeological features may have been removed by ploughing but the thick topsoil covering may ‘mask’ the geophysical response of these remnants. This masking effect has shown to influence the survey success with gradiometry and in particular electromagnetism within low conductivity soils (Davis *et al*. 1997; Powlesland *et al.* 2006). This is particularly noticeable when the remnants of the WWII look out point, including bricks, iron sheeting and iron nails were not identified at all with the electromagnetism surveys but was interpreted with magnetometry and magnetic susceptibility. After the topsoil was removed, EM38 surveying over the trenches revealed increases in conductivity values over the ring ditches (from ~2 mS/m to ~5 mS/m) (Section 5.2), providing evidence the topsoil masked the results when using electromagnetism. Even with the aid of the final geophysical model (Section 5.5), it is still difficult to interpret the ring ditches with electromagnetism due to the masking effect. The geophysical model is therefore most appropriate for use with the resistivity surveys or with electromagnetism surveys after the removal of topsoil.

A further survey was performed by Dr. Peter Morris using a Bartington Type 601 magnetic gradiometer (Figure 6.1). Although a slight trace of four of the ring ditches could be recognized, the geophysical variations were again very subtle and were disrupted by large amounts of magnetic clutter. The high disturbance at 50 m east and 35 m north corresponds to the magnetic anomaly at NGR: 329541 700019 identified with the magnetometry survey performed with the GEM GSM-19T proton precession magnetometer (Figure 4.16). Another feature of interest is the linear anomaly trending SSW-NNE but additional surveying and excavation would be required to identify this anomaly. Despite limited evidence of archaeology, this data reveals more archaeology than the magnetometer survey measuring magnetic gradient in Section 4.3 (Figure 4.16). Morris (*Personal Communication,* 2010) has argued two reasons for this. Firstly, he suggested the bottom sensor could have been set-up closer to the ground surface (~25–50 cm) and thus measuring more of the magnetic changes in the near surface. Secondly, the survey grid spacing of 2 m x 2 m was perhaps too large making it less likely to detect the subtle geophysical variations. A smaller grid spacing was considered but due to the time consuming nature of this technique it was only possible to perform the survey on a grid spacing of 2 m x 2 m. Despite this survey having slightly more success in showing geophysical variations relating to subsurface archaeology, this data still supports the other geophysical surveys in suggesting that there are limited archaeological features on Newton Farm.

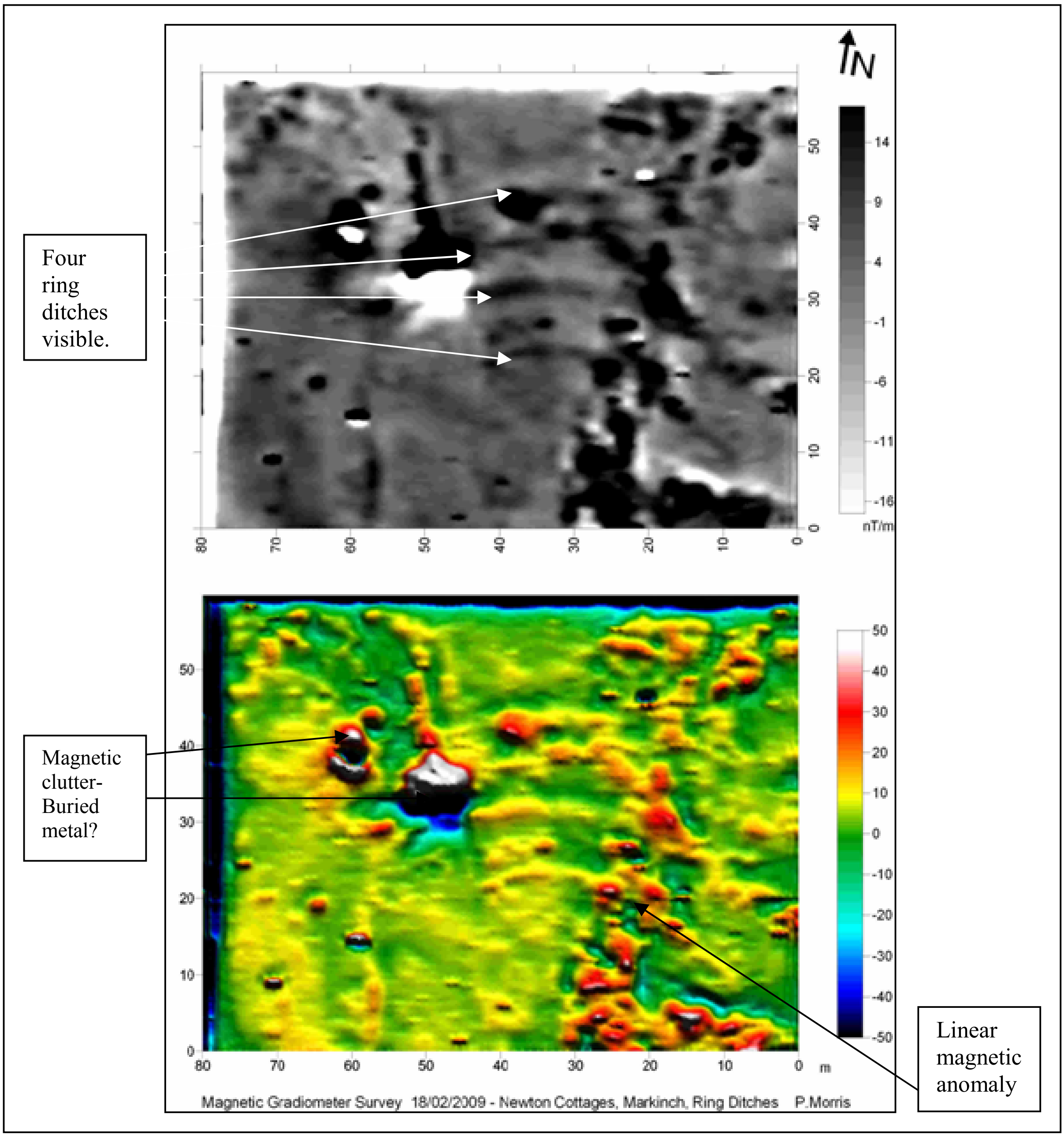

Figure 6.1. The magnetic gradiometer presented results using a Bartington Type 601 magnetic gradiometer on an 80 x 60 m grid with a line spacing of 1 m and in-line sampling of 25 cm in the northern extent of Field 1 (Morris, *Personal Communication,* 2009).

Other possible buried features (probably metallic bodies) were identified with DC resistivity and magnetometry (e.g. GR: 329643 703017) but understanding exactly what these features are would require further excavation.

6.2 Ditch Analysis

Although it was only possible to take samples from two of the ring ditches in one specific location (Figure 5.6a and Appendix C), the results from XRF, XRD and grain size analysis revealed, like the geophysical survey and excavation, that there was only a minor difference between the ditch infill and surrounding sediment. This data suggests that the ring ditches were likely to have been infilled with the surrounding sediment. This similarity between the ditch infill and surrounding sediment made it hard to interpret the ring ditches with the geophysical survey and during excavation and therefore proper excavation only took place on the northern trenches.

Phosphorous levels within soils are known to increase in areas of previous human occupation (Schlezinger & Howes, 2002). It could therefore be suggested that the rise of phosphorous seen within the two ditches was caused by previous human occupation on the site (Appendix C.2). However as it was not possible to perform extensive sampling and as this rise in phosphorous was only 0.07%, it cannot be assumed that human occupation was the only cause of this. For example, as Holliday and Gartner (2006) note, this rise could come from enrichment by soil fertilizer because ditches often retain more phosphorous along with water than the surrounding areas.

Some brief examination of the sediment in the field indicated that there were no visible sedimentary structures within the ditch infill and the grainsize, colour, sorting and composition seemed relatively homogenous throughout. This evidence suggests the ditches could have been infilled by aggradation of windblown deposits with surrounding sediment from the area (French *et al.* 2005). However there were also occasional cobbles (up to 100 m diameter) within the ditch infill and due to their size it is unlikely these were moved into the ditches by natural processes suggesting that man may have had some influence on ditch infilling at times.

As Doerge (1999) notes, electrical conductivity of soil is predominantly determined by porosity, water content, salinity level, cation exchange capacity (CEC) and temperature. As salinity and temperature can be assumed constant, it could be suggested that as the ditches contain sediment with a mean grain size (~140-180 μm) larger than the surrounding sediment, this could allow higher porosity (larger void space) for fluids to reside therefore providing better growth conditions leading to the formation of cropmarks. However, both ditches contain sediment with a larger standard deviation of grain size (~60 μm larger) than the surrounding sediment, suggesting that the grains could be slightly less well sorted leading to lower porosity. A likely scenario is that the ditches retain more moisture through either having differing porosity, permeability or higher % of clay minerals (e.g. montmorillonite and illite) than their surroundings. As XRD did not identify any significant quantities of clay minerals it is likely that grain size and porosity/permeability is the dominant contributing factor for causing the cropmarks. Further study into the packing properties (fabric) of the in situ sediment would help understand whether porosity is the controlling factor in forming these cropmarks, nevertheless the laboratory data collected provides further evidence to explain why the geophysical survey failed to show any significant geophysical variations relating to the ring ditches.

6.3 The Nature of the Soil

After the initial desk study and geophysical surveying, it was evident that the site consisted of very low conductivity sands and gravels. These soils also drain fluids particularly well (high hydraulic conductivity) meaning that during times of limited precipitation, as when the survey was performed, the conductivity values would be particularly low. Due to the nature of the soil (low conductivity sands) and the extensive covering of disturbed plough-soil, the chances of success with the geophysical survey, particularly with electromagnetism, was limited. If the survey was performed at a time when precipitation rates were higher the survey may have shown larger geophysical variations.

As Sheets and Hendrickx (1995) and Reedy and Scanlon (2003) found when operating the Geonics EM31 and EM38 respectively, there is a linear relationship between total soil water content and bulk soil electrical conductivity. As seen in Section 4.2.3, it was found that ground conductivity showed a relationship with topography, suggesting that the electromagnetism surveys performed on Newton Farm revealed that soil electrical conductivity was lower in Field 1, likely to be due to lower soil water content. This, in addition to the low conductivity nature of the soil led to very low conductivity values over Field 1 making it hard to detect any significant variations in the geophysical response with electromagnetism.

6.4 Archaeology

In terms of archaeology the excavation was of limited success. As shown by the extensive geophysical survey, archaeological features were few and far between and even though specific areas were targeted for excavation, it is unlikely that any other areas would have been worthwhile investigating. Ditch analysis and the limited number of artefacts found suggest the site was used very little and may have been restored to its natural state soon after being built. The full archaeological interpretations can be viewed in the Rathmell archaeological report (Appendix D.1).

CHAPTER 7: FUTURE WORK

Due to limited success recognizing subsurface archaeology using geophysics together with excavation, it has been suggested in the final archaeological report by Rathmell Archaeology (Appendix D.1) to investigate no further. However, the following suggestions for future work might help to improve and further the project if desired.

7.1 Ground Penetrating Radar (GPR)

GPR can be used as a first-look technique or a fill-in method between excavations and can provide estimates of depth of the archaeological features (Reynolds, 1997). As the site consists of sediments with very low conductivity values, GPR increases the likelihood of success (Gaffney & Gater, 2003). Watters (2004) is one of many geophysicists to have been successful using GPR when other methods such as electromagnetism and DC resistivity have proved to be of limited success in detecting subsurface features beneath cropmarks. This method has proved to be successful detecting archaeological features such as ditches and pits even when the sediment within the ditches is similar to the surroundings (Figure 7.1). In addition, three dimensional data analysis and visualization software could be applied to the geophysical data in order to extract the third dimension element. This would give a more realistic interpretation of the subsurface archaeology and geologic variations (Watters, 2007).

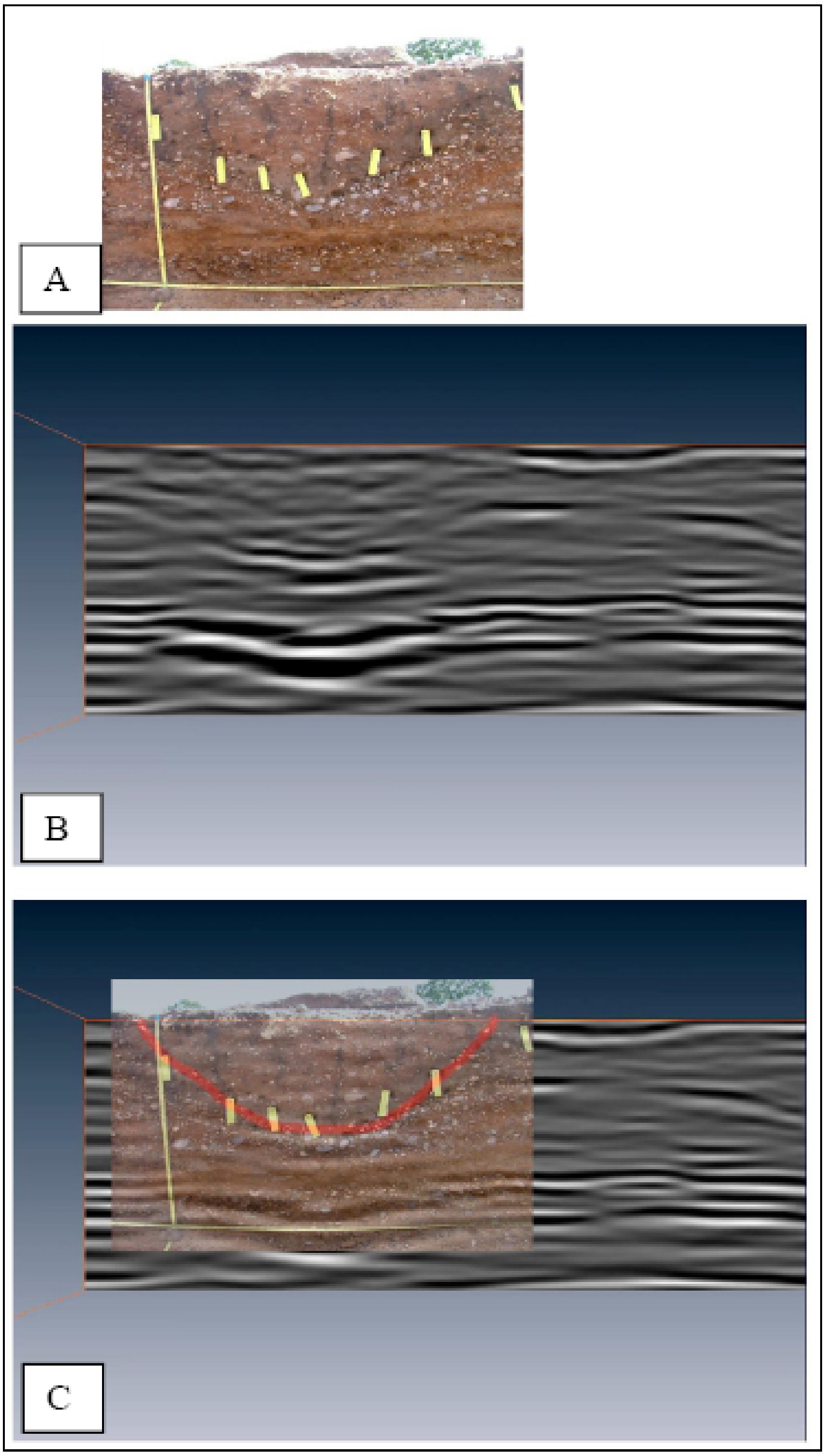

Figure 7.1. GPR used successfully to map a Neolithic ring ditch. The photograph (A) shown is of the corresponding two dimensional GPR anomaly (B) and then this photograph is shown to overlay the GPR presented data (C). N.B. No scale provided (from Watters, 2007).

7.2 Phosphate Analysis

Phosphate detection is probably the most popular geochemical method used in archaeology. As noted previously, human occupation enriches soils with phosphorous and therefore can inform us about the presence of past human intensity and occupation (Terry *et al*. 2000; Holliday & Gartner, 2006). Phosphorous enrichment can occur anthropogenically from addition of human and animal waste, refuse and soil fertilizer (Holliday & Gartner, 2006). Soil phosphorous exists in many forms and analysis of each reveals different results (See Holliday & Gartner, 2006). Clark (1996) suggests that sandy soils, much like the soils on Newton Farm, tend to be the least successful with phosphate analysis due to phosphates being easily lost to drainage. However there is some debate to suggest that phosphates can be drawn back to the surface by vegetation (Clark, 1996) and therefore could indicate areas of human occupation.

CHAPTER 8: CONCLUSIONS

The main aim of this investigation was to understand the size and nature of the archaeology and any other significant subsurface features present on Newton Farm using a range of geophysical techniques. During the course of the investigation the following conclusions were made:

- The resistivity survey was successful in detecting geological variations within the subsurface but failed to recognize any significant archaeological features other than two ring ditches and some buried (probably modern) metallic items.

- The electromagnetism surveys failed to show any significant archaeology with both the EM31 and EM38 in vertical and horizontal dipole mode. The surveys did however show a relationship between topographic variations and ground conductivity, with high conductivities at lower topography and low conductivities at higher topography.

- Magnetometry and magnetic susceptibility successfully located areas of archaeology and areas of previous human activity. These methods were particularly useful in detecting what were later discovered to be the remains of a WWII look out point.

- Surveying of the trenches after the topsoil was removed confirmed the hypothesis that topsoil 'masked' the results with electromagnetism. This gives additional useful information for future surveys of the influence topsoil may have in restricting the success with electromagnetism.

- Ditch sediment analysis showed grain size and composition of the ditch infill and surrounding sediment were similar causing adjustment of the geophysical model. This similarity between the ditch infill and surrounding sediment meant there were only subtle changes in ground conductivity within the site and ultimately limited the success in interpreting any subsurface archaeology.

- GPR could provide a much more successful survey of the site and reveal more archaeology within the subsurface, however geophysical evidence and excavation suggests it may be more appropriate to abandon further research.

- As long as ground conditions are suitable and geophysics can be constrained by ground truth knowledge, geophysical techniques can be used successfully to provide detailed mapping of subsurface features.

REFERENCES

ABDU, H., ROBINSON, D.A. & JONES, S.B. 2007. Comparing bulk soil electrical conductivity determination using the DUALEM-1S and EM38-DD electromagnetic induction instruments. *Soil Science Society of America Jounal*, **71,** 189.

ABEM. (2010) ABEM TERRAMETER SAS 4000 Specification. [WWW] http://www.abem.se/products/sas4000/ABEM_TerrameterSAS4000.pdf (January 25, 2010).

AERIAL ARCHAEOLOGICAL RESEARCH GROUP (AARG). (2009) Anatomy of a cropmark. [WWW] http://www.univie.ac.at/aarg/php/cms/Aerial-Archaeology/short-introduction-to-aerial-archaeology (July 15, 2009).

BARCLAY, G.J. & RUSSELL-WHITE, C.J. 1993. Excavations in the ceremonial complex of the fourth to second millennium BC at Balfarg/Balbirnie, Glenrothes, Fife. *Proc Soc Antiq Scot,* **123**, 43-210.

BARTINGTON. (2009) MS2 Magnetic Susceptibility System. http://www.bartington.com/templates/asset-relay.cfm?frmAssetFileID=122 (August 22, 2009).

BATES, M.R., BATES, C.R. & WHITTAKER, J.E. 2007. Mixed method approaches to the investigation and mapping of buried quaternary deposits: Examples from southern England. *Archaeological Prospection*, **14**, 104-129.

BERNSTONE, C., DAHLIN, T., OHLSSON, T. & HOGLAND, W. 2000. DC resistivity mapping of internal landfill structures: two pre-excavation surveys. *Environmental Geology,* **39**, 360-368.

CENTRAL FEDERAL LANDS HIGHWAY DIVISION. (2009) The DC resistivity arrays. [WWW] http://www.cflhd.gov/agm/engapplications/RoadwaySubsidence/522IndentRoadbedExpanClays.htm (June 29, 2009).

CLARK, A.J. 1996. *Seeing Beneath the Soil. Prospecting Methods in Archaeology.* Batsford, London.

CRANE, P. & POUCHER, P. 2009. Crugiau cemmaes nevern Pemrokeshire. Geophysical survey report No 2009/36. Dyfed Archaeological Trust.

DAVIS, J.G., KITCHEN, R.N., SUDDITH, K.A. & DRUMMOND, S.T. 1997. Using electromagnetic induction to characterize soils. *Better Crops*, **81,** 6-8.

DOCHARTAIGH, B.O. 2002. Water borehole prognosis BGS report No: GR_011078_1. *Georeports.* BGS.

DOERGE, T.1999. Soil Electrical Conductivity Mapping. *Crop Insights,* **19**, 1-5.

FRENCH, C. A.I., LEWIS, H.A., SCAIFE, R. & ALLEN, M. 2005. New perspectives on Holocene landscape development in the southern English chalklands: The upper Allen valley, Cranborne Chase, Dorset. *Geoarchaeology*, **2**, 109–34.

GAFFNEY, C.F. & GATER, J.A. 2003. Revealing the buried past: geophysics for archaeologists. John Wiley & Sons, Ltd. London.

GEONICS LIMITED. (2005) Ground conductivity meters. [WWW] http://www.geonics.com/html/conductivitymeters.html (July 12, 2009).
GISCOGEO. (2006) GSM-19T Proton Precession Magnetometer/Gradiometer. [WWW] http://www.giscogeo.com/pages/magm19t.html (July 12, 2009).

HEWSON, M., HANCOX, E. & K. BAIN. 2005. *Catholme Ritual Landscape Ground Truthing Project 2004: Post-excavation assessment. Aggregates Levy Sustainability Fund (ALSF) Where Rivers Meet Phase II Report 1*. English Heritage, London.

HOLLIDAY, V. T. & GARTNER, W. G., 2006. Methods of soil P analysis in archaeology. *Journal of Archaeological Science.* **34**. 301-333.

JONES, D. M. 2008. *Geophysical survey in field evaluation*. English Heritage Publishing. Swindon.

LE BORGNE, E. 1955. Susceptibilité magnétique anormal de sol superficial. *Annals of Geophysics,* **11**, 399–419.

LE BORGNE, E. 1960. Influence du few sur les propriétiés magnétiques du sol et du granite. *Annals of Geophysics,* **16**, 159–195.

LETHANGIE, J. 2009. Discussion on the history of farming at Newton Farm. [Conversation] (Personal communication, June 10, 2009).

LEWIS, J. 2003. Results of geophysical surveys at two barrow sites in Cheddar and Priddy Parishes, Mendip. *Proc. Univ. Bristol. Soc,* **23**, 9-15.

MANSON, B. 2009. Discussion on the history of Newton Farm. [Conversation]. (Personal Communication, June 14, 2009).

MERCER, R.J. 1981. The excavation of a Late Neolithic henge-type enclosure at Balfarg, Markinch, Fife, Scotland, 1977-78. *Proc Society of Antiquaries of Scotland,* **111**, 63-171.

MERCER, R.J., JORDAN, D., RUSSELL-WHITE, C.J. & BARCLAY, G.J. 1988. Neolithic henge-type enclosure at Balfarg: A re-assessment of the evidence for an incomplete ditch circuit. *Proc. Society of Antiquaries of Scotland,* **118**, 61–67.

MILSOM, J. 2003. *Field Geophysics.* Wiley & Sons, University College London.

MORRIS, P. 2009. The Bartington gradiometer survey [email] (Personal communication, June 18, 2009).

MORRIS, P. 2010. Discussion of the gradiometer results [email] (Personal communication, March 12, 2010).

MURDIE, R.E., GOULTY, N.R., WHITE, R.H., BARRATT, G., CASSIDY, N.J. & GAFFNEY, V. 2003. Comparison of Geophysical Techniques for Investigating an Infilled Ditch at Bury Walls Hill Fort, Shropshire. *Archaeological Prospection,* **10**, 265–276.

MYTUM, H. & WEBSTER, C. (2003) Geophysical surveys at defended enclosures in the neighbourhood of Castell Henllys, Pembrokeshire. [WWW] http://www.coflein.gov.uk/pdf/AENT17_06 (January 20, 2010).

POWLESLAND, D., LYALL, J., HOPKINSON, G., DONOGHUE, D., BECK, B., HARTE, A. & STOTT, D. 2006. Beneath the and Remote Sensing, Archaeology, Aggregates and Sustainability: a Case Study from Heslerton, the Vale of Pickering, North Yorkshire, UK. *Archaeological Prospection*, **13**, 291–299.

REEDY, R. C, & SCANLON, B. R. 2003. Soil water content monitoring using electromagnetic induction. *Journal of Geotechnical and Geoenvironmental Engineering*, **10**, 1028–1039.

RENFREW, C. & BAHN, P. 2001. Archaeology: Theories, methods and practice. Thames and Hudson, New York.

REYNOLDS, J. M. 1997. *An introduction to applied and environmental geophysics.* John Wiley and Sons Ltd, Chichester.

RCAHMS. (2010) Brown Caterthun. [WWW] http://canmore.rcahms.gov.uk/en/site/34969/details/brown+caterthun/ (February 10, 2010).

RCAHMS. (2010) Mains of Edzell. [WWW] http://canmore.rcahms.gov.uk/en/site/34987/details/mains+of+edzell/ (February 10, 2010).

SCHLEZINGER, D.R. & HOWES, B.L. 1999. Organic phosphorus and elemental ratios as indicators of Prehistoric human occupation. *Journal of Archaeological Science,* **27**, 479-492**.**

SHEETS, K. R. & HENDRICKX, J.M.H. 1995. Noninvasive soil water content measurement using electromagnetic induction. *Water Resources Research,* **10**, 2401-2409.

TERRY, R.E., HARDIN, P.J., HOUSTON, S.D., JACKSON, M.W., NELSON, S.D., CARR, J. & PARNELL, J. 2000. Quantitative phosphorus measurement: A field test procedure for archaeological site analysis at Piedras Negras, Guatemala. *Geoarchaeol. Int. J.* **15**. 151–166.

TOPCON POSITIONING. (2010). Topcon HiPer Pro. [WWW] http://www.topconpositioning.com/products/gps/geodetic-receivers/integrated/hiper-pro.html (January 25, 2010).

YOUNG, T. (1998) Using the Geonics EM31. [WWW] http://www.geoarch.co.uk/field/em31.html (June 27, 2009).

WATTERS, M.S. 2004. GPR: a tool for archaeological management. *Proceedings of GPR 2004, Tenth Intemational Conference on Ground Penetrating Radar, 21-24 June, 2004*, Delft, The Netherlands.

WATTERS, M.S. 2007. *New methods for archaeo-geophysical data visualization.* Unpublished Ph.D. thesis, The University of Birmingham.

WALDEN, J., OLDFIELD, F. & SMITH, J.P. 1999. *Environmental Magnetism: a practical guide.* Quarternary Research Association, London.

APPENDICES

APPENDIX A: BOREHOLE DATA

A.1: Location of BGS Borehole Data

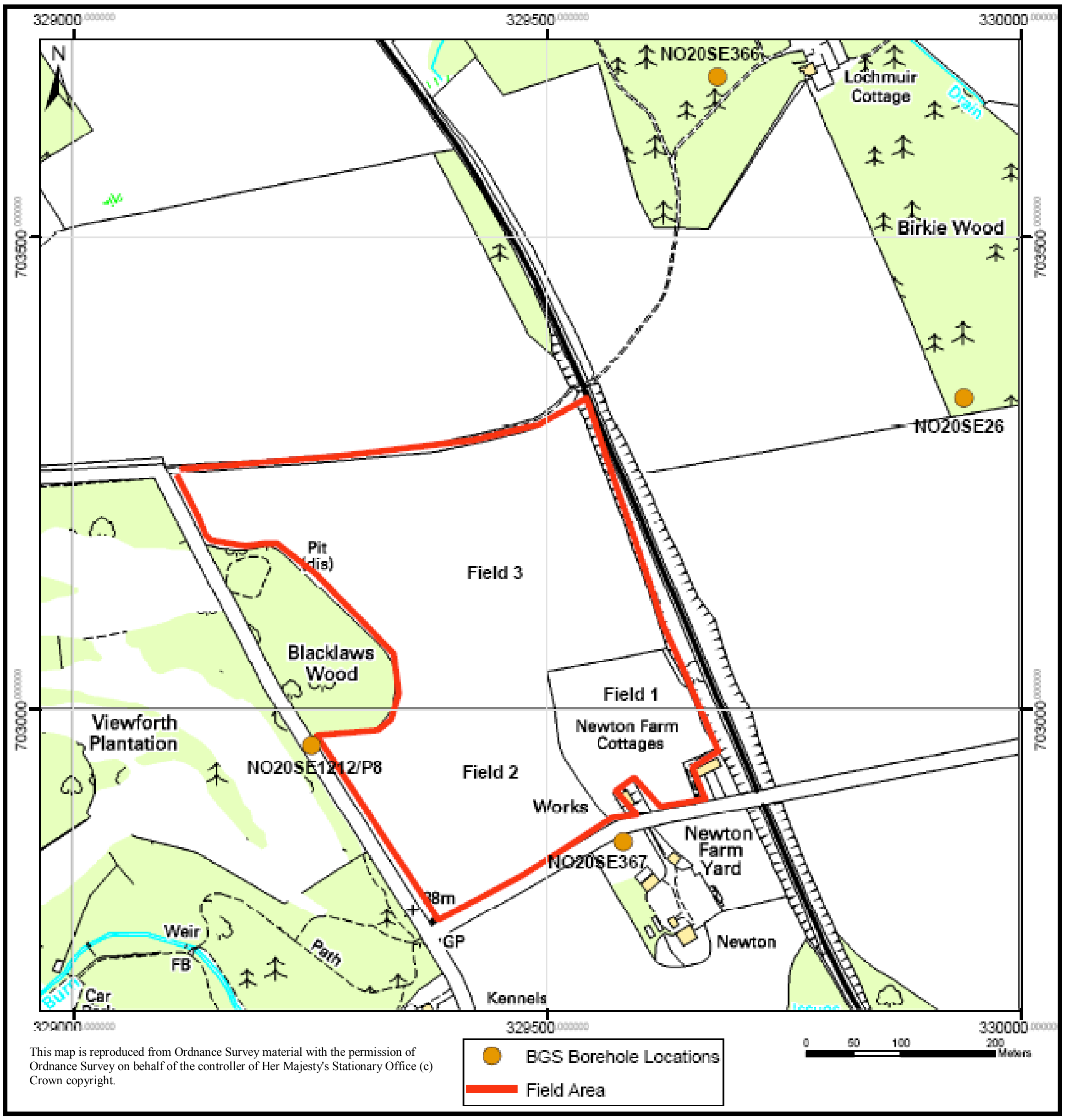

Figure A.1.1. The location of the four boreholes near Newton Farm used to define the geological conditions for preparation of the geological and geophysical model. Each borehole is labelled on map.

A.2: Summary of Borehole Data

The BGS borehole data from the 4 sites was conglomerated to form an expected model of the geology beneath Newton Farm. As boreholes NO20SE367 and NO20SE1212/P8 were closest to the main site it was assumed these would have the most likely reflection on the underground geology of Newton Farm and therefore had more bias in the production of the summary below.

Geological Classification	Lithology / Description of Strata	Thickness	Depth	B.H.
Head	Made ground	0.5 m	0.5 m	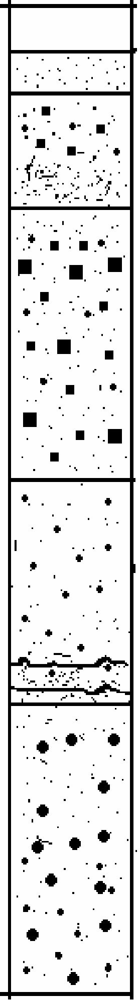
	Soil, sandy loam	0.5 m	1.0 m	
	Clay, sandy, stony, red-brown, sub-angular to sub-rounded, clasts up to 30 mm. Clasts- red and yellow sandstones, quartzite, dolerite and coal. Sandier with depth.	1.5 m	2.5 m	
Glacial sand and gravel	a) Sandy gravel Gravel: fine to coarse-grained with cobbles up to 100 mm, sub-rounded to rounded, red and yellow sandstone, dolerite and quartzite. Sand: fine, medium and coarse-grained, sub-angular to sub-rounded, quartz, felspar and lithics. Fines: occasional thin silty clay seams (red/brown).	6 m	8.5 m	
	b) Pebbly sand Gravel: fine, sub-rounded, sandstone and occasional coal clasts. Sand: fine and medium-grained with coarse sub-rounded to well rounded, quartz, feldspar and lithics. Fines: silt, spread widely and as laminae increasing with depth. Light brown.	3 m	11.5 m	
	c) Sandy gravel Gravel: fine to coarse with cobbles up to 100 mm, sub-rounded to rounded, red and yellow sandstone, dolerite and lower quantities of andesite, quartzite, vein-quartz, felsite, siltstone and mudstone. Sand: fine to coarse-grained, fining upwards, angular to sub-rounded, predominantly quartz and feldspar. Fines: rare silt, light brown	13 m	24.5 m	

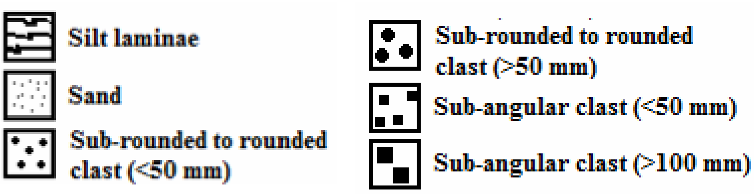

Figure A.1.2. Combined data from the 4 boreholes to come up with a hypothetical borehole model for Newton Farm (not to scale).

APPENDIX B: FIELD SURVEY

B.1: Theory of Geophysical Techniques

B.1.1: *DC Resistivity*

In simple terms DC resistivity passes electrical currents into the ground and resistance to the flow of the currents is measured. The ability of allowing current flow is directly related to the interstitial water retained in the soil and any salts that may be present (Gaffney & Gater, 2003). These waters carry charge as electrolytes (Reynolds, 1997).

Resistivity geophysical methods are based on Ohm's Law (R=V/I) where the resistance (R) is established by calculating the current (I) flowing through the material and observing the change in voltage (V). As the current is kept constant, the resistance can be calculated by accessing the change in voltage. Resistivity (ρ= R(A/l)) where A is the cross-sectional area and l is the length of the material, is a more useful property, which is a measure due to the material itself. It will not change with the amount or shape of that material (Gaffney & Gater, 2003). A direct current is passed through the ground by two electrodes and the resulting voltage induced (resistance) in the ground, which may or may not be affected by subsurface variations, is then sampled by two electrodes between these two points, giving an apparent resistivity.

The apparent resistivity for the Wenner Array is calculated with the following equation:

$$\rho_\alpha = 2\,\pi\, a\,(V/I)$$

Where, ρ_α = apparent resistivity
a = electrode spacing
V= Voltage
I=Current

B.1.2. *Electromagnetism*

EM methods primarily use the response of the ground to the propagation of EM waves. EM energy is transported into the ground by induction which occurs when an object/material is magnetized due to the introduction of an external magnetic field and then is demagnetized after removal of the external field. For FDEM a sinusoidally varying alternating current is passed through the transmitter coil (Milsom, 2003). This transmitter coil then induces an alternating magnetic field which can penetrate the ground energizing it with 'time-varying electromagnetic fields'. Faraday's Law, EMFc= M_{TC}^{*} (d_{IT}/dt) where EMFc is the electromotive force, M_{TC} is the mutual inductance and d_{IT}/dt is the time rate of change of current, suggests that the 'time-varying electromagnetic fields' induce eddy currents and electromotive forces within subsurface conductors (Reynolds, 1997). The induced fields (secondary fields) are then picked up by the receiver coil where two currents are measured, the current direct from the transmitted coil (primary field) and the currents induced in the ground (Figure 3.6). The differences between the primary and secondary fields indicate the presence of a conductor and its properties. For this survey the secondary field is measured by electronically separating the transmitted and induced fields into the real component in-phase with the transmitted field, and the quadrature (quad-phase) component which is 90^{o} out-of-phase with the transmitted field. In systems with the option of two dipole modes, vertical dipole mode has a better depth of penetration than horizontal dipole mode because the vertical field can couple better with material in the earth than the horizontal field (Abdu *et al.* 2007).

B.1.3: *Magnetometry (Gradiometry)*

Surveying was carried out with a proton precession magnetometer measuring the vertical gradient of the total magnetic field. This consists of two sensing elements mounted above each other on a vertical pole. The sensing elements consist of hydrocarbon fluid with a larger number of protons (Milsom, 2003). A current is passed through a copper coil wound around the sensing element creating a magnetic field to which the proton moments are aligned. When the current is removed the protons align with the ambient magnetic field which is both the Earth's magnetic field and that of any magnetic anomalies (Clark, 1996). These two measurements, the Earth's magnetic field and that of magnetic anomalies, are then subtracted from one another therefore leaving only the measurement of features local to the instrument.

B.1.4: *Magnetic Susceptibility*

Gradiometers respond to the change in magnetic susceptibility, however in some cases the absolute value can be just as useful, particularly in archaeological sites that have minimal physical imprint (Gaffney & Gater, 2003). Iron compounds are relatively insoluble which means they often concentrate in the soil. Enhanced topsoil magnetism involves the development of ferrimagnetic compounds from other forms (Clark, 1996). The main cause for magnetic susceptibility enhancement is through burning (Le Borgne, 1955; 1960). Le Borgne (1955, 1960) found that the alternation of reducing and oxidizing conditions enabled the conversion of haematite to maghaemite with magnetite as an intermediate stage. Clark (1996) notes that all magnetically susceptible natural materials have a characteristic 'susceptibility spectrum'. This 'susceptibility spectrum' is a calculation of the natural materials susceptibility variation with change in frequency. By sampling this frequency spectrum, dual frequency measurement can supply information on the nature and size distribution of the magnetic minerals present (Clark, 1996).

B.2: GEOPHYSICAL EQUIPMENT SPECIFICATIONS AND OPERATING PROCEDURES

B.2.1: ABEM Terrameter SAS 4000 Resistivity

Table B.2.1. Technical Specifications: Terrameter SAS 4000 Resistivity, IP & SP (from ABEM, 2010).

General	Memory Capacity More than 1 500 000 readings Display LCD, 200 x 64 pixels. 8 lines of 40 char. Multifunction connector Current and potential for all four channels including RS232 communication for external devices as PC, LOG & Imaging External devices LUND Imaging System, SAS LOG Power Optional Clip-on rechargeable power pack or external 12V DC through SAS-EBA Casing Rugged cast Aluminium case, meets IEC IP 66 Weight 5.3 kg Dimensions 105 x 325 x 270 mm (W x L x H) with SAS-EBA Ambient temperature -5°C to + 50°C, operating
Receiver: Resistivity	Number of channels 4 bipolar, galvanically isolated Input impedance 10 M Ω minimum Resolution (theoretical) 30 nV WI Accuracy (typical) 1 % WI Precision (measured) better than 0,1 % (in the range 4 - 200, Ω at 1 second integration) Dynamic range Up to 140 dB plus 64 dB automatic gain (at 1 second integration)
Transmitter	Output current 1,2,5,10,20,50,100,200,500,1000 mA (operator set or autoranging) Maximum output voltage 400 V (800 V peak-to-peak) Maximum output power 100 W Cycle type in resistivity mode Plus-Minus-Minus-Plus Cycle type in IP mode Plus-Zero-Minus-Zero Pulse length 0.1 to 4 seconds Output current accuracy Better than 0,5 % at 100 mA

Abem Terrameter SAS 4000 Resistivity Simplified Operating Procedure

1) Electrodes connected to cable roll with 1 m interval spacing. The two centre cable rolls are then attached to the Lund imaging system.

2) Turn on Lund imaging system, press red button selecting ‘resistivity’.

3) Press red button again until screen says ‘Protocol #1: CRAD4lX8’ then press red.

4) Automatic electrode check runs.

5) If all ok then the system will automatically start to record. If system says faulty electrodes check the transect for bad electrode connections before starting to record.

6) When complete the system automatically goes to screen ‘Protocol #2: GRAD4SX8’. Press red button.

7) System will again check for any faulty electrodes and automatically record after.

B.2.2: *Geonics EM31*

Table B.2.2. Technical Specifications: Geonics EM31 (from Geonics Limited, 2005)

Measured Quantities	1.Apparent conductivity in millisiemens per metre (mS/m) 2: In-phase ratio of the secondary to primary magnetic field in parts per thousand (ppt)
Primary Field Source	Self-contained dipole transmitter
Sensor	Self-contained dipole receiver
Intercoil Spacing	3.66 metres
Operating Frequency	9.8 kHz
Power Supply	8 rechargeable 'C' cells (approx. 20h continuous)
Measuring Ranges	Conductivity: 10, 100, 1000 mS/m In-phase: +/- 20ppt
Measurement Resolution	+/- 0.1% of full scale
Measurement Accuracy	+/- 5% at 20 mS/m In-phase: 0.03 ppt
Noise Levels	Conductivity: 0.1 mS/m In-phase: 0.03 ppt
Data Storage	Data stored used the Allegro CX handset running Geomar 'Trackmaker 31'.
Dimensions	Boom: 4.0m extended, 1.4m stored Shipping Case: 145 x 38 x 23 cm
Weight	Instrument: 12.4 kg Shipping: 28 kg

Geonics EM31 Operating Procedure (Young, 1998)

Initial Set-up

1) Check batteries (has to be above ±4.4 V).

2) Attach transmitter coil tube.

3) Set to 'OPER' and check the zero reading. Tolerance is ±1 mS/m.

4) Turn off and attach receiver tube.

Equipment Functional Checks

5) Set 'RANGE' switch to 100 mS/m.

6) Use 'Coarse' and 'fine' compensation tools in 'OPER' mode to adjust in-phase meter.

7) Check phase by ‘MODE’ switch set to ‘phase’. Noting the meter reading and rotating the ‘coarse’ control one click clockwise. If within +/- 0.2, phase correct.

8) If different with the coarse control in original position, adjust the PHASE potentiometer ¼ turn clockwise or anticlockwise until correct.

9) Sensitivity Test: ‘MODE’ switch set to ‘comp’ and ‘coarse control rotated one click clockwise. Conductivity reading should increase by 22 to 26 mS/m.

Operating Procedure

10) Instrument rests on hip with use of strap. ‘MODE’ switch set to ‘OPER’.

For removal of the data from the EM31 to computer

1) Memory ‘flash’ card removed from Allegro handset.

2) Data transferred from memory card to computer hard drive and given individual file names.

3) Data converted into ‘xyz’ file using Trackmaker software.

4) Opened up in Microsoft Excel and displayed with ‘Surfer’ for quick analysis.

5) Data transferred to Minitab (dbase file extension) for final processing.

6) ArcMap used for final presentation and analysis of data.

B.2.3: ***Geonics EM38***

Table B.2.3. Technical specifications: Geonics EM38 (from Geonics Limited, 2005)

Measured Quantities	1: Apparent conductivity in millisiemens per metre (mS/m) 2: In-phase ratio of the secondary to primary magnetic field in parts per thousand (ppt)
Primary Field Source	Self-contained dipole transmitter
Sensor	Self-contained dipole receiver
Intercoil Spacing	1 metre
Operating Frequency	14.6 kHz
Power Supply	9V PP3 battery (30 hours continuous)
Measuring Ranges	Conductivity: 1000 mS/m In-phase: +/- 29ppt
Measurement Resolution	+/- 0.1% of full scale
Measurement Accuracy	+/- 5% at 30 mS/m
Noise Levels	Conductivity: 0.5 mS/m In-phase: 0.02ppt
Data Storage	External using the Allegro CX handset running Geomar 'Trackmaker 38'. Output: Serial
Dimensions	Instrument: 106 x 15 x 3.6 cm Shipping Case: 117 x 19x 13 cm
Weight	Instrument: 3 kg Shipping: 10 kg

Geonics EM38 Operating Procedure (edited from Geonics Limited, 2005).

Initial Set-up

1) EM38 set to 1000 mS/m.

2) Check battery by switching power switch to 'BATT'. Needs to be between -1500 and -720.

Calibration

Calibration should be carried out at least 3 times per day.

3) Turn on. When the EM38 is on the ground in vertical mode, switch to Q/P mode and use Q/P reading to zero using the Q/P zero control knob.

4) Set mode switch to I/P and set the I/P reading to zero using the I/P Coarse and Fine controls. Return back to Q/P and ensure the Q/P reads zero and note the position of the I/P Coarse control knob.

5) A one-step clockwise rotation of the I/P Coarse Control knob should not change the reading.

6) When the EM38 is lifted ~1.5 m above the ground and in horizontal mode, set the Q/P and I/P readings to zero as in steps 3 and 4.

7) With mode switch set to the Q/P position, adjust the Q/P Zero control so that an arbitrary value appears on the display. Without changing the instrument height, rotate to vertical mode and note the reading. Subtract the horizontal reading from the vertical reading.

8) With the mode switch still in Q/P position and the instrument in horizontal mode, rotate the Q/P Zero Control until the display reads the value calculated in step 7. When this is done and the EM38 is rotated back to vertical mode the reading should be double that of the horizontal reading.

For proper setting of instrument zero: When the instrument is at least 1.5 metres above the ground, the Q/P reading should satisfy the equation:

$$V=2H$$

V= vertical dipole mode reading.

H=horizontal dipole mode reading.

In some cases, as on Newton Farm, there is no change in the reading when rotating the dipole from one position to the other (V=H). This occurs when the ground is highly resistive. Therefore, the reading of both dipoles should be adjusted to zero, with the equation V=2H still satisfied.

<u>For removal of the data from the EM38 to computer</u>

The same process was used as for the EM31 (Section B.2.2).

B.2.4: *GEM GSM-19T Proton Precession Magnetometer*

Table B.2.4. Technical specifications: GEM GSM-19T Proton Precession Magnetometer specifications (from Giscogeo, 2006).

Sensitivity:	<0.1 nT (0.2 nT at 1 or 2 sec rate with 'W' option)
Resolution:	0.01 nT
Absolute Accuracy:	1 nT
Dynamic Range:	10,000 to 120,000 nT
Gradient Tolerance:	Over 7000 nT/m
Sampling Rate:	1 reading per 3 to 60 sec, (1 to 60 sec for 'W' walking option)
Operating Temperature:	-40C to +60C
Storage:	4 Mb
Console Dimensions:	223 x 69 x 240 mm
Sensor Dimensions:	170 x 71 mm diameter cylinder
Console Weight:	2.1 kg
Sensor + Staff Weight:	2.2 kg

GEM GSM-19T Proton Precession Magnetometer Simplified Operating Procedure

1) Connect equipment together allowing 56 cm between the two sensors making sure both sensors face the same direction.

2) Press A > SURVEY.

3) Press nf > for each new block.

4) Press C.

5) Press F 4 times in succession.

6) Line # > check correct line increment increases by 2 (2 m).

7) Line increment > leave at 0.

8) Station # > set to new station start.

9) Station increment > set to "+2" (+2 m).

10) EOL increment > Leave at +2 (+2m).

11) F > OK > Start survey using any key.

<u>For removal of the data from magnetometer to computer</u>

1) Computer operated in MS-DOS mode and GSM-19T handset connected.

2) Gemlink software operated.

3) GSM-19T turned on and correct field selected (press F for ok then A for data).

4) Data saved in excel and transferred to Minitab for processing and ArcMap for final presentation.

B.2.5: Bartington MS2 Magnetic Susceptibility Specifications

Table B.2.5a. Technical specifications: Bartington MS2 Meter (from Bartington, 2009)

Measuring range-volume specific -mass specific	1-9999 x 10-5 SI (10-6 CGS) 1-9999 x 10-8 SI (10-6 CGS)
Resolution - volume specific	2 x 10-6 SI (2 x 10-7 CGS) on x0.1 range. The resolution achieved will depend on temperature drift and environmental noise.
Internal battery	0.7 Ah sealed NiMH give 8 hours continuous use before recharge is required
Enclosure material	High impact ABS
Operating temperature	10oC to 40oC
Weight	1.2kg
Dimensions	260 x 158 x 50mm
Sensor cable	50 ohm TNC to TNC, 1m length
Battery charger inlet	2.1mm socket, 6-18VDC, 100mA maximum, polarity protected
RS232 interface	1200/9600 baud selected on rear panel
Interface connector	4-way rear panel Fischer socket

Table B.2.5b. Technical specifications: MS2B Dual Frequency Sensor (from Bartington 2009)

Calibration accuracy	1% (10ml calibration sample provided)
Measurement period x 1 range x 0.1range	1.5s SI (1.2s CGS) 15s SI (12s CGS)
Operating frequencies: LF HF	0.465kHz ±1% 4.65kHz ±1%
Amplitude of applied field	250µT peak ±10% (LF & HF)
Maximum resolution	2 x 10-6 SI (vol) (2 x10-7 CGS) (LF & HF)
HF/LF cross calibration	0.1% worst case (can be adjusted using calibration sample)
Temperature induced drift:	Sample to sensor differential ±0.05 x 10-5 SI/ºC/minute (LF& HF) (±0.05 x 10-6 CGS/ºC/minute)
Enclosure material	High impact ABS
Weight	0.7kg
Dimensions	210 x 145 x 110mm

B.3: HiPer Pro Topcon integrated RTK GPS Specifications

Table B.3. Technical specifications: HiPer Pro Topcon GPS (from Topconpositioning, 2010).

Tracking	
Signal	GPS/GLONASS L1/L2 C/A and P Code & Carrier WAAS/EGNOS
Channel	40
Cold Tracking	<60 seconds
Warm Tracking	<10 seconds
Reacquisition	<1 seconds
Accuracy	
Static	3mm +.5ppm, horizontal, 5mm +.5ppm vertical
RTK/Kinematic	10mm + 1ppm horizontal, 15mm + 1ppm vertical
Physical	
Enclosure	Aluminium construction
Dimensions	158.5 x 113 x 173 mm
Weight	1.65 kg
Color	Topcon Grey
Environmental	
Operating Temperature	-30 to +55 degrees Celsius
Storage Temperature	-20 to +35 degrees Celsius
Humidity	95 %
Power	
Internal Battery	Li-ion, 4000 mAh, 7.4V x 2 batteries
Operating Time	14+ (10 TX) Hours
External Power	1 port(s)
Input Voltage	6 to28 V DC, 2 minimum charge
Power Consumption	4.2 Watts
Battery Charger	AC Adaptor
Charging Time	unknown Hours
Communication	
Bluetooth	1.1 comp.
USB	1.1 Version
Serial Port	A/D port, 460800,230400,115200(Default),57600, 38400,19200,9600,4800,2400,1200,600, 300 Baudrate, RTS/CTS Flow Control, 7, 8(Default) Length, 1 (Default), 2 Stop bit, None (Default), odd, even Parity
Key and LED	
Key	3: on/off, Function, Reset
LED	4: Satellite, data status, battery, modem status
Memory	
Internal Memory	Compact flash card
Capacity	1024 (optional) MB
Logging Time	53 Hours
Connectors	
External Power Port	1 port(s), 5 pin ODU
External Antenna Connector	TNC connector
Radio Antenna Connector	BNC connector
Serial Port	2 (Port A and D) port(s), 7 pin ODU

B4: EM38 Vertical Mode-Trenches

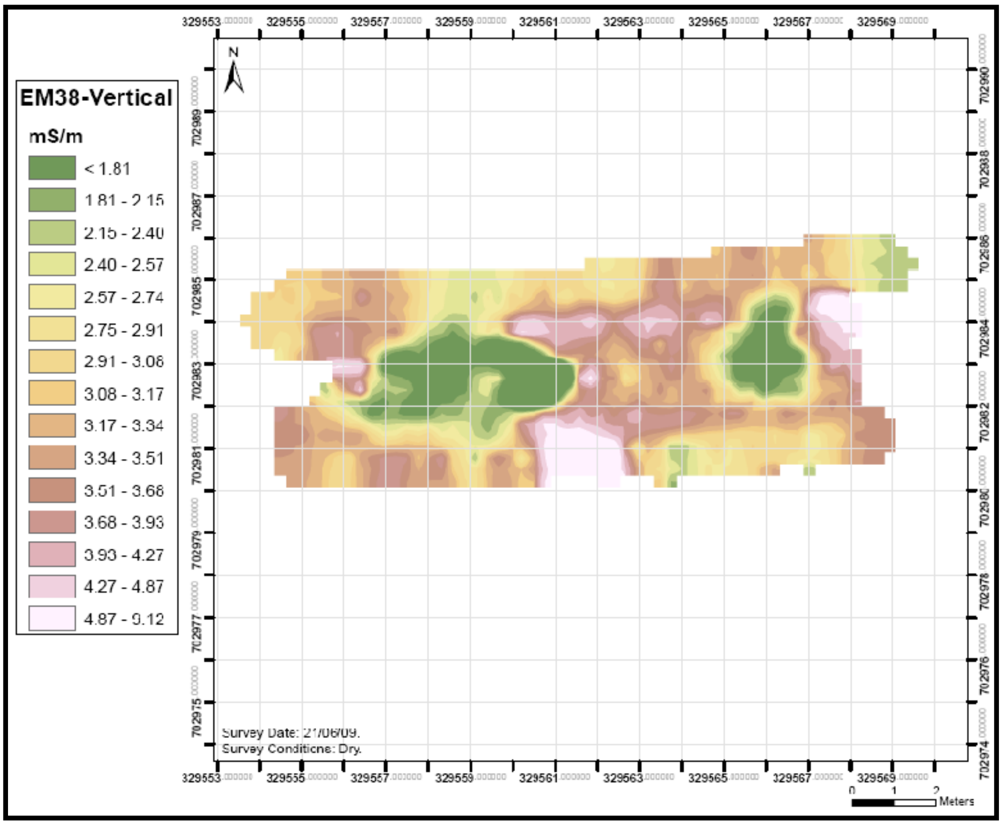

Figure B.4.1. EM38 vertical mode (Q/P) of Trench 2 without topsoil covering.

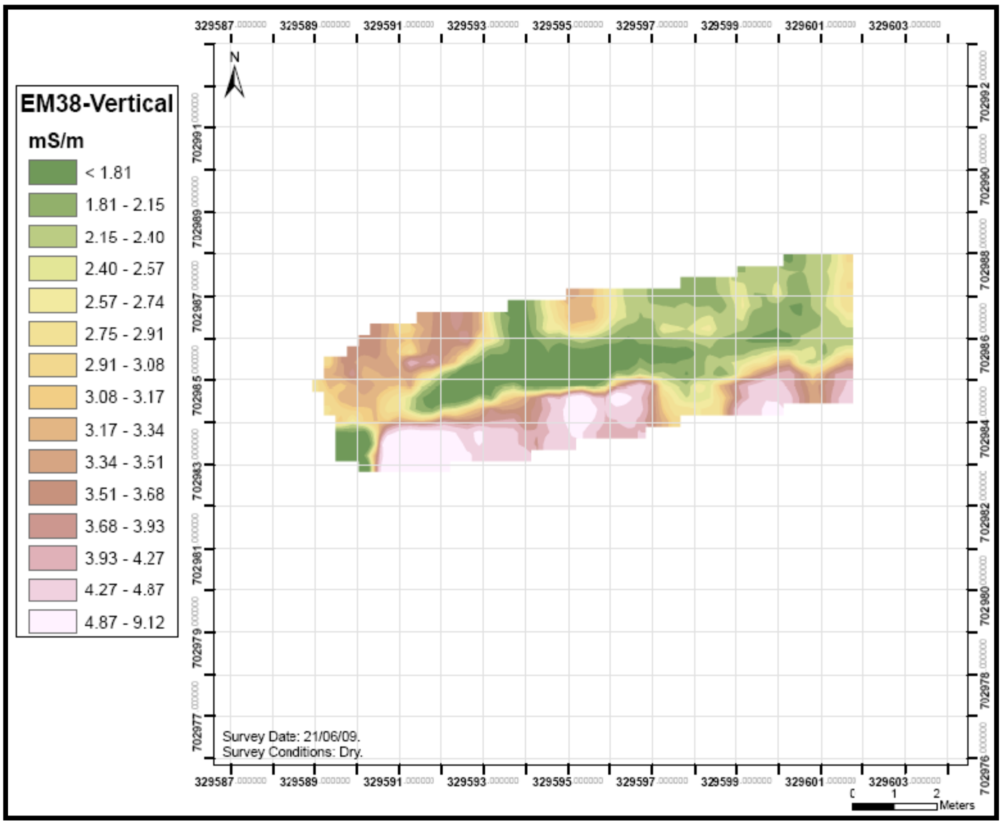

Figure B.4.2. EM38 vertical mode (Q/P) of Trench 3 without topsoil covering.

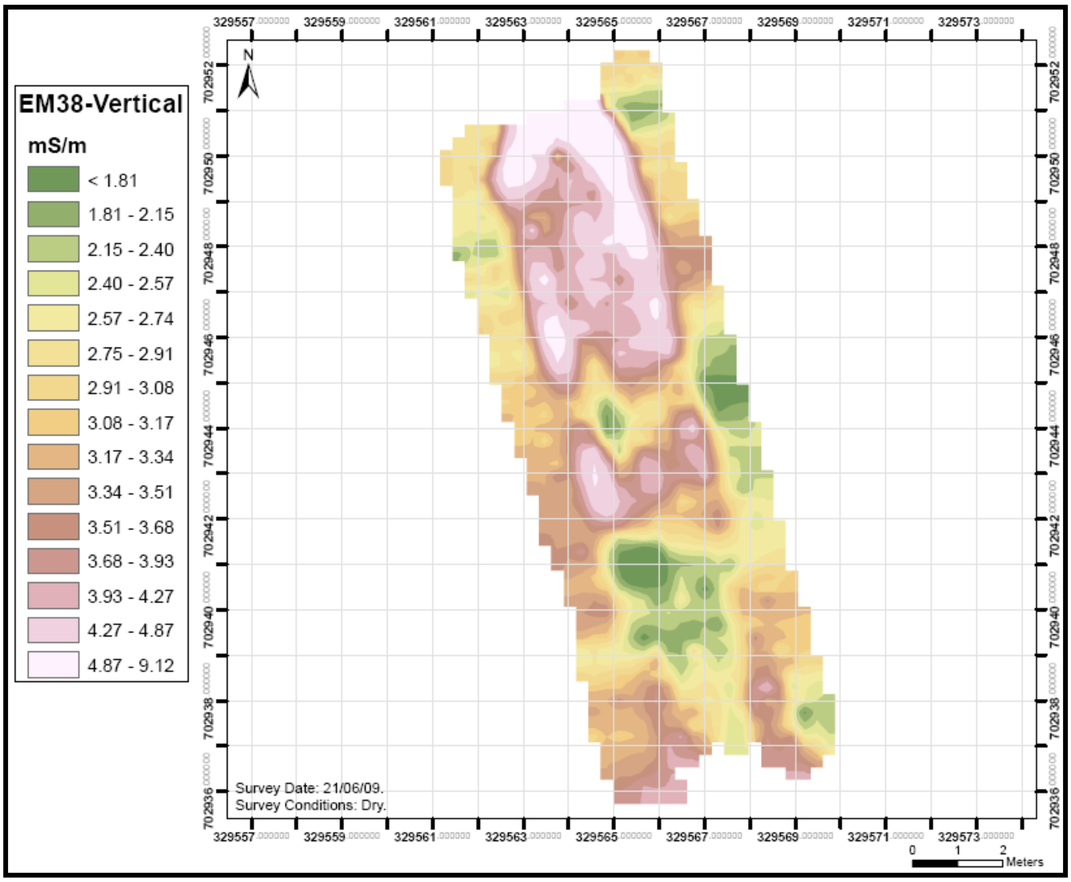

Figure B.4.3. EM38 vertical mode (Q/P) of Trench 4 without topsoil covering

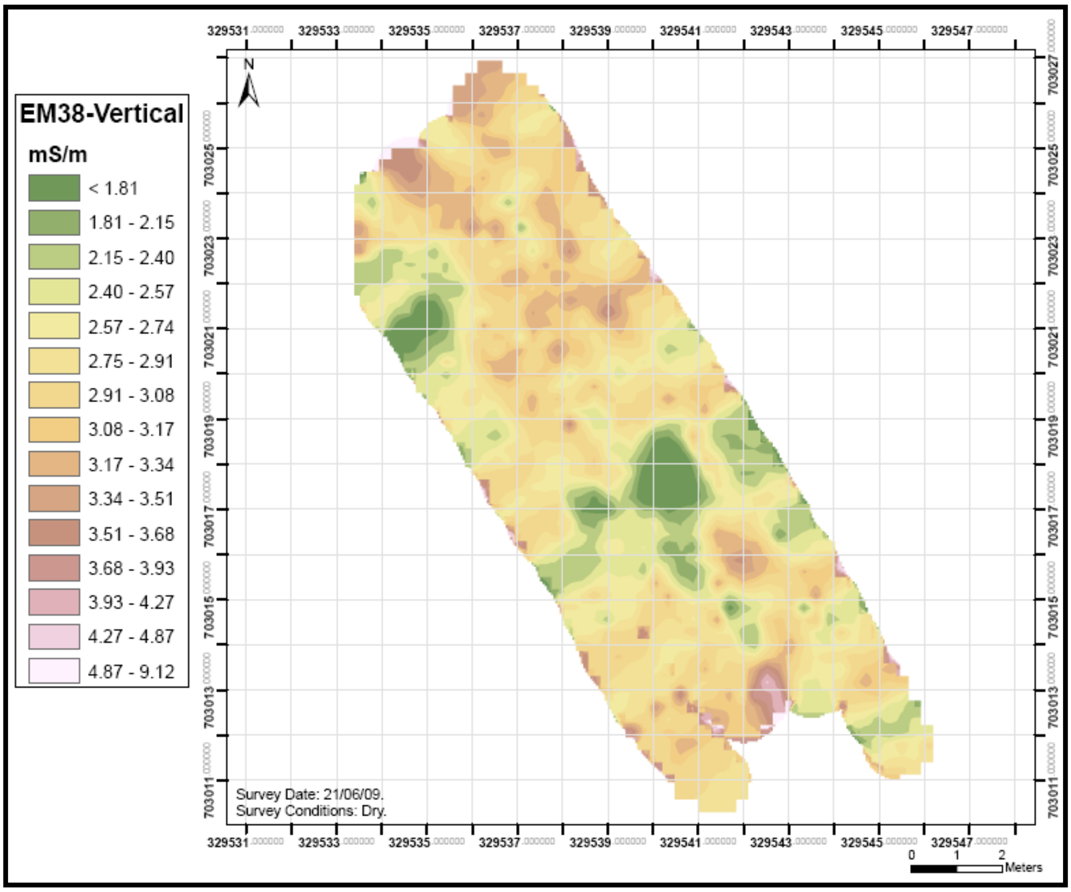

Figure B.4.4. EM38 vertical mode (Q/P) of Trench 5 without topsoil covering

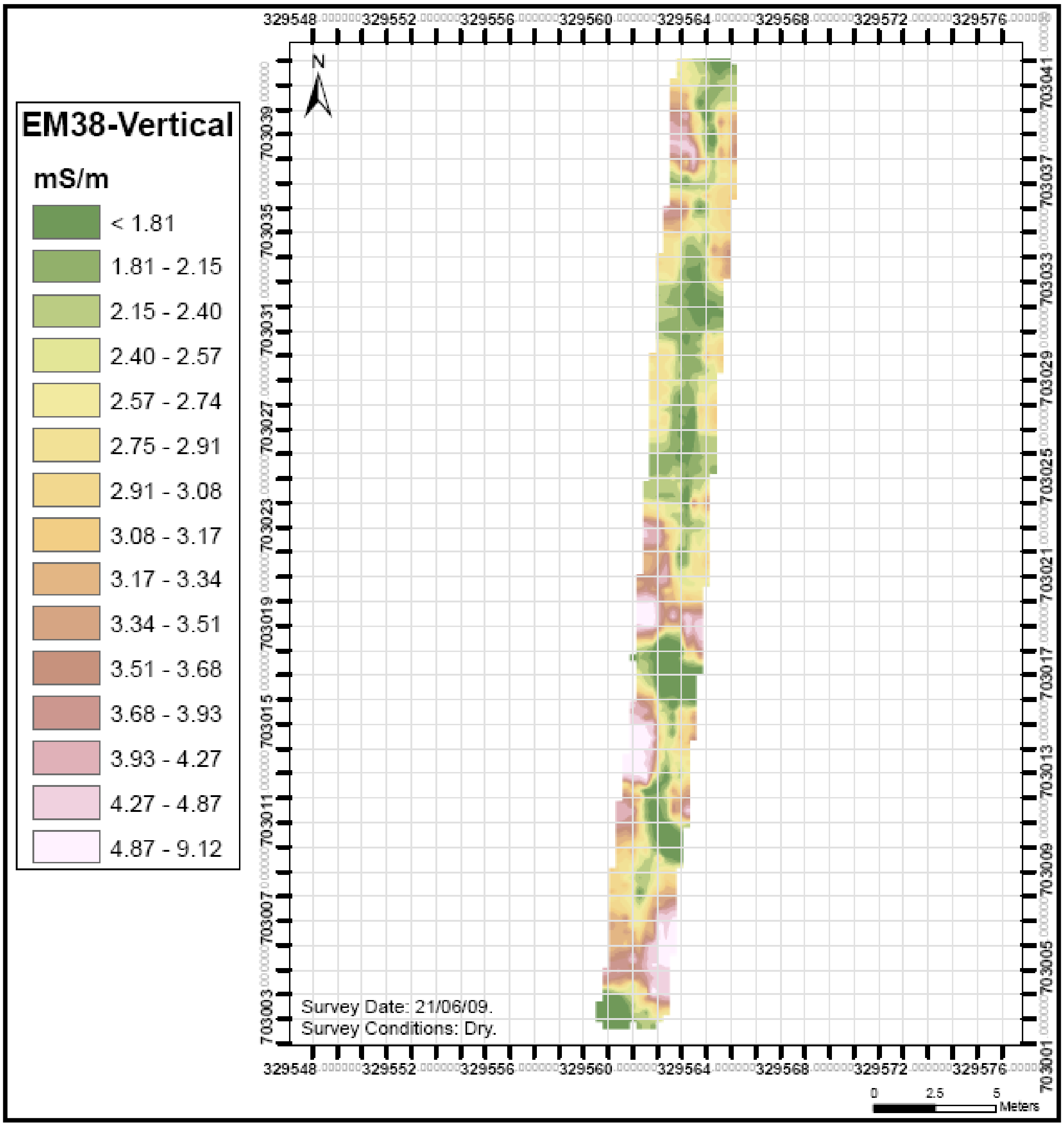

Figure B.4.5. EM38 vertical mode (Q/P) of Trench 6 without topsoil covering.

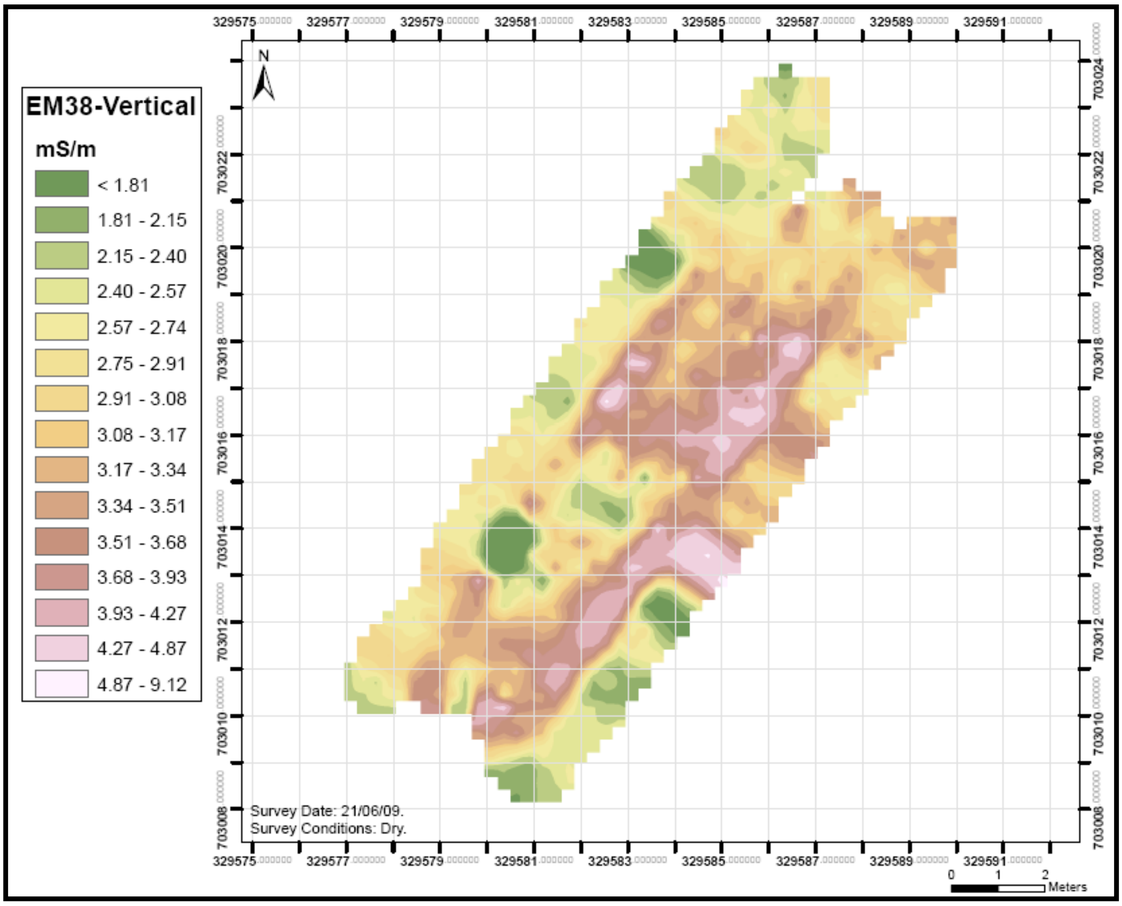

Figure B.4.6. EM38 vertical mode (Q/P) of Trench 7 without topsoil covering.

B.5: Magnetic Susceptibility HF Results

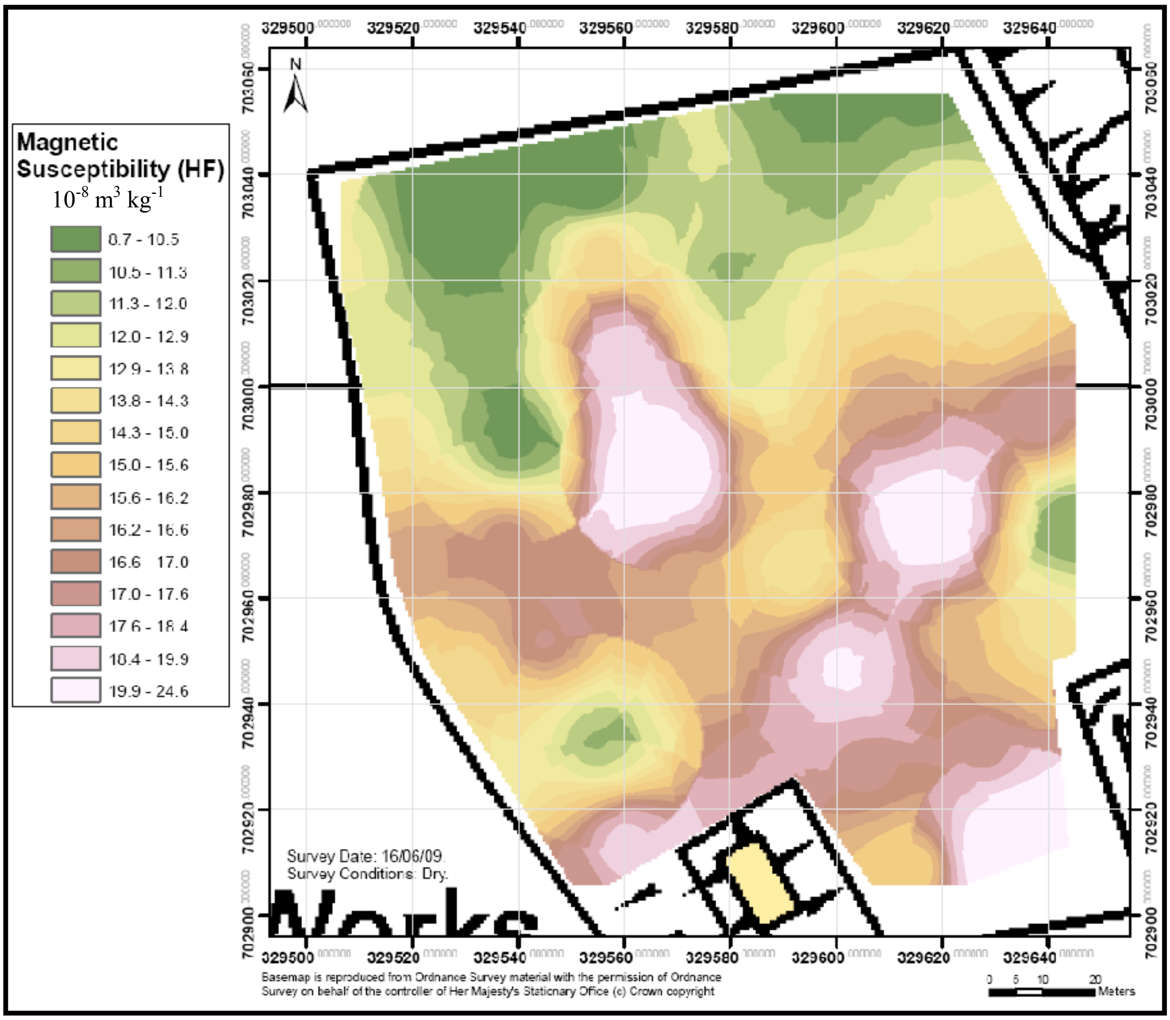

Figure B.5.1. Magnetic susceptibility high frequency results using the Bartington MS2 magnetic susceptibility meter.

B.6: Frequency Dependent Magnetic Susceptibility ($\chi_{fd\%}$)

Frequency dependent magnetic susceptibility was calculated using the following equation:

$$\chi_{fd\%} = (\chi_{lf} - \chi_{hf} / \chi_{lf}) \times 100$$

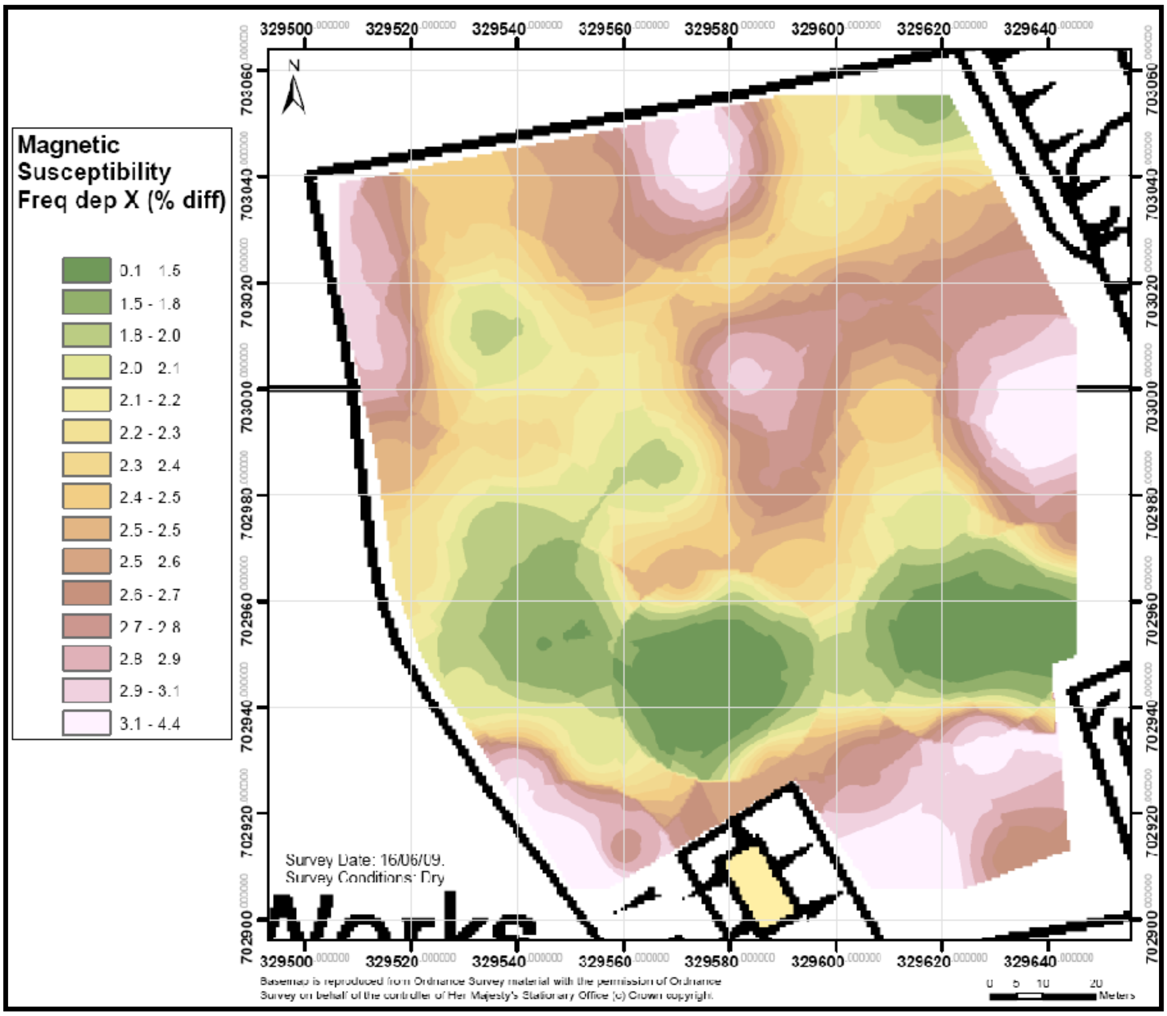

Figure B.6.1. Frequency dependent susceptibility results using the Bartington MS2 magnetic susceptibility meter.

APPENDIX C: DITCH ANALYSIS

The image below shows the location of samples taken from the two ring ditches fully excavated in Trench 6 with the sample references referred to throughout the investigation.

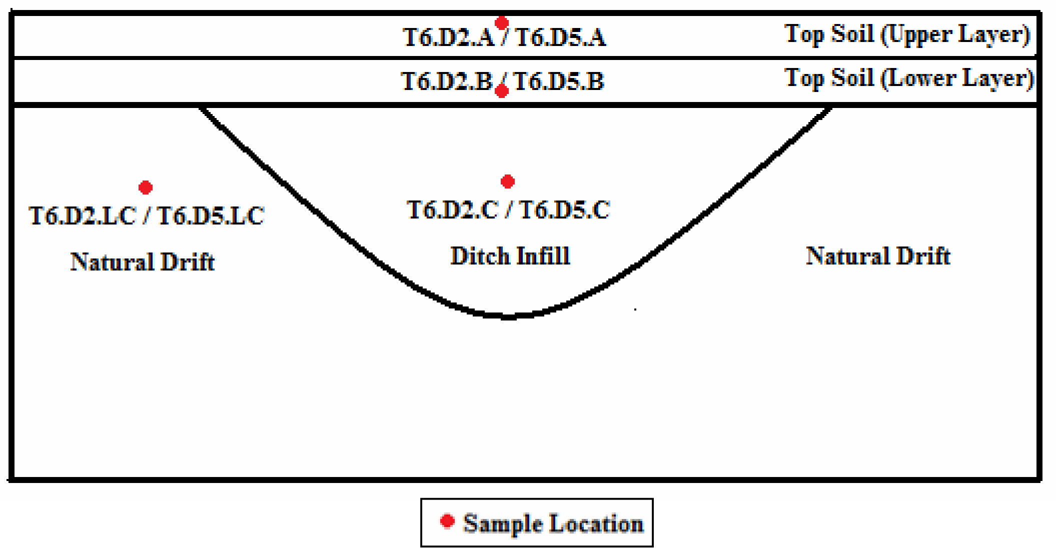

Figure C1. The sample locations with references within Trench 6 on Field 1.

C.1: Grain Size Results

When running grain size analysis using the Coulter LS230, three cycles of measurements are performed automatically. The first cycle is likely to give measurements including some clay particles, particularly clay coating some of the grains. Therefore the third cycle measurements show the true representative of the grain sizes as they have been subject to water filtering three times.

Figures C.1.1 – C.1.4 show the similarities between ditch infill and the surrounding sediment for both ditches within Trench 6.

Table C.1.1. First cycle measurement showing grain size data from two ditches sampled in Trench 6

First Cycle Measurement	Ditch 2 (T6.D2.C1)	Left of Ditch 2 (T6.D2.LC1)	Ditch 5 (T6.D5.C1)	Left of Ditch 5 (T6.D5.LC1)
From (µm)	0.375	0.375	0.375	0.375
To (µm)	2000	2000	2000	2000
Mean (µm)	612.8	462.8	558.2	385
Median (µm)	443.9	319	418.9	272.5
Mean/Median Ratio	1.38	1.451	1.333	1.413
Mode (µm)	390.9	429.2	390.9	356.1
S.D. (µm)	518.5	460.5	473.4	419.3

Table C.1.2. Second cycle measurement showing grain size data from two ditches sampled in Trench 6

Second Cycle Measurement	Ditch 2 (T6.D2.C2)	Left of Ditch 2 (T6.D2.LC2)	Ditch 5 (T6.D5.C2)	Left of Ditch 5 (T6.D5.LC2)
From (µm)	0.375	0.375	0.375	0.375
To (µm)	2000	2000	2000	2000
Mean (µm)	581.9	452.5	534.7	380.9
Median (µm)	416.6	305.7	403.9	265
Mean/Median Ratio	1.397	1.48	1.324	1.438
Mode (µm)	390.9	429.2	356.1	356.1
S.D. (µm)	514.9	462.5	469.6	425.9

Table C.1.3. Third cycle measurement showing grain size data from two ditches sampled in Trench 6

Third Cycle Measurement	Ditch 2 (T6.D2.C3)	Left of Ditch 2 (T6.D2.LC3)	Ditch 5 (T6.D5.C3)	Left of Ditch 5 (T6.D5.LC3)
From (µm)	0.375	0.375	0.375	0.375
To (µm)	2000	2000	2000	2000
Mean (µm)	587	447.7	540.8	371.9
Median (µm)	423.7	301.6	404.1	258.6
Mean/Median Ratio	1.385	1.484	1.338	1.438
Mode (µm)	390.9	429.2	356.1	356.1
S.D. (µm)	519	458.1	479.1	419.2

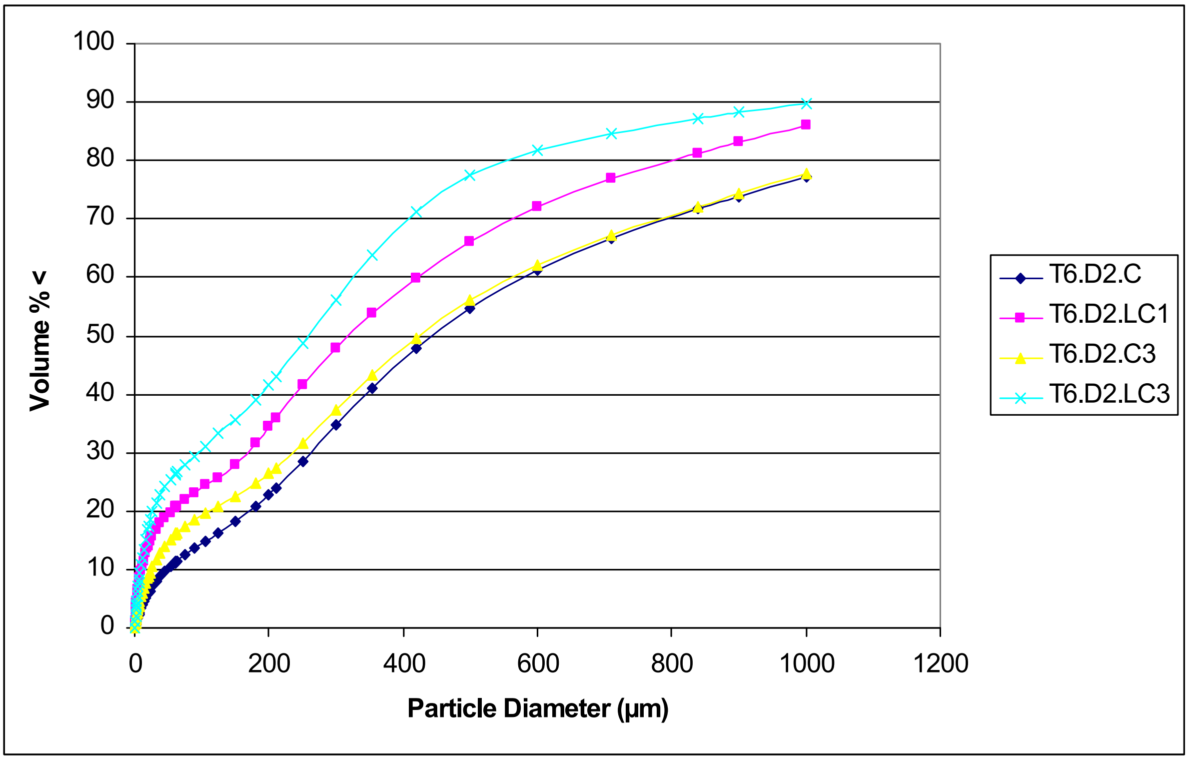

Figure C.1.1. Graph showing the particle diameter (µm) with volume (%) for Trench 6, Ditch 2 (1st and 3rd cycles).

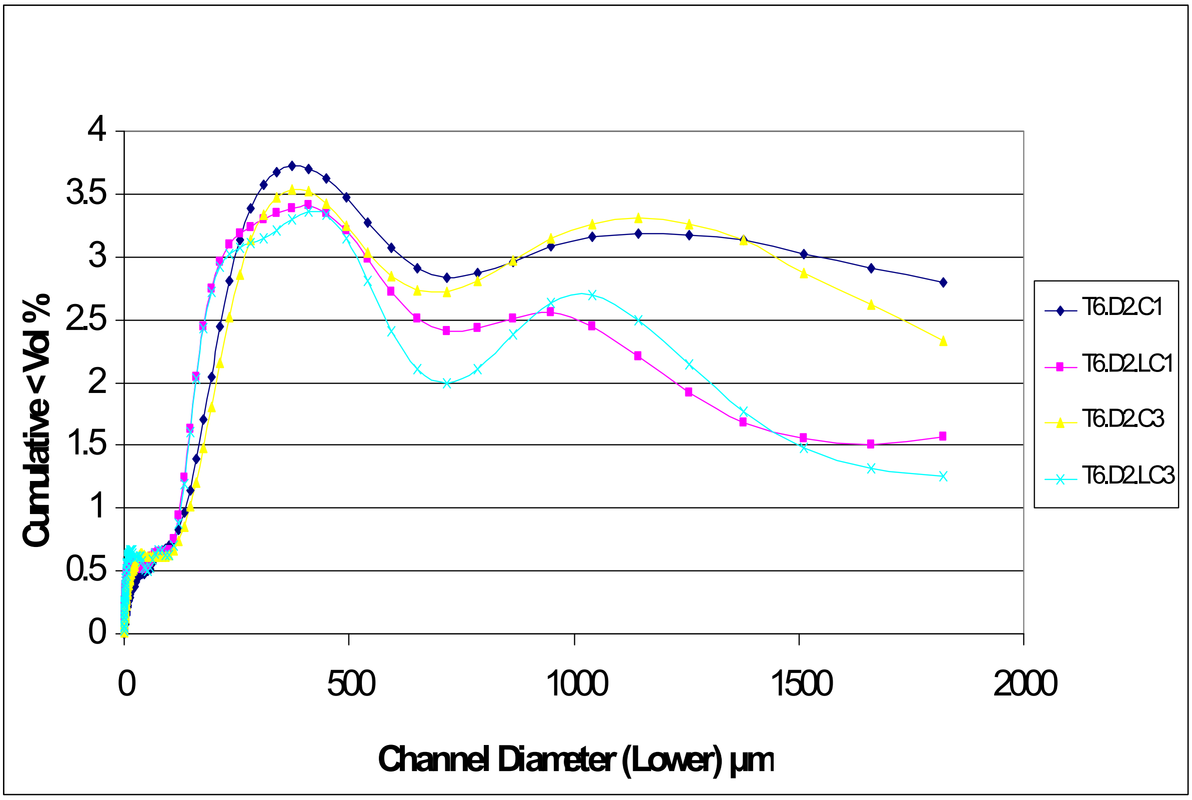

Figure C.1.2. Graph showing the channel diameter (µm) with cumulative volume (%) for Trench 6, Ditch 2 (1st and 3rd cycles).

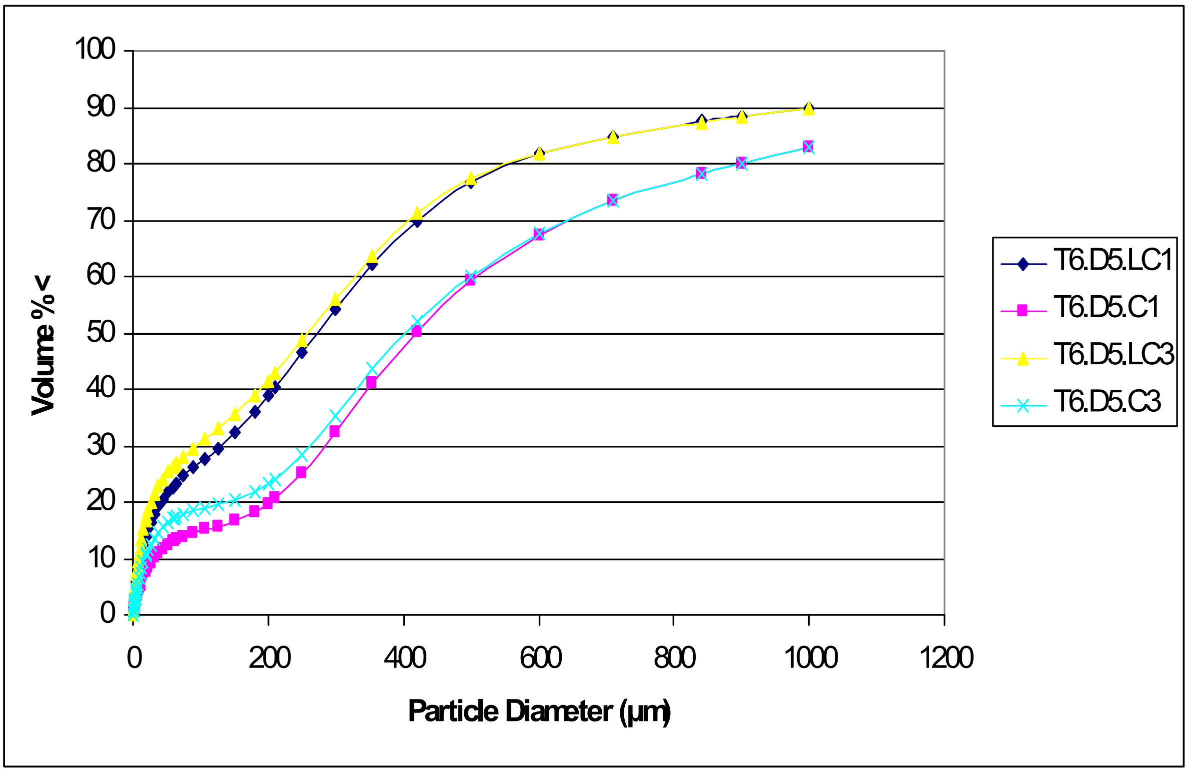

Figure C.1.3. Graph showing the particle diameter (µm) with volume (%) for Trench 6, Ditch 5 (1st and 3rd cycles).

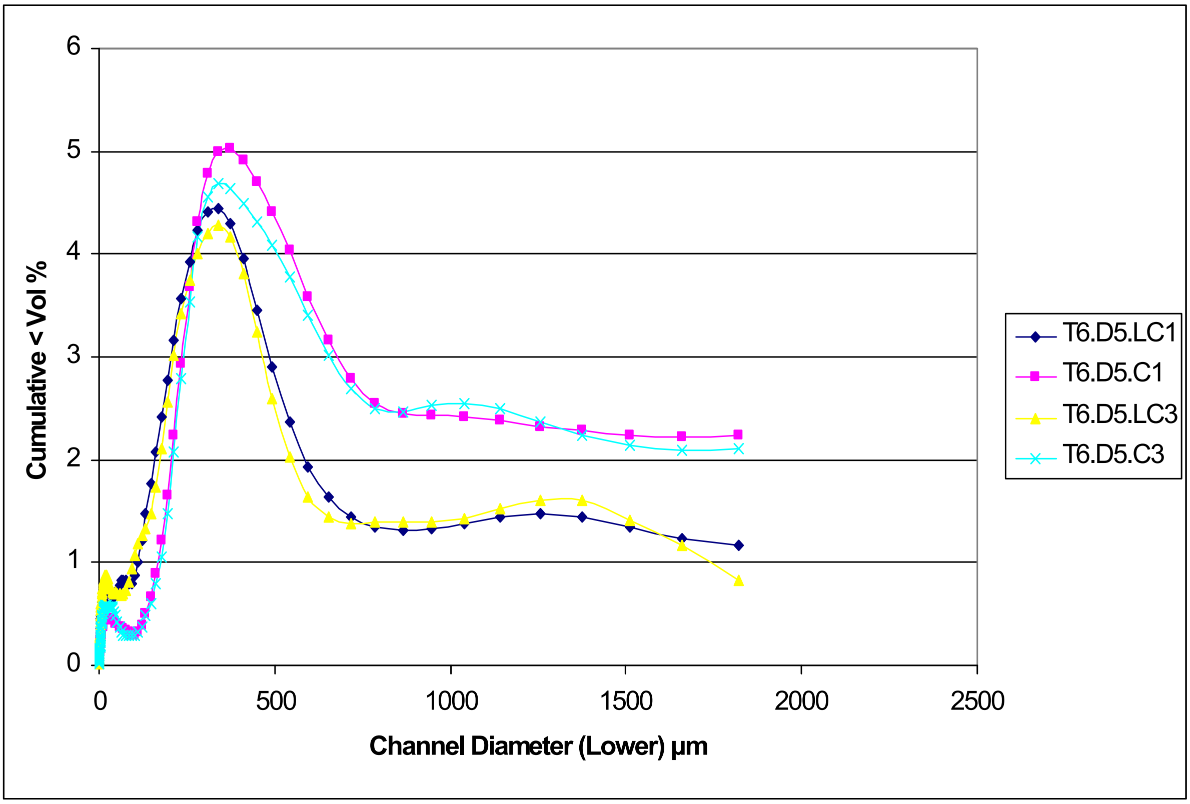

Figure C.1.4. Graph showing the channel diameter (µm) with cumulative volume (%) for Trench 6, Ditch 5 (1st and 3rd cycles).

C.2: XRF Results

XRF was performed to determine major and trace element chemistry of the ditch samples collected. Major element chemistry is of prime importance for this comparison thus glass fusions were not needed. Preparation for XRF analysis involved the following steps:

1) Samples dried in oven at constant temperature (~37°C).
2) Samples sieved with 50 mm grating to remove pebbles.
3) 40 g of sample measured and placed in a tungsten TEMA mill for 1 minute 30 seconds then poured into new sample bags.
4) Between each run the equipment was cleaned with a pure quartz run then air blasted and wiped down with acetone.
5) Press powder pellets were formed by mixing 7 g of ground sample and 1g of wax.
6) These mixed samples were then compressed with an applied pressure of 10 tonnes using a tungsten carbide hydraulic press to form the press powder pellet.
7) The pellets were then analysed using an X-Lab polarised energy dispersive spectrometer.

The accuracy and precision of the XRF results were determined by comparing standards run by Mr. Angus Calder with published values obtained from www.geoanalyst.com.

Table C.2.1. XRF- Major Elements (%)

Sample Reference	**Na_2O** %	**MgO** %	**Al_2O_3** %	**SiO_2** %	**P_2O_5** %	**SO_3** %	**Cl_2O** %	**K_2O** %	**CaO** %	**TiO_2** %	**Fe_2O_3** %	Total %
T6.D2.A	0.58	0.50	3.71	31.16	0.15	0.01	0.04	1.26	0.37	0.30	2.32	40.4
T6.D2.B	0.52	0.38	3.50	32.65	0.14	< 0.01	0.03	1.21	0.33	0.29	2.09	41.2
T6.D2.C	0.50	0.25	3.43	32.61	0.08	< 0.01	0.04	1.24	0.20	0.26	1.89	40.5
T6.D2.LC	0.58	0.30	3.41	34.23	0.01	< 0.01	0.04	1.43	0.20	0.21	1.89	42.3
T6.D5.A	0.52	0.25	3.11	32.96	0.13	0.01	0.04	1.13	0.29	0.24	1.73	40.4
T6.D5.B	0.48	0.16	3.22	34.14	0.09	< 0.01	0.03	1.17	0.17	0.23	1.74	41.4
T6.D5.C	0.49	0.12	3.10	35.26	0.08	< 0.01	0.04	1.18	0.14	0.22	1.64	42.3
T6.D5.LC	0.56	0.27	3.42	34.30	0.01	< 0.01	0.04	1.28	0.13	0.24	1.76	42.0
Precision	0.09	0.03	0.05	0.12	0.01	0.00	n/a	0.02	0.01	0.00	0.01	
Accuracy	1.55	3.46	0.93	0.23	10.16	n/a	n/a	1.08	4.03	2.75	2.74	

Table C.2.2. XRF- Trace Elements (ppm)

Sample Reference	V ppm	Cr ppm	Mn ppm	Ni ppm	Cu ppm	Zn ppm	Ga ppm	Ge ppm	As ppm	Se ppm	Br ppm	Rb ppm	Sr ppm	Y ppm	Zr ppm	Nb ppm	Mo ppm
T6.D2A	72.1	48.0	645.1	16.0	23.6	46.1	7.6	< 3	5.4	< 0.8	9.3	34.7	127.4	9.7	180.6	6.6	< 1
T6.D2.B	60.6	33.0	616.0	8.9	19.9	41.8	6.2	< 3	5.5	< 0.9	11.0	33.8	106.4	8.6	197.6	5.9	< 1
T6.D2.C	48.6	30.9	604.2	9.9	18.0	38.9	6.7	< 3	4.9	< 0.9	12.1	32.5	99.1	8.4	221.7	5.6	< 1
T6.D2.LC	56.4	40.2	487.8	6.8	29.4	19.4	6.5	< 3	5.8	< 0.9	3.4	35.3	112.2	9.6	213.2	4.9	< 1
T6.D5.A	47.4	31.7	587.7	11.9	18.5	42.1	7.0	< 3	4.7	< 0.9	11.3	31.3	95.4	7.8	177.9	5.4	< 1
T6.D5.B	48.6	28.1	772.2	5.3	17.8	34.2	6.4	< 3	4.3	< 0.9	12.7	34.3	87.3	8.2	190.5	5.1	< 1
T6.D5.C	52.5	36.1	867.9	7.4	16.2	38.0	6.6	< 3	3.4	< 0.9	6.3	34.3	83.3	7.6	194.5	5.2	< 1
T6.D5.LC	45.2	31.7	347.6	8.2	13.9	23.9	5.7	< 3	4.0	< 0.9	3.8	35.0	93.9	7.4	200.1	6.0	< 1
Precision	3.0	3.1	n/a	2.3	2.1	4.7	0.9	n/a	2.9	0.5	1.0	3.0	4.4	2.0	4.6	2.1	0.3
Accuracy	4.7	2.2	n/a	0.9	3.4	6.7	4.0	n/a	3.7	0.4	0.4	1.0	8.8	1.2	10.5	5.7	0.5

Sample Reference	Ag ppm	Cd ppm	In ppm	Sn ppm	Sb ppm	I ppm	Cs ppm	Ba ppm	La ppm	Ce ppm	Pr ppm	Nd ppm	Tl ppm	Pb ppm	Bi ppm	Th ppm	U ppm
T6.D2.A	< 1	< 1	< 1	1.3	0.5	2.4	< 3	303.3	7.1	24.0	< 5	12.8	< 3	22.7	< 1	3.5	< 1
T6.D2.B	< 1	< 1	< 1	1.2	0.6	3.8	< 3	287.0	9.2	22.4	< 5	14.7	< 3	17.2	< 1	2.8	< 1
T6.D2.C	< 1	< 1	< 1	0.6	< 0.3	5.1	< 3	336.6	8.9	21.7	< 5	11.5	< 3	10.1	< 1	3.1	< 1
T6.D2.LC	< 1	< 1	< 1	1.1	0.4	0.5	< 3	326.0	9.1	24.7	< 5	11.0	< 3	8.2	< 1	3.5	< 1
T6.D5.A	< 1	< 1	< 1	1.4	0.4	4.3	< 3	256.2	7.5	17.8	< 5	12.4	< 3	19.2	< 1	2.7	< 1
T6.D5.B	< 1	< 1	< 1	0.5	< 0.3	4.2	< 3	258.3	6.9	20.1	< 5	11.2	< 3	9.5	< 1	3.1	< 1
T6.D5.C	< 1	< 1	< 1	0.9	0.4	3.9	< 3	268.6	6.9	17.9	< 5	11.1	< 3	8.3	< 1	1.9	< 1
T6.D5.LC	< 1	< 1	< 1	1.2	0.5	0.9	< 3	303.5	4.8	17.5	< 5	10.9	< 3	8.6	< 1	2.8	< 1
Precision	n/a	n/a	n/a	n/a	n/a	n/a	n/a	6.6	1.7	2.7	n/a	2.7	0.5	4.7	n/a	1.6	1.0
Accuracy	n/a	n/a	n/a	n/a	n/a	n/a	n/a	15.2	4.3	4.0	n/a	3.4	0.2	7.7	n/a	1.1	0.5

C.3: XRD Results

The following two XRD graphs show a comparison of the ditch infill sediment to the surrounding sediment for both ditches identified in Trench 6 (T6.D2.LC/T6.D2.C and T6.D5.LC/T6.D5.C). XRD was used to identify the major mineral phases within the samples. The powdered samples were analysed on plates using a Philips PW1050/Hiltonbrooks DG2 X-Ray Diffraction machine. The results are presented in Figures C.3.1 and C.3.2.

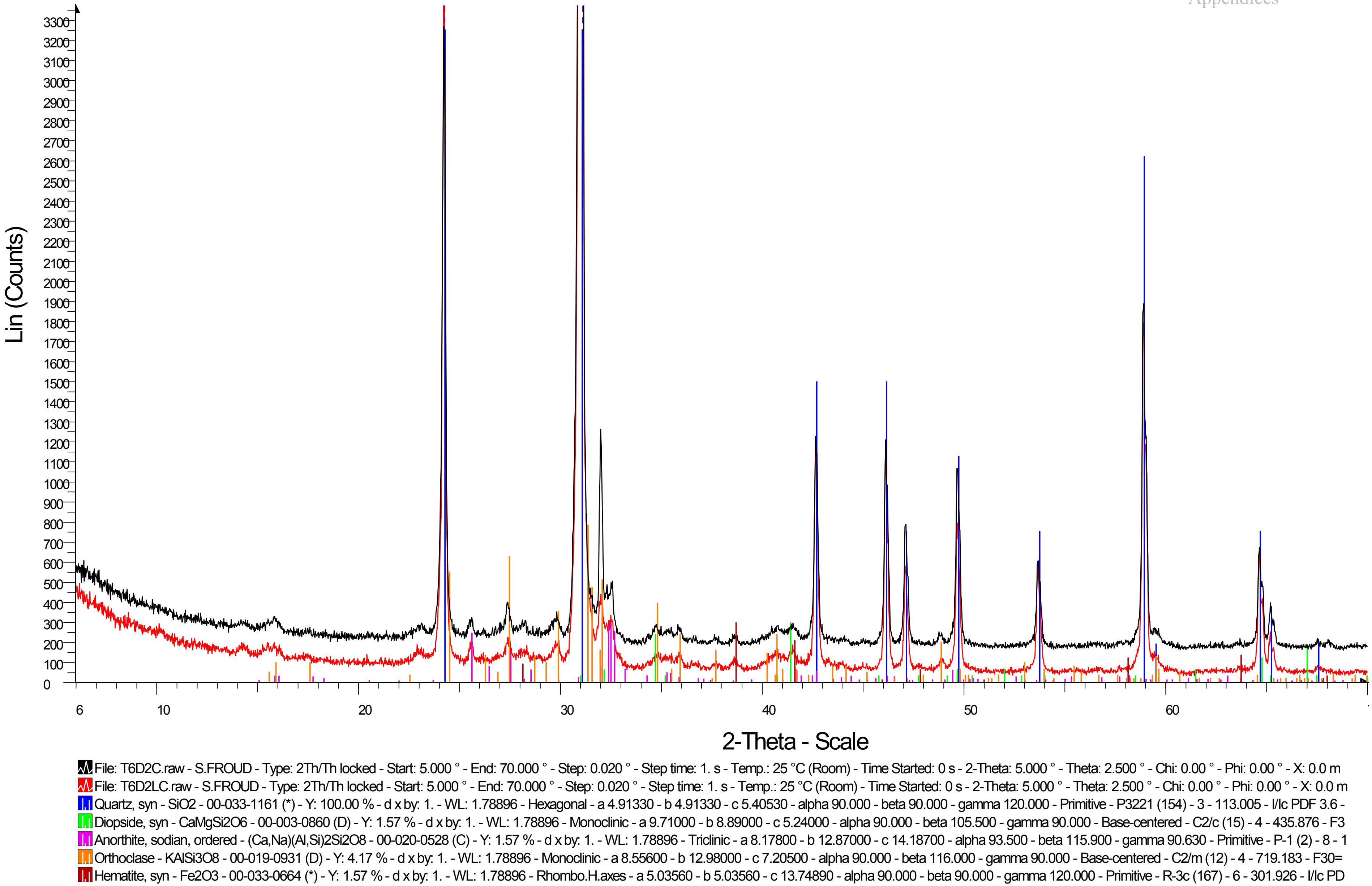

Figure C.3.1. XRD data for T6.D2.C (ditch infill) and T6.D2.LC (natural drift).

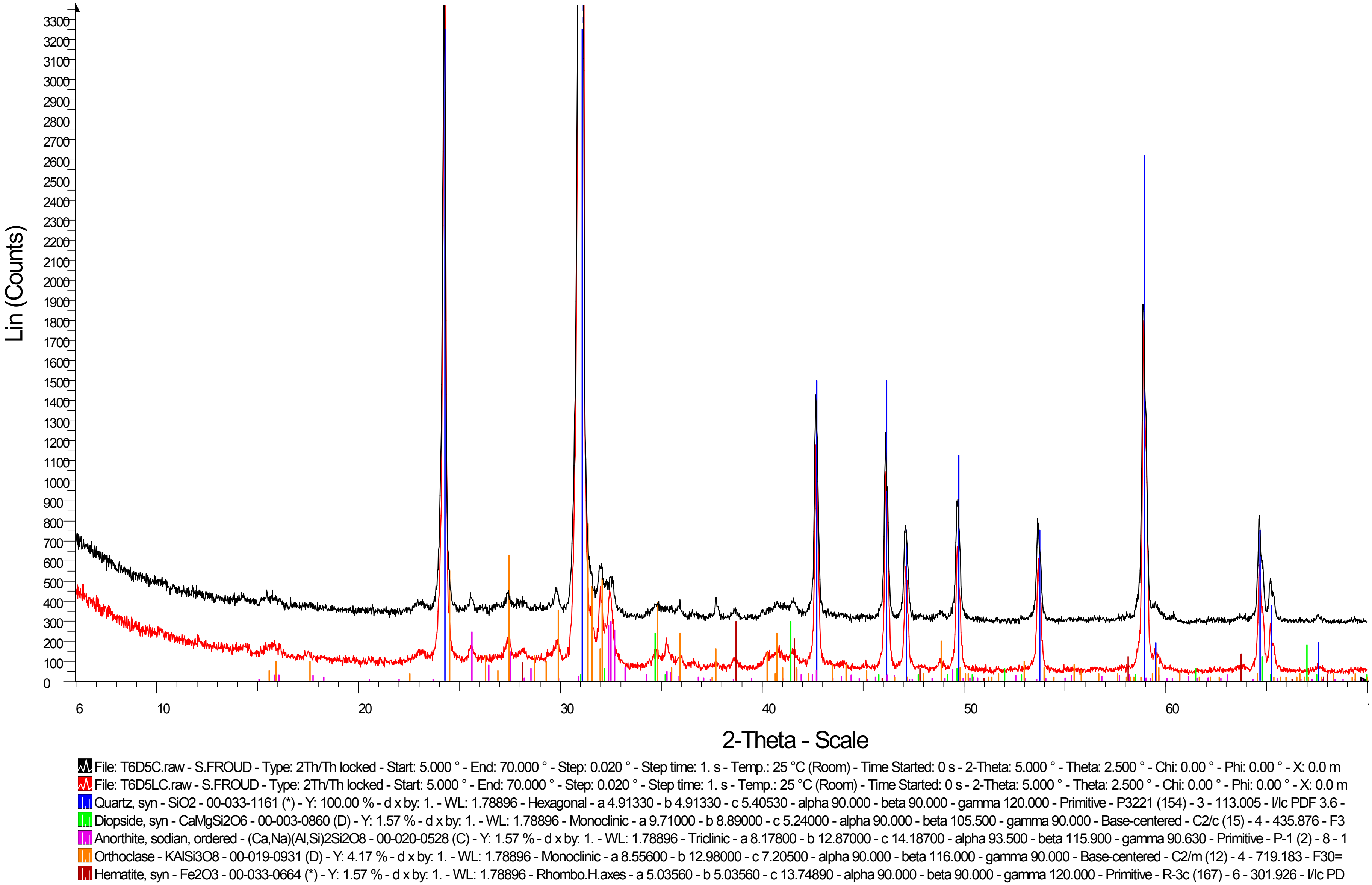

Figure C.3.2. XRD data for T6.D5.C (ditch infill) and T6.D5.LC (natural drift).

C.4: Excavation Imagery

Trench 2

The remaining findings from trench 2 not displayed in Section 5.2 marking the position of the WWII look out point/spot light.

Figure C.4.1. The extent of Trench 2 with excavation in progress (person for scale).

Figure C.4.2. Loose bricks found relating to WWII feature (camera case for scale).

Figure C4.3. 'Jeffrey's' Edinburgh Lemonade bottle found within the WWII remains (hand for scale).

Trench 3

Figure C.4.4. Two features thought to be ring ditches being excavated but it was very hard to locate the boundaries upon excavation (person for scale).

Trench 5

Figure C.4.5. Plough scars visible 50 cm deep.

Figure C.4.6.A possible ring ditch excavated.

Figure C.4.7. An unidentified linear feature within the southern half of Trench 5.

Trench 6

Figure C.4.8. The full length of Trench 6 with excavation in progress (person for scale).

Figure C.4.9. Ditch 2, one of only two ring ditches that were identified.

Figure C.4.10. Ditch 5, the second of two ring ditches identified.